DOE/ET/27111-5

Annual Report

SALINITY VARIATIONS AND CHEMICAL COMPOSITIONS OF WATERS IN THE FRIO FORMATION, TEXAS GULF COAST

by

R. A. Morton, C. M. Garrett, Jr., J. S. Posey,
J. H. Han, and L. A. Jirik

Prepared for the
U.S. Department of Energy
Division of Geothermal Energy

Under Contract No. DE-AC08-79ET27111

Bureau of Economic Geology
The University of Texas at Austin
Austin, Texas 78712

W. L. Fisher, Director

November 1981

DISCLAIMER

"This report was prepared as an account of work sponsored by an agency of the United States Government. Neither the United States Government nor any agency thereof, nor any of their employees, makes any warranty, express or implied, or assumes any legal liability or responsibility for the accuracy, completeness, or usefulness of any information, apparatus, product, or process disclosed, or represents that its use would not infringe privately owned rights. Reference herein to any specific commercial product, process, or service by trade name, trademark, manufacturer, or otherwise, does not necessarily constitute or imply its endorsement, recommendation, or favoring by the United States Government or any agency thereof. The views and opinions of authors expressed herein do not necessarily state or reflect those of the United States Government or any agency thereof."

This report has been reproduced directly from the best available copy.

Available from the National Technical Information Service, U.S. Department of Commerce, Springfield, Virginia 22161.

Price: Printed Copy A06
Microfiche A01

Codes are used for pricing all publications. The code is determined by the number of pages in the publication. Information pertaining to the pricing codes can be found in the current issues of the following publications, which are generally available in most libraries: Energy Research Abstracts, (ERA); Government Reports Announcements and Index (GRA and I); Scientific and Technical Abstract Reports (STAR); and publication, NTIS-PR-360 available from (NTIS) at the above address.

CONTENTS

Figures

ABSTRACT

Waters produced from sandstone reservoirs of the deep Frio Formation exhibit spatial variations in chemical composition that roughly coincide with the major tectonic elements (Houston and Rio Grande Embayments, San Marcos Arch) and corresponding depositional systems (Houston and Norias deltas, Greta-Carancahua barrier/strandplain system) that were respectively active along the upper, lower, and middle Texas Coast during Frio deposition. Waters of the upper coast typically have relatively high salinities (maximum total dissolved solids >80,000 mg/L), high calcium (200 to 9,000 mg/L), high sodium (>15,000 mg/L), relatively high potassium (>150 mg/L), low to moderate Cl/Na ratios (1.4 to 1.9), and high Cl/Br ratios (>400). When compared with adjacent areas of Frio production, waters of the middle coast have lower salinities (maximum total dissolved solids <80,000 mg/L), low calcium (27 to 2,900 mg/L), low sodium (<15,000 mg/L), low potassium (<150 mg/L), low to moderate Cl/Na ratios (1.2 to 1.8), and low to intermediate Cl/Br ratios (55 to 400). Deep South Texas waters from the lower coast (Kenedy and Kleberg Counties) also have high salinities (maximum total dissolved solids >80,000 mg/L, extremely high calcium (1,800 to 34,000 mg/L), high sodium (>15,000 mg/L), high potassium (>150), extremely high Cl/Na ratios (>2), and low Cl/Br ratios (<250). Calcium concentrations actually exceed sodium concentrations in some South Texas waters.

Within an area, salinities are usually depth dependent, and primary trends closely correspond to pore pressure gradients and thermal gradients. Salinities decrease near the base of hydropressure but increase at intermediate pressure gradients (0.465 psi/ft and 0.7 psi/ft); maximum salinities in the geopressured zone generally occur where pressure gradients are between 0.7 and 0.75 psi/ft. At higher pressure gradients (>0.75 psi/ft) salinities decrease with depth. Changes in calcium and sodium concentrations with depth commonly parallel those

of total dissolved solids; however, changes in other ions and ionic ratios with depth are more gradual and usually do not coincide with salinity changes or the temperature and pressure regimes.

Where data are available (mainly in Brazoria County) the increases in TDS and calcium with depth coincide with the zone of albitization, smectite-illite transition, and calcite decrease in shales. Whether or not the increase in potassium with depth corresponds to a decrease in K feldspar is uncertain. Many of the high salinity waters of the upper coast can be explained by salt dissolution according to the Cl/Br ratio, but high salinity waters in South Texas are not as easily explained using the same criteria.

Waters have fairly uniform salinities when produced from the same sandstone reservoir within a fault block or adjacent fault blocks with minor displacement. In contrast, stratigraphically equivalent sandstones separated by faults with large displacement usually yield waters with substantially different salinities owing to the markedly different thermal and pressure gradients across the faults that act as barriers to fluid movement.

INTRODUCTION

The methane dissolved in formation waters at high temperatures and pressures represents a vast but dilute resource that remains largely undeveloped because many uncertainties are associated with exploration and commercialization. One of the most critical and least understood physical factors affecting the resource is salinity of formation waters. Knowing the chemical composition and ionic concentration of brines in geopressured aquifers can be important for several reasons. First of all, methane solubility is partly controlled by the salinity of formation water. Secondly, the degree of corrosion and scaling of

surface equipment largely depends on the chemical characteristics of produced waters, and thirdly, the chemical compatibility of produced waters with shallower ground waters may control the long-term disposal of spent geothermal fluids.

Although this study is part of an ongoing effort to assess and delineate Gulf Coast geopressured geothermal energy, its application is not limited to those alternate energy sources. Indeed equally important are the applications directed toward improved exploration and development of conventional hydrocarbons. For example, salinity data are needed to determine the compatibility of formation and completion fluids. Moreover they are critical to the calibration of electric logs from which petrophysical parameters and reserve estimates are derived.

A primary objective of the study was to evaluate the local and regional structural and stratigraphic controls on formation water salinity in the Frio Formation of Texas. This formation was selected because (1) chemical analyses of Frio waters were available from field samples, company files, and published sources (Jessen and Rolshausen, 1944; Fowler, 1970; Kharaka and others, 1977), (2) the regional geologic framework of the Frio Formation has been established (Bebout and others, 1978; Galloway and others, in press), and (3) the Frio continues to be one of the most active exploration targets and prolific producers of hydrocarbons in the Texas Gulf Coast.

PRIOR STUDIES OF FORMATION WATER SALINITY

Mechanisms for Concentration and Dilution

Numerous physical and chemical mechanisms have been suggested to explain the wide range of subsurface salinities and their systematic and random changes

observed in deeper parts of sedimentary basins. For the purposes of dissussion, these explanations can be broadly grouped according to their primary cause (original water, fluid migration, water-rock interaction). However, the grouping does not imply that the geochemical processes are mutually exclusive.

Original Water

Extreme salinity variations occurring over short lateral or vertical distances have sometimes been explained as differences related to the original environment of deposition, and indeed where evaporation rates are high, shallow ground waters in coastal sand bodies can exhibit a large range in salinities (fresh water to 250,000 ppm) and high salinity gradients (Amdurer, 1978). On the other hand, the preponderance of evidence suggests that the physical and geochemical alterations that occur at depth and over geologic time are far more important than the salinity at the time of deposition (White, 1965). The few attempts to demonstrate a causal relationship between depositional environments and salinity have been based on limited data. Consequently, the general relationships described by Timm and Maricelli (1953) for low salinity water in marine sediments and high salinity water in nonmarine equivalents are probably fortuitous and other explanations are equally valid.

Fluid Migration

Ionic concentrations greater than sea water, commonly found at depth (Dickey, 1969; Manheim and Horn, 1968), have been attributed to physical processes including sediment compaction and dewatering of thick shale intervals that act as semipermeable membranes. According to its proponents, this process, termed ionic filtration (salt sieving, reverse osmosis), selectively allows the migration of water molecules through the sediment while movement of ions is retarded (De Sitter, 1947; McKelvey and Milne, 1962; Bredehoeft and others, 1963;

Engelhardt and Gaida, 1963; White, 1965). Such hyperfiltration would result in increases in salinity with depth and increases in pore-water salinity of shale relative to that of adjacent sandstones.

High salinity brines in deep aquifers may also be partly explained by dissolution and ionic diffusion from nearby salt (Minor, 1934; Rittenhouse, 1967; Manheim and Horn, 1968; Manheim and Bischoff, 1969; Kharaka and others, 1977) or by charging by brines (Magara, 1978) derived from underlying evaporites, but proximity to salt is not requisite for high salinities (White, 1965). Other explanations for abnormal concentrations involving fluid movement, such as evaporation (Mills and Wells, 1919) or gravity segregation (Mangelsdorf and others, 1970), have been dismissed previously because of quantitative considerations (Russell, 1933; Kharaka and Berry, 1974).

Water-Rock Interactions

With the physical compaction and fluid migration that accompanies sediment burial are chemical reactions that cause dissolution of rock components, precipitation of authigenic minerals, and transformation of one mineral species to another. These diagenetic alterations are certainly better understood today than a decade ago, when Burst (1969) first described the transformation of expandable clay minerals to nonexpandable forms at temperatures above 200°F. This transformation causes the release of water from interlayer positions. The low ionic concentration of this structured water would contribute to the dilution of shale pore water (Hedberg, 1967; Schmidt, 1973).

Geopressured Sediments

In Gulf Coast sediments below the top of geopressure, where undercompacted shales exhibit higher porosities, reversals in trends toward lower salinities have been widely reported (Myers and Van Siclen, 1964; Dickey, 1969; Dickey and

others, 1972; Jones, 1969, 1975; Overton and Timko, 1969; Fowler, 1970; Schmidt, 1973; Fertl, 1976). However, laboratory analyses of waters produced from hydropressured and geopressured aquifers show that the decrease in salinity near the top of geopressure does not necessarily persist with depth. In fact, trends of increasing as well as decreasing salinities can be documented.

Hedberg (1967) and Schmidt (1973) and Jones (1969, 1975) suggested that under certain conditions, salinities in shales are less than salinities in adjacent sandstones. The dynamic interaction of geopressures and osmotic pressures may explain the salinity contrasts; however, Manheim and Horn (1968) contend that subsurface pressure gradients are inadequate to accomplish hyperfiltration in the face of osmotic pressures.

In summary, formation waters with salinities less than that of normal sea water (35,000 mg/L) are thought to be caused by the presence of original connate waters of the depositional environment, the flushing by meteoric water in the shallow subsurface, and the dilution by membrane-filtered water. Higher salinities are commonly thought to be caused by residuals remaining after hyperfiltration and/or clay mineral diagenesis, or caused by products of salt dissolution and other water-rock interactions. Given the diversity of diagenetic chemical reactions and the unusually high thermal and pressure gradients to which the rocks have been subjected, it appears that several mechanisms could explain the wide variability in chemical composition of waters in the Frio Formation.

Frio Formation

Both local and regional studies of subsurface brines have been published for hydropressured and geopressured sediments along the Texas Gulf Coast. Studies of limited areal extent focused on the Frio Formation in Matagorda County (Myers and Van Siclen, 1964), Brazoria County (Fowler, 1970), and the

Houston-Galveston and Corpus Christi areas (Kharaka and others, 1977). Except for Myers and Van Siclen (1964), these studies relied on produced formation waters to develop interpretations of salinity changes with depth. Jessen and Rolshausen (1944) also used chemical analyses of produced waters to describe regional variations in the Frio Formation at depths generally less than 8,000 ft where normal pressure gradients are usually encountered.

Salinities derived from electric logs and reported measurements for Tertiary aquifers have been mapped regionally by Core Laboratories (1972), Jones (1975), and Wallace and others (1977). In the Core Lab report, map units for sediments younger than the Wilcox Group consist of uniform depth intervals (2,000 ft) that cross stratigraphic subdivisions and ignore facies changes. Furthermore, these maps portray average salinities in the hydropressured zone and use a data base equivalent to about one water analysis per county. Jones (1975) and Wallace and others (1977) also used resistivity measurements to map regional salinities for the Wilcox Group, the Frio Formation, and the Miocene sediments in the Rio Grande Embayment. These maps suggest that the South Texas area is characterized by low salinities. However, available field measurements indicate salinities substantially higher than those mapped by Jones (1975) in Kenedy County. On the other hand, Wallace and others (1977) estimated higher salinities that are similar to those obtained from waters produced in the Candelaria area. The most frequently cited explanations for salinity variations in the Frio Formation are the combined processes of hyperfiltration and clay mineral diagenesis (Myers and Van Siclen, 1964; Fowler, 1970; Jones, 1975; Wallace and others, 1977), although Kharaka and others (1977, 1978) favor the influence of salt dissolution.

SAMPLING AND ANALYTICAL PROCEDURES

Field collection of water samples (fig. 1) and chemical analyses of those samples by the Mineral Studies Laboratory (MSL) established a basic framework for the study of formation water salinities in the Frio of the Texas Gulf Coast. Candidate wells for sampling were selected on the basis of geographic location, depth of producing zones in the Frio Formation, and appropriate gas to water ratios (<100 mcf/bbl). One hundred five wells were sampled for formation fluids during the summer of 1981. Eighty of these were judged valid and are included in Appendix A. The 80 wells sampled were located in 45 oil and/or gas fields producing from the Frio at depths greater than 7,000 ft. A summary of samples obtained from various depths is as follows: 6 samples from 7,000 to 8,000 ft; 15 samples from 8,000 to 9,000 ft; 15 samples from 9,000 to 10,000 ft; 20 samples from 10,000 to 11,000 ft; 14 samples from 11,000 to 12,000 ft; 7 samples from 12,000 to 13,000 ft; 1 sample from 13,000 to 14,000 ft; and 2 samples from 14,000 to 15,000 ft.

Field Techniques

When possible, water samples of producing wells were obtained at the wellhead. Occasionally samples were obtained from the separator, the heater-treater, or in some cases storage tanks located away from the well. Each sample was collected at a point in the production system nearest the wellhead that would have the least possibility for contamination. Plastic containers (100 ml beakers) and funnels used in the collection process were thoroughly cleaned to eliminate possible contaminants. In addition glass wool was used to remove oil and solid contaminants carried in the flow stream. After obtaining approximately 2 liters of water, temperature and pH values were measured using a 200°

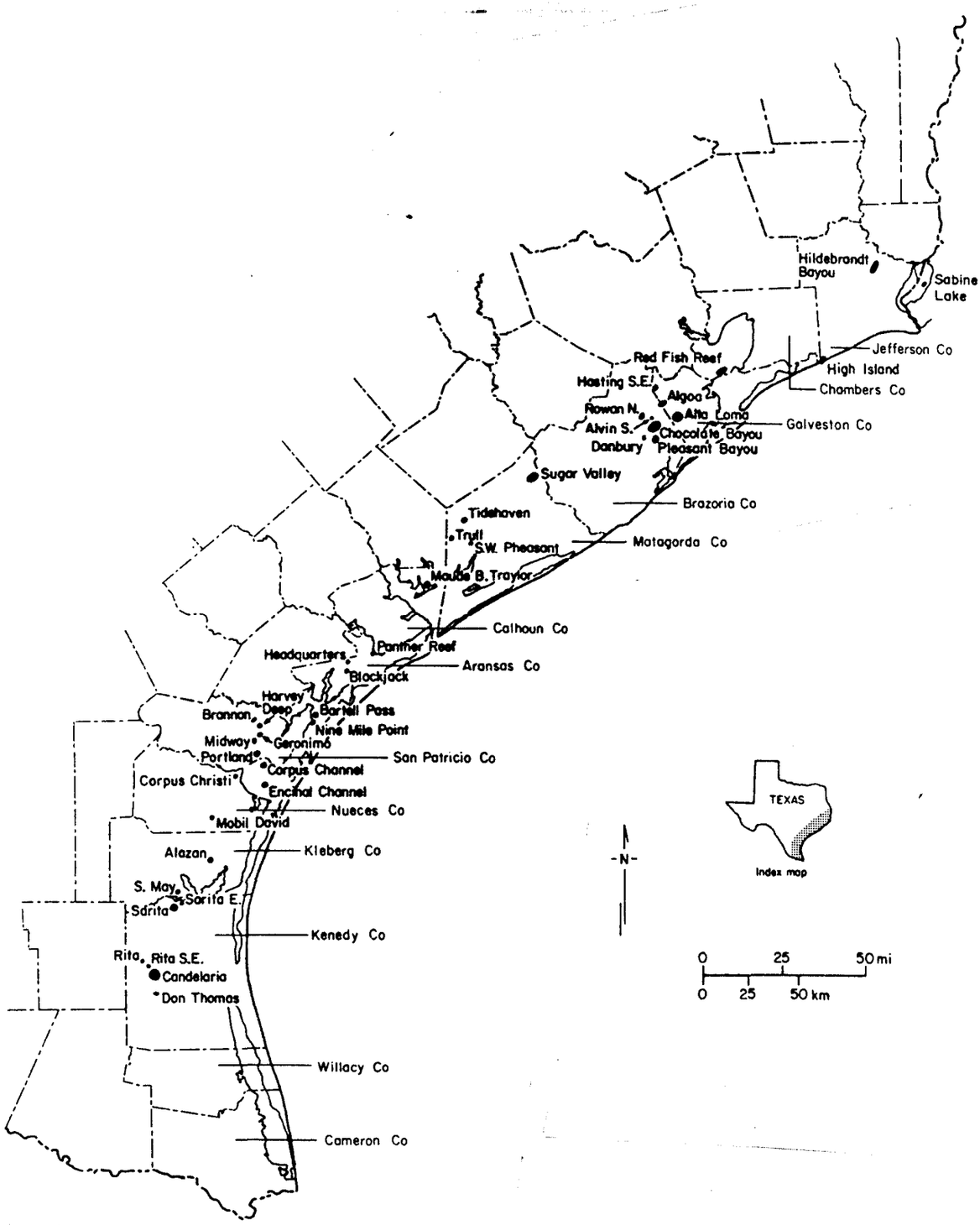

Figure 1. Locations of oil and gas fields along the Frio trend from which water samples were collected and analyzed. Chemical analyses are presented in Appendix A. Some field locations are generalized to include geographic (north, south, east, west) subdivisions.

centigrade thermometer and a Sargent Welch model PBC pH meter. Alkalinity was also measured in the field.

Four samples were collected from each well. First, a 250 ml plastic bottle was filled with water that had been filtered through glass wool. The water was treated with 1.25 ml of chloroform for later laboratory measurement of nutrients. Next, approximately 1,000 ml of raw untreated sample was passed through a filter system consisting of a hand-powered air pump connected to an enclosed cylinder with 0.45 μ millipore filter paper. A 250 ml plastic bottle was filled with filtered sample, capped, labeled, and preserved for later laboratory measurement of chlorides. A sample for determining the presence and concentration of various metals was prepared by placing 2.5 ml of 6N HCl in a 500 ml plastic bottle which was then filled with the filtered sample. Laboratory measurements could then be obtained for these elements at a later date. The fourth bottle for each well sampled was prepared for laboratory measurement of silica by filling a 100 ml plastic bottle with 25 ml of filtered sample and 75 ml of distilled de-ionized water.

Laboratory Techniques

The Mineral Studies Laboratory (MSL), an element of the Bureau of Economic Geology, performed all chemical analyses listed in Appendix A. The inductively coupled plasma emission spectrometer (ICP) method was used as a relatively inexpensive, rapid, analytical technique, which provided simultaneous measurements of major, minor, and trace elements in the water samples. Tests, conducted by the MSL, have shown that results using this technique are comparable to those from atomic absorption spectrophotometry. Elements normally analyzed by ICP for this study included sodium (Na), potassium (K), magnesium (Mg), calcium (Ca), aluminum (Al), iron (Fe), titanium (Ti), manganese (Mn), strontium (Sr), boron (B), and phosphorus (P). Depending on the condition of the sample and the

objective of the task, other techniques were employed for elements difficult to analyze by ICP.

Elements or compounds not on ICP band and therefore analyzed manually as single components included chloride (Cl), fluoride (F), bromide (Br), sulfate (SO_4), ammonia (NH_3), silica (SiO_2), bicarbonate (HCO_3), concentration of hydrogen ions (pH), and total dissolved solids (TDS).

A quality assurance program was carried out by the MSL for all samples analyzed to provide a mechanism for determining accuracy of results and for correcting inadequacy of methods. Steps taken to ensure accuracy included: (1) comparison of analyses with certain reference standards. These reference standards are from the United States Geological Survey (USGS); National Bureau of Standards; Department of Energy, Mines, and Resources of Canada; South African Committee for Certified Reference Materials; reference samples from the International Working Group (Paris, France); standard seawater (IAPSO Carlottenlund, Denmark); synthetic water standards (EPA); and standard stock solution prepared in the MSL from ultra-pure elements or compounds. (2) Reference materials of comparable chemical composition were selected as controls during each batch of sample analyses. (3) Elements difficult to analyze were examined using several different methods, and methodology was revised to eliminate discrepancies. (4) Independent cross-checking of analyses by lab personnel eliminated personal bias. (5) Coordination between MSL and field geologists assured proper sampling and subsequent sample handling. (6) Cross-checks were made with various laboratories, using different techniques for analyzing control water samples (USGS), for accuracy and reproducibility of results. High accuracy can be demonstrated by comparing the analyses for Pleasant Bayou No. 2 (Appendix A) with those reported by Kharaka and others (1980). The error estimated by the cation-anion balance (Appendix A), which is generally less than 3 percent, also provides an internal check on the accuracy of the data.

Sources of Variability

The variability of salinity measurements can be partitioned according to (1) sampling and analytical differences, (2) dilution and contamination, and (3) in situ reservoir differences involving the physical and chemical environment as well as geological time. Multiple water samples from the same well (including Pleasant Bayou No. 2) that were analyzed by the same and different labs indicate that salinity variations of 10 percent or less are attributable to field collection and sample treatment techniques, laboratory methods, operator error, units of measurement, minor time dependent changes in brine composition at the wellhead, and the like. The second source of error, attributed to unrepresentative field data, is difficult to assess. Salinities determined from drill stem tests may be contaminated with mud filtrate, whereas water produced in association with hydrocarbons is subject to dilution by condensed water vapor or by downhole fluid treatments such as acidizing or hydraulic fracturing. In each of these cases, measured salinities could be much less than actual salinities. These sources of error are minimized by using analyses from wells having low gas to water ratios (<100 mcf/bbl) and considerable elapsed time since well completion or stimulation.

Another source of variability is the difference that results when log-derived salinities are compared with water analyses. Most studies of subsurface salinities in the Gulf Coast have been partly or completely based on electric log calculations using SP and R_{wa} measurements assuming sodium chloride water. Such log-derived salinities are tentative at best because they are subject to serious error, and a universally accepted method of calculation has not been identified. In the Red Fish Reef area, salinities are underestimated in the hydropressured zone and overestimated in the geopressured zone (fig. 2). Thus, salinity trends interpreted from log calculations are not always in agreement with those interpreted from water analyses.

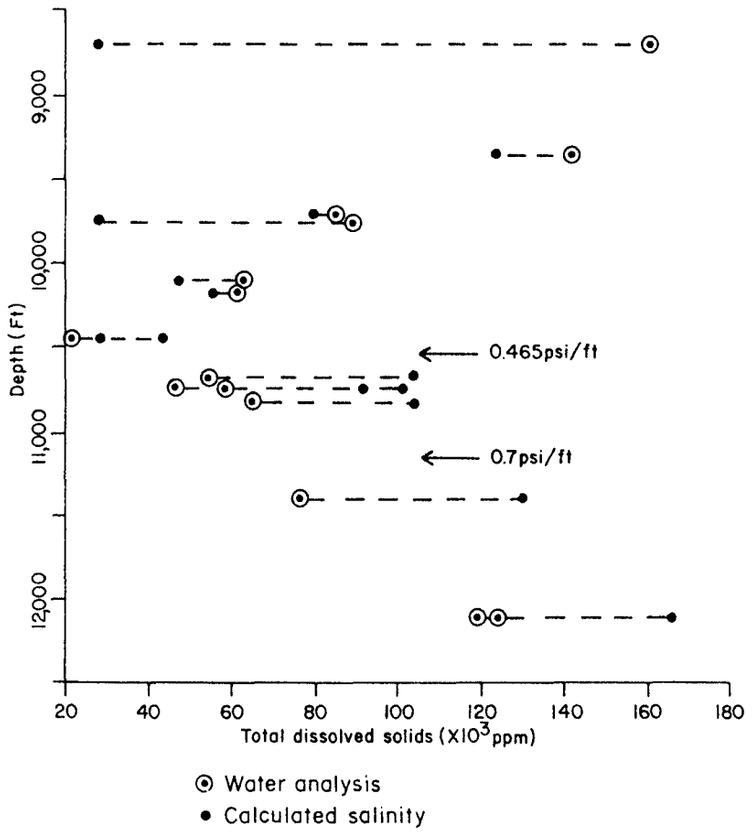

Figure 2. Plot of total dissolved solids versus depth for Red Fish Reef area.

FIELD STUDIES

Red Fish Reef Area

The Red Fish Reef area includes the Red Fish Reef and Red Fish Reef S.W. fields in Chambers County, Texas (fig. 1). Water analyses data from Red Fish Reef S.W. was provided by Sun Oil Company, and data from the Red Fish Reef field was provided by Exxon Corporation. The Sun data are from State tracts 288 and 307. The Exxon data are from State tracts 225 and 246, about 3 mi to the north. Water analyses from the two Exxon wells (Appendix A), have similar concentrations of total dissolved solids when compared to earlier analyses provided by Exxon Corporation of the same wells.

Water analyses are from sandstone reservoirs within the Frio Formation, which is defined as the sandstone-rich sequence underlying the Anahuac Shale. The top of the Frio is commonly picked by the Heterostegina marginulina zone. In the Red Fish Reef area, the top of the Frio occurs at a depth of about 8,700 ft.

Structure

The structure of the area is uncomplicated. Both the Red Fish Reef and the Red Fish Reef S.W. fields are in one major strike-aligned fault block on the downdip side of a large growth fault. Only minor faults with less than 100 ft of displacement cut the wells themselves. Each field is on an anticline oriented east-west or parallel to the major growth fault trend.

Stratigraphic Relationships

Wells in the area penetrate the upper and middle Frio sediments and part of the lower Frio sediments as delineated by Galloway and others (in press). The base of the Frio is reached at a depth of over 15,000 ft in the area (Stout,

1961) but is not reached by wells sampled in this study (Appendix A). Sand packages are easily correlated and are consistent across the entire area.

Electric log (SP) patterns of the sand bodies in the area are of two types. In the upper Frio and lower Frio, SP patterns are blocky and range from 50 to 150 ft thick. Sandstone packages are laterally continuous in the strike direction, but they thin in both updip and downdip directions. Sand-to-shale ratios range from 30 to 40 percent. The sands of the middle Frio, however, are thinner (10 to 50 ft) and not as blocky. Shale breaks between the sand beds are 50 to 150 ft thick, and sand/shale percentages are 10 to 20 percent. Minor faulting occurs within this middle Frio sequence.

At the time of deposition of the Frio Formation, the upper Texas coast was dominated by the Houston Delta system situated in the Houston Embayment (Galloway and others, in press). Sediments were supplied from several different points along the coast into a basin structurally complicated by salt diapirism. There was constant switching of delta lobes accompanied by destructional marine reworking and inundation of abandoned sites (Galloway and others, in press).

The Red Fish Reef area was always on the fringe of the main deltaic deposition and along strike or distal to the main delta lobes. The blocky, strike-oriented sandstones of the upper and lower Frio Formation resemble strandplain facies deposited in a broad interdeltaic area, whereas the thinner sands of the middle Frio with serrated SP patterns resemble distal delta-front sediments. Some of the thinner sandstone beds probably represent storm-generated deposits.

Geochemical Trends

In the Red Fish Reef area, salinity data (total dissolved solids) are available from depths of about 9,000 ft in the middle Frio to depths of over 12,000 ft in the lower Frio (fig. 2). Values of total dissolved solids range from 20,000 to 160,000 mg/L. Total dissolved solids decrease with depth in the

normal pressure zone (fig. 2) but increase with depth through the transition zone of intermediate pressure gradients (0.465 to 0.7 psi/ft). Calcium concentrations follow a similar trend of decrease then increase with depth, and the point of inflection again coincides with the top of abnormal pressure. The chloride to sodium ratio, however, is uniform with depth and remains at about 1.65 over the entire depth interval.

Chocolate Bayou Area

Structure

The overall structure of the Chocolate Bayou field area (figs. 1 and 3) is represented by a large, low-relief anticline with associated smaller closures bounded by several major and minor contemporaneous growth faults. Axial diameter of the large anticline is about 8 mi in a northwest-southeast direction. The smaller closures developed in the updip part of the area form shallower producing fields, such as West Chocolate Bayou and Rowan fields (figs. 1 and 3). The Rowan field marks the updip limit of the regional Frio depocenters, which were associated with growth faults and domal structures within a salt-withdrawal basin. Downdip of the East Chocolate Bayou field, Halls Bayou field occurs in the downthrown block of a major growth fault that also separates the Chocolate Bayou anticline from the Alta Loma field in the eastern part of the area (fig. 3).

The top of the Frio Formation is displaced from 500 ft in the updip fields to more than 1,000 ft in the downdip fields (fig. 4). Generally displacement in the same fault zone increases with depth because of rollover into the fault. Maximum displacement is more than 3,000 ft in the lower unit (T5 marker) between East Chocolate Bayou and Halls Bayou fields.

The increased number of growth faults with depth complicates the structure of deeper units, and rollover and subsequent thickening of the stratigraphic

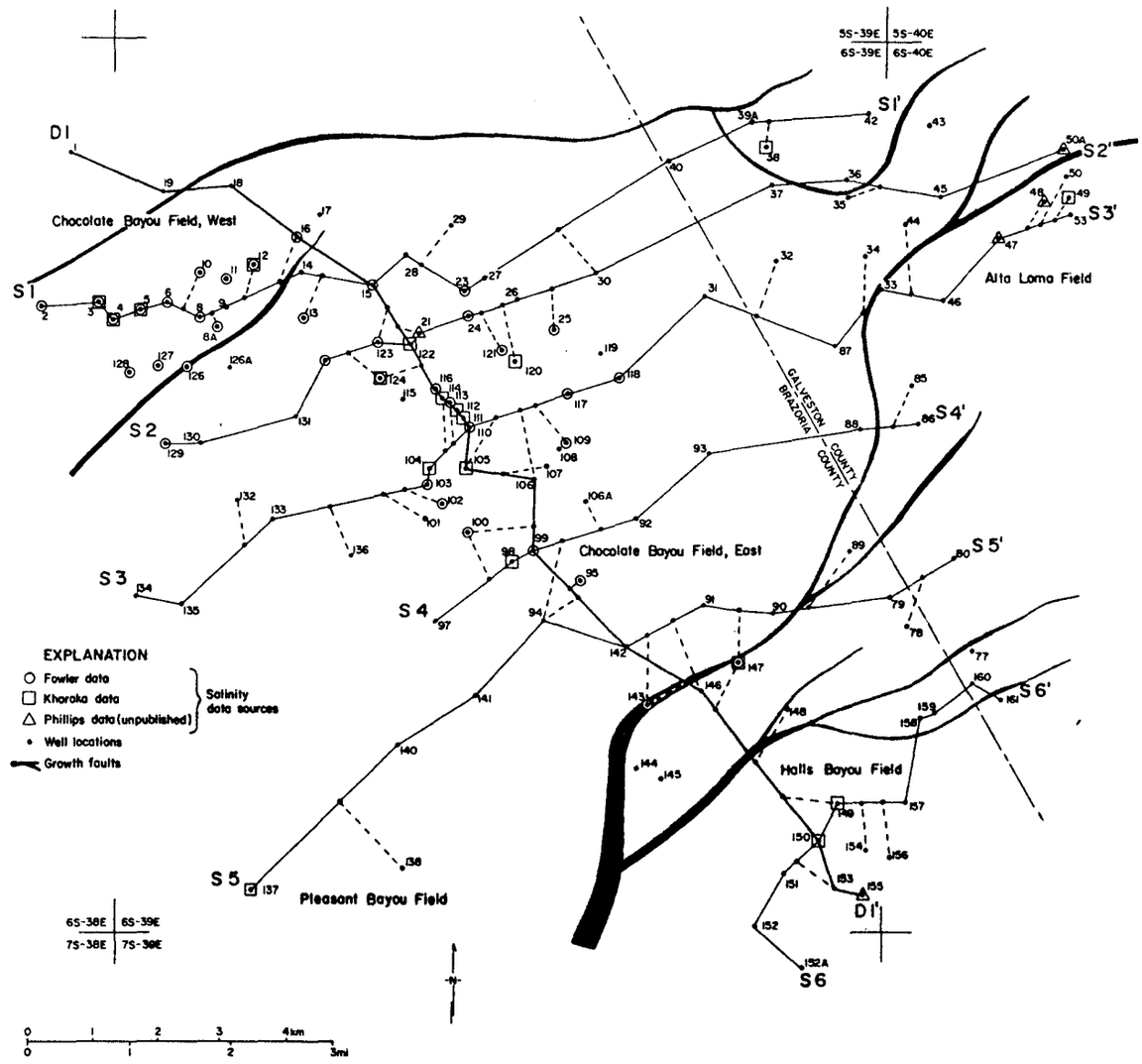

Figure 3. Location map of wells, cross sections, and sources of salinity data in the Chocolate Bayou field area. Dotted lines represent projections of wells onto cross-section lines.

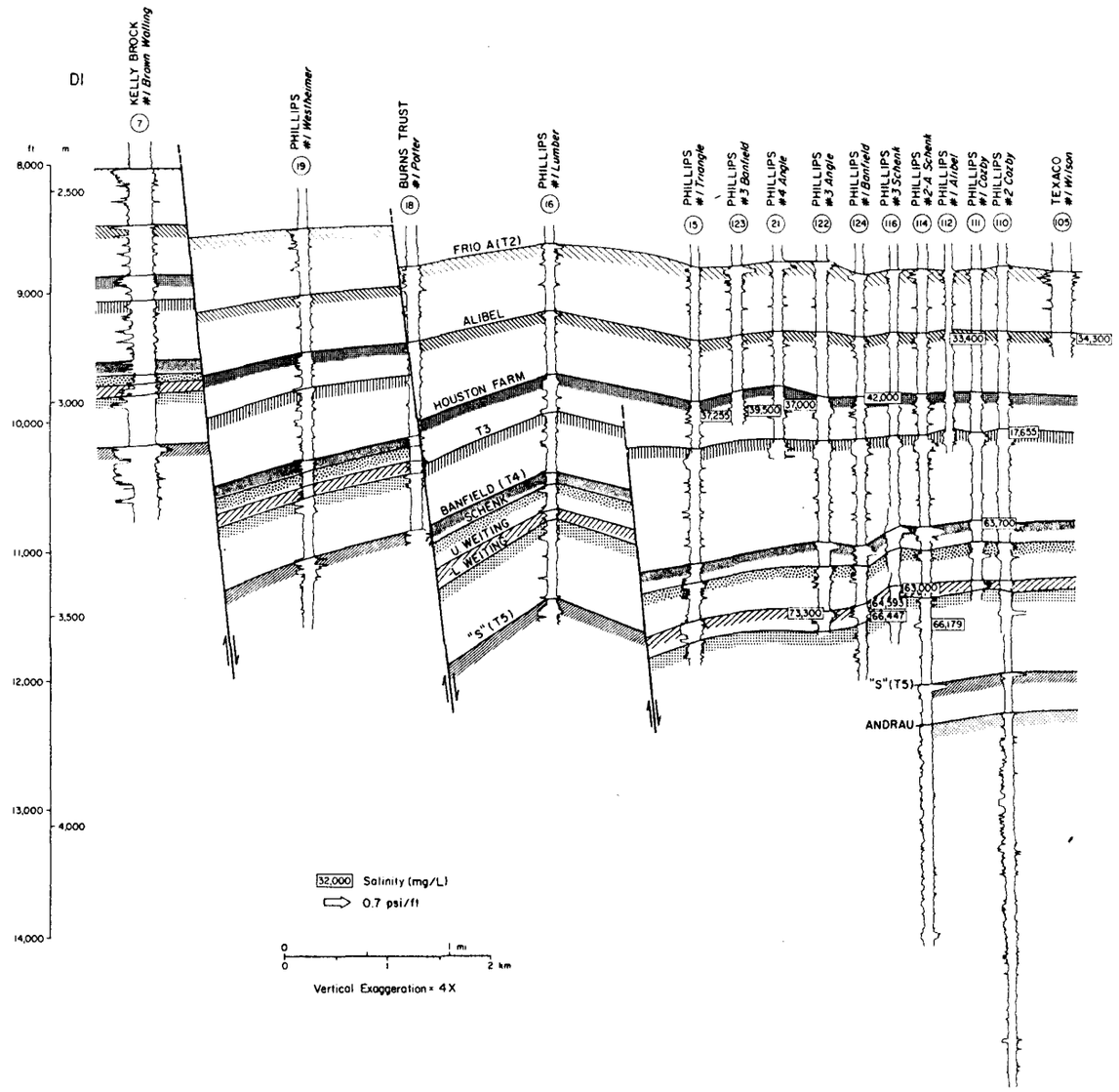

Figure 4. Structural dip cross section, Chocolate Bayou field. Section line shown in figure 3.

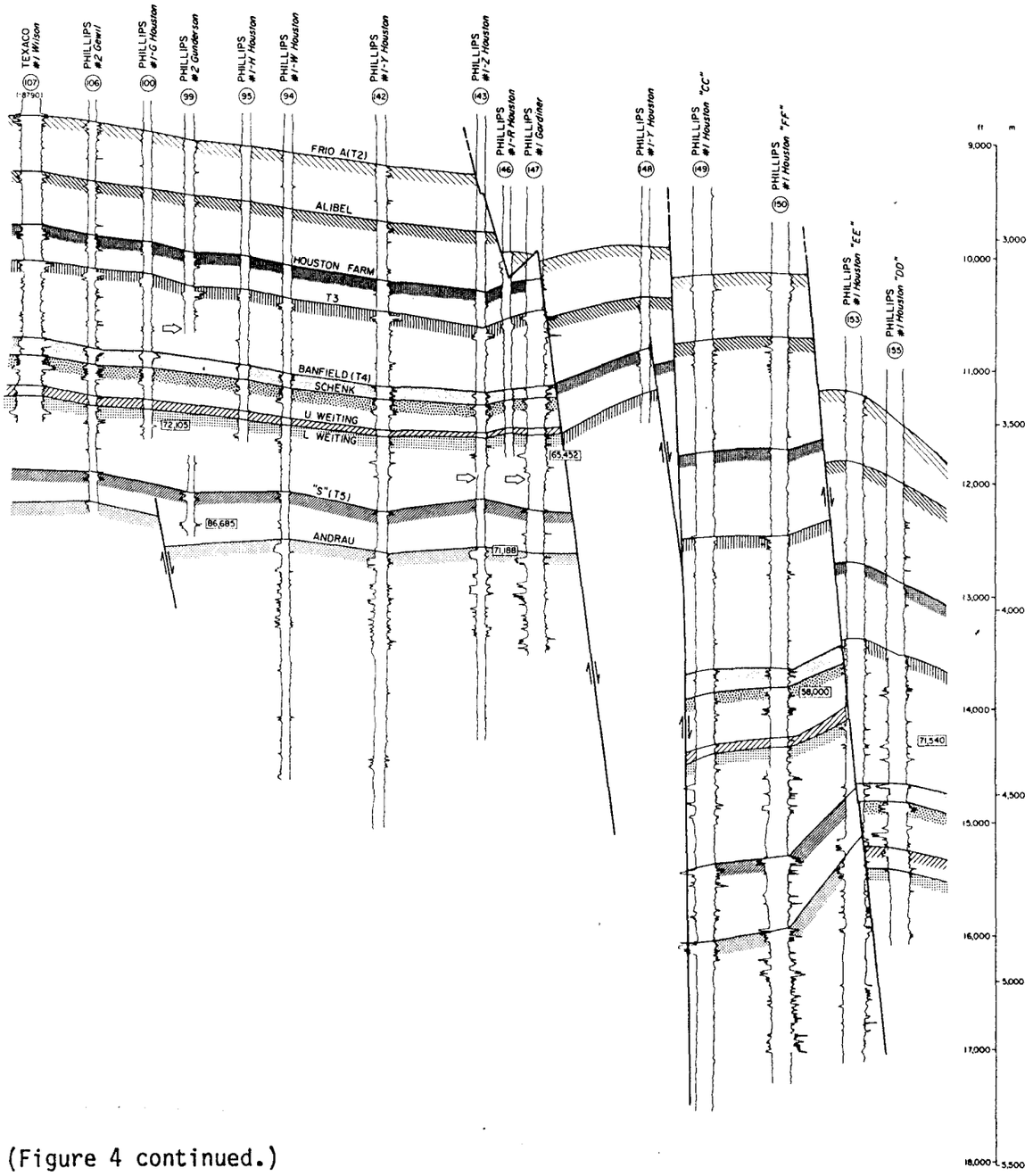

(Figure 4 continued.)

units near the faults become more significant in the deeper downthrown side of the Halls Bayou field.

Origin of the Chocolate Bayou anticline is not well understood. Bebout and others (1978) reported that the structural setting of the Chocolate Bayou area was controlled by the rapid deposition of large volumes of sediments, the loading of which resulted in subsidence accompanied by salt withdrawal into nearby salt domes. Neither regional rollover near growth faults nor direct upward movement of salt affected the development of the large anticline in the Chocolate Bayou field. As shown in a stratigraphic section (fig. 5), this anticline apparently formed as a result of differential subsidence contemporaneous with Frio deposition. The greatest subsidence occurred along the flanks of the developing folds, while the least subsidence was associated with the fold axis.

Stratigraphic Relationships

The Frio Formation of the Chocolate Bayou field area has been interpreted as thick progradational deltaic deposits. To facilitate interpretation, the interval was subdivided into several stratigraphic units, which closely correspond to micro-paleontological markers (T markers) established by Bebout and others (1978). Each stratigraphic subdivision consists of several genetic units that can be correlated with individual sandstone beds.

Alternating sequences of sandstone and shale having maximum thicknesses of 100 ft underlie the Andrau sandstone (fig. 4). However, these thick sandstones are not differentiated in terms of genetic significance. Overall depositional style in this area is characterized by repetitive accumulations of progradational deltaic lobes and expansion of stratigraphic units resulting from differential subsidence and a number of contemporaneous growth faults.

The distribution of sandstone in the Frio Formation (fig. 4) shows that the rate of subsidence commonly exceeded the rate of progradation, especially on the

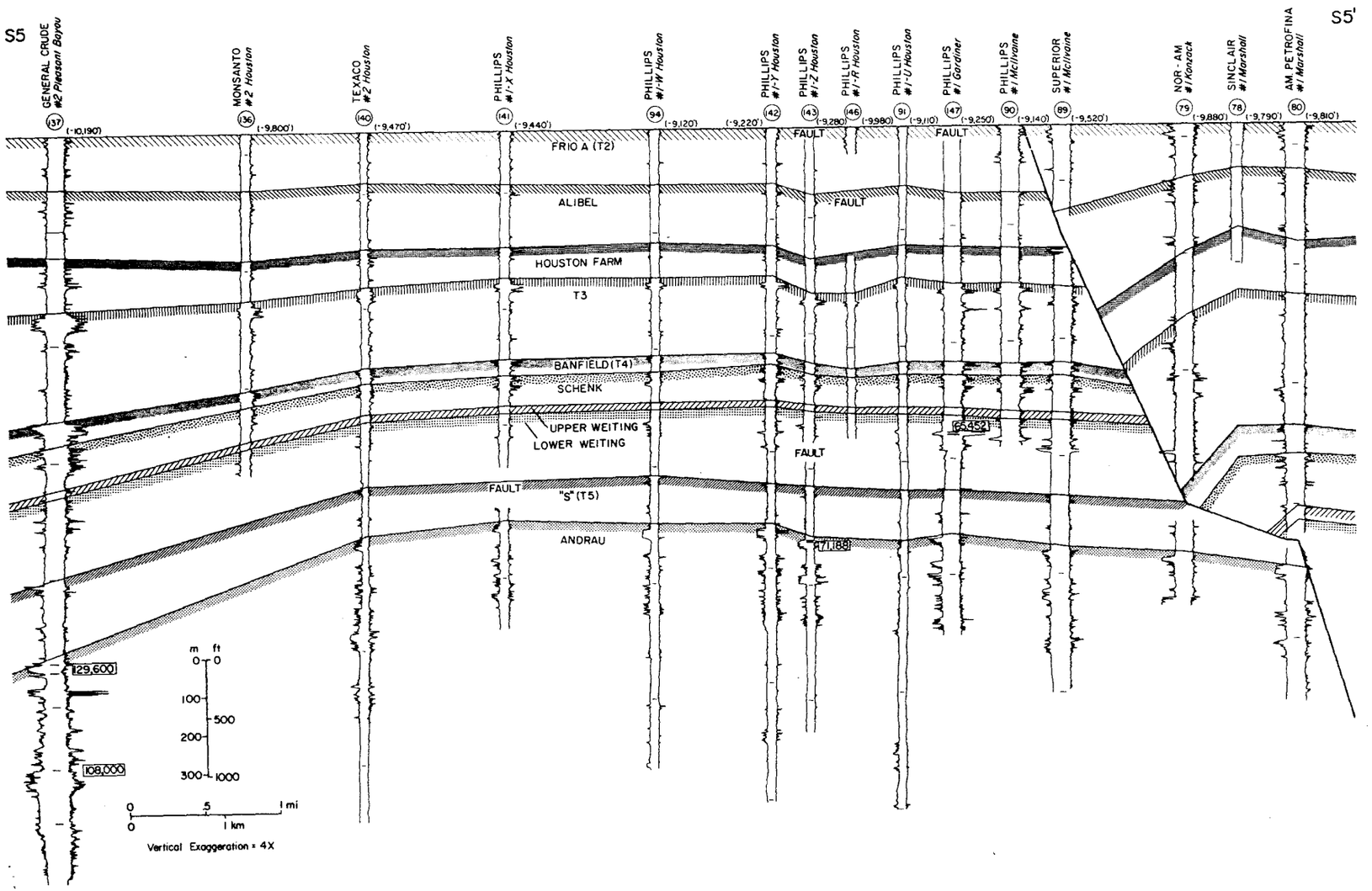

Figure 5. Stratigraphic strikè cross section, Chocolate Bayou field. Section line shown in figure 3.

downthrown side of major growth faults. In the lower Frio Formation, below the Banfield (T4) sand (figs. 4, 5, and 6), a major depocenter was developed on the flank of a salt-withdrawal syncline that was encountered in the Pleasant Bayou No. 2 test well (fig. 5). Uniform thickening of the discrete stratigraphic intervals in the well was recognized by detailed correlation with nearby wells. As subsidence decreased after Banfield (T4) time, major depocenters shifted to the northeastern part of the Chocolate Bayou field. Geometries of each genetic sandstone in the Chocolate Bayou field show lobate-arcuate morphologies, which suggest the Frio Formation of Chocolate Bayou field was deposited by river-dominated deltas. Interpretations of core descriptions (Morton and others, 1981) suggest that a variety of deltaic depositional settings are represented including shoreface, distributary-mouth bar, distributary channel, subaerial levee, and interdistributary subenvironments.

The Frio A sandstone (figs. 4, 7, and 8), the uppermost sandstone unit of the Frio Formation, exhibits one depositional axis parallel to depositional strike and another dip-oriented depositional axis trending northwest-southeast that passes through the middle part of the structural high of the Chocolate Bayou field (fig. 8). This dip- oriented axis is considered to be a distributary channel of the arcuate-cuspate delta that developed during late Frio time.

Upper Weiting (figs. 9 and 10) and "S" sandstones in the lower Frio are laterally persistent (figs. 5 and 6) and become thinner and pinch out basinward in this area. However, net-sandstone maps show broad, lobate distributary patterns. Accordingly, these sandstones are assumed to be distal delta-front facies.

Changes of depositional direction and associated depocenters can be determined from net-sandstone maps of different stratigraphic horizons (figs. 8 and 10). Sandstone distributary patterns may be influenced by shifts of distributary channels and subsequent delta abandonment during deposition in this area.

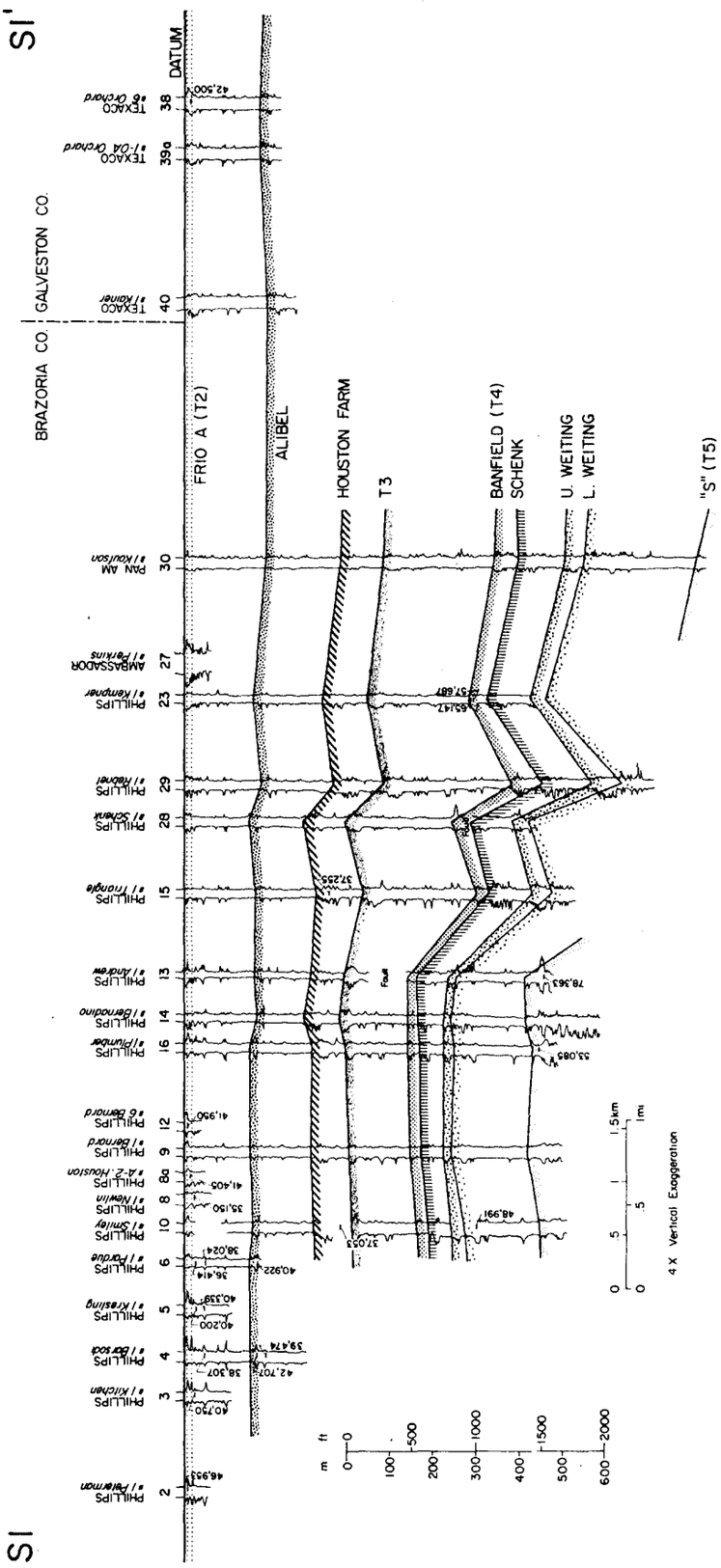

Figure 6. Stratigraphic strike cross section, Chocolate Bayou field. Section line shown in figure 3.

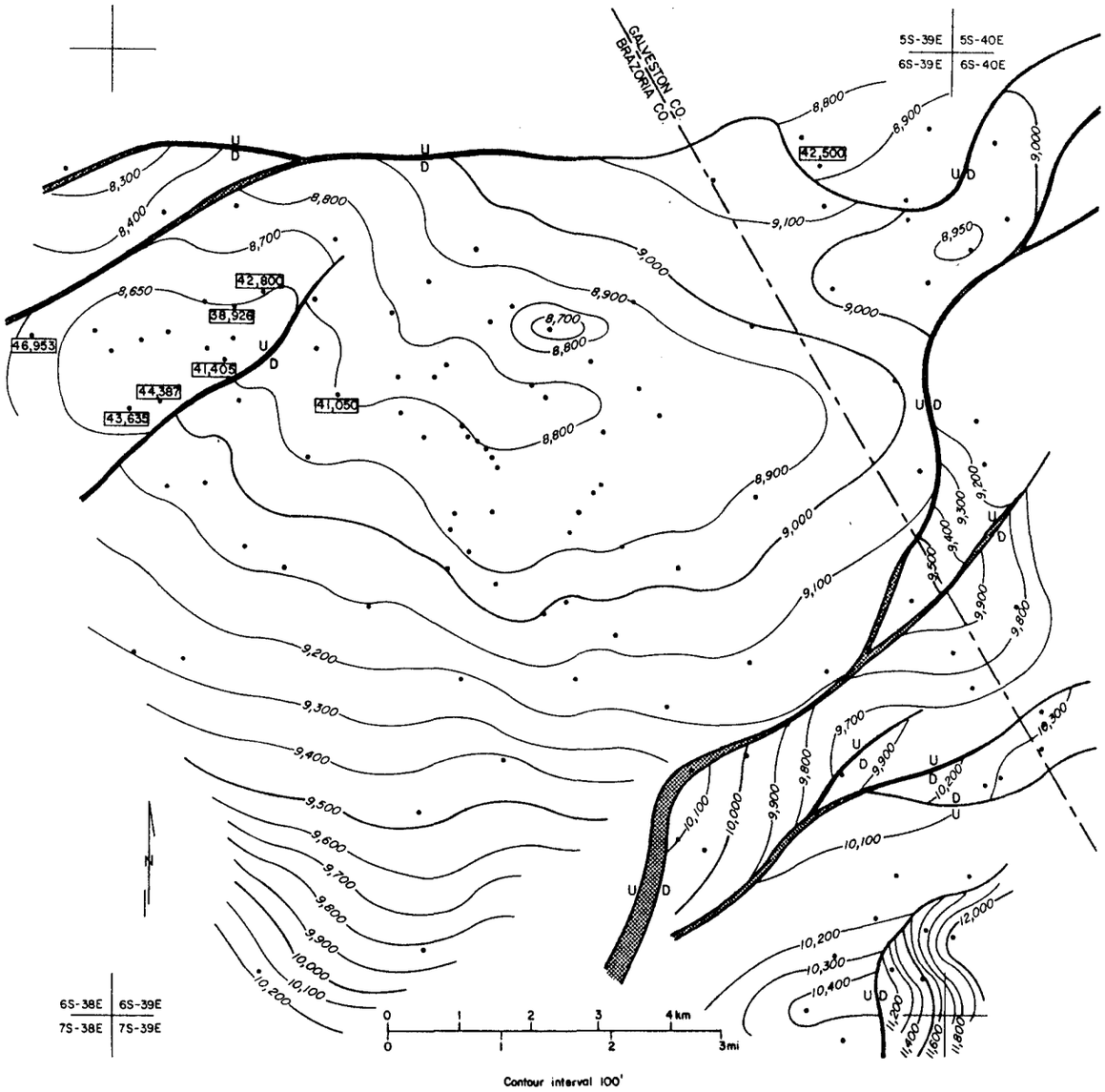

Figure 7. Structure map of the top of Frio A sandstone. Salinity data are mainly from West Chocolate Bayou field.

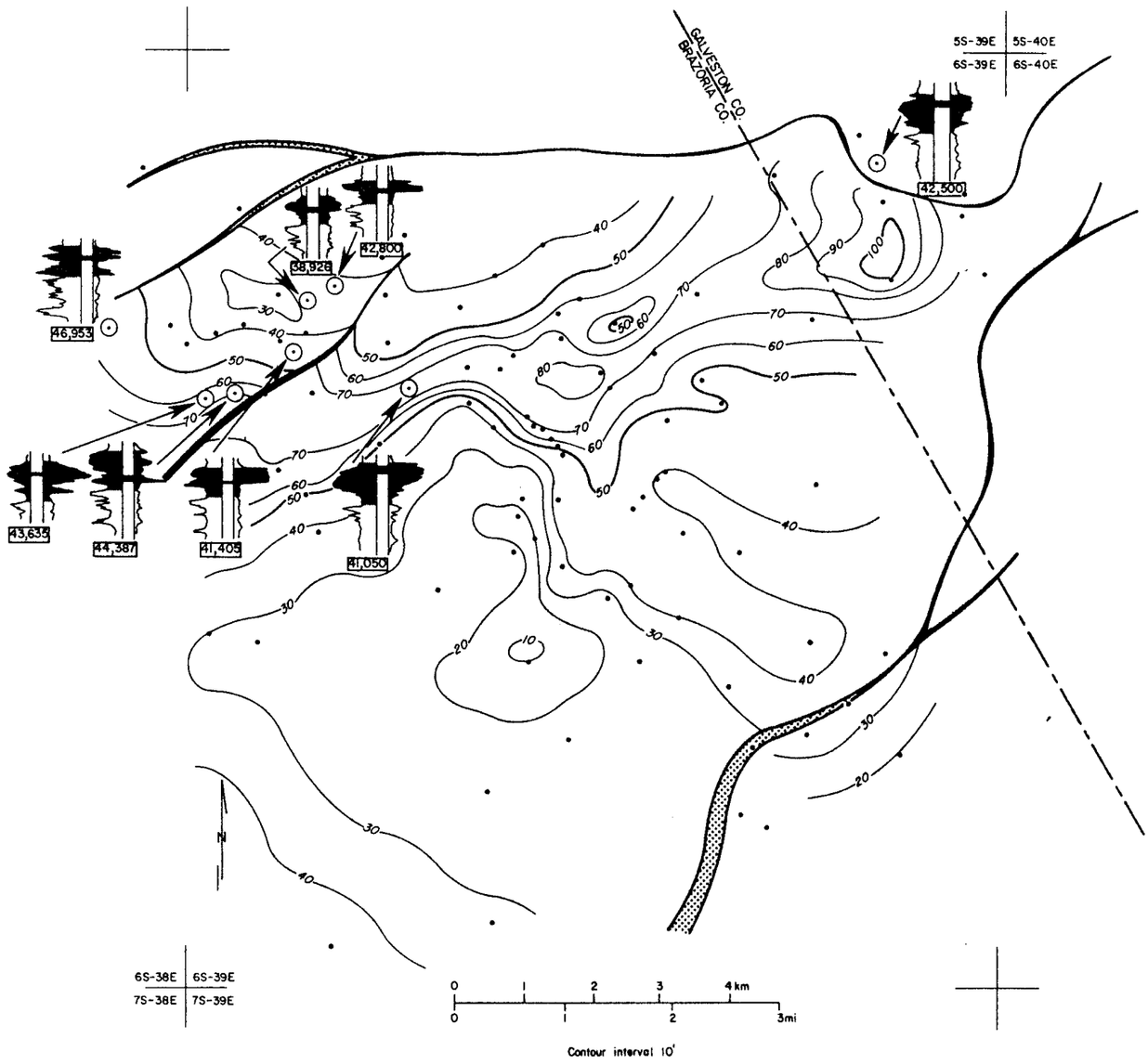

Figure 8. Isopachous map of Frio A sandstone. Shaded log sections and numbers in boxes below indicate thicknesses of the sandstones and salinity values, respectively.

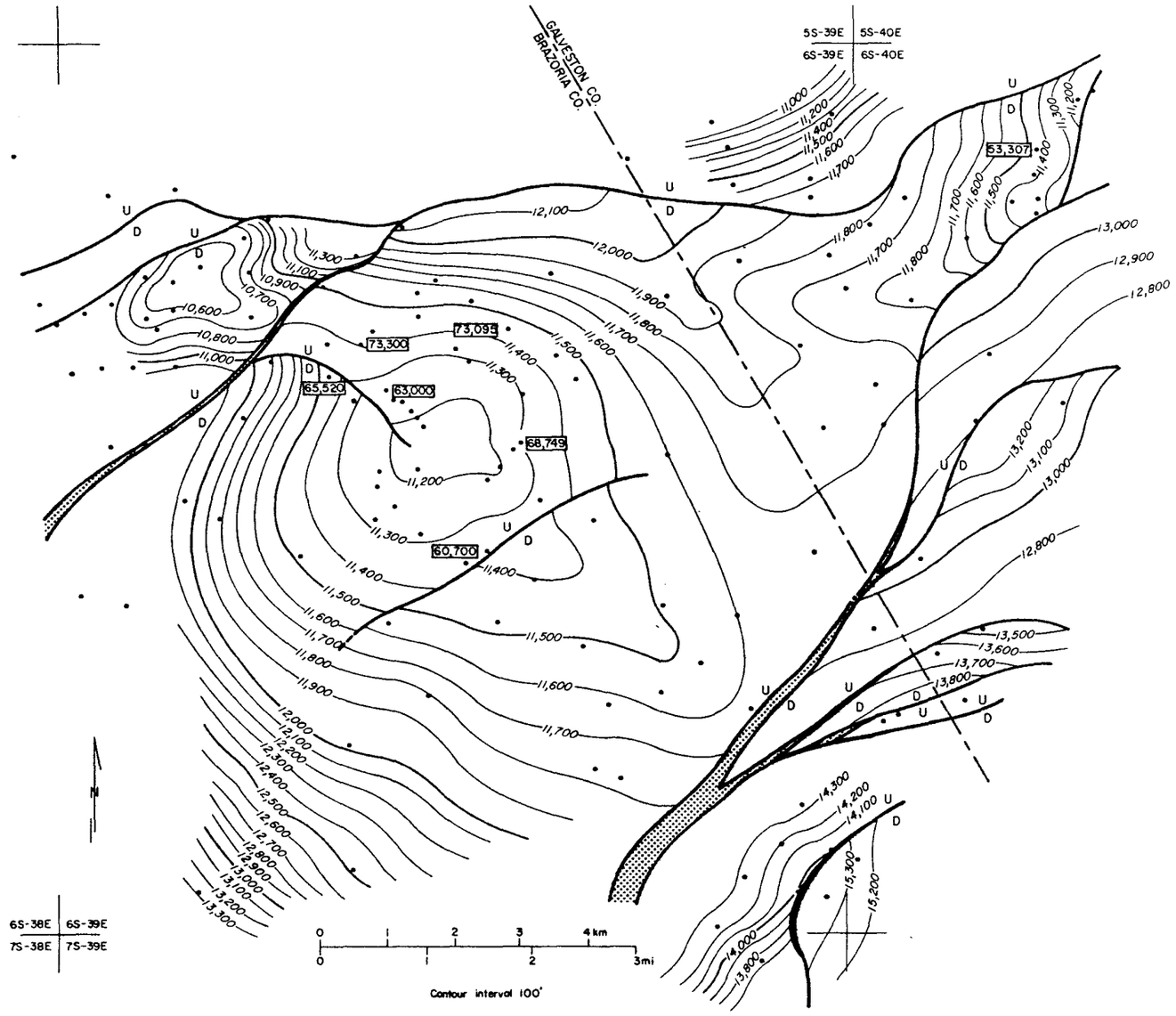

Figure 9. Structure map of top of the Upper Weiting sandstone. Numbers in boxes represent salinity values.

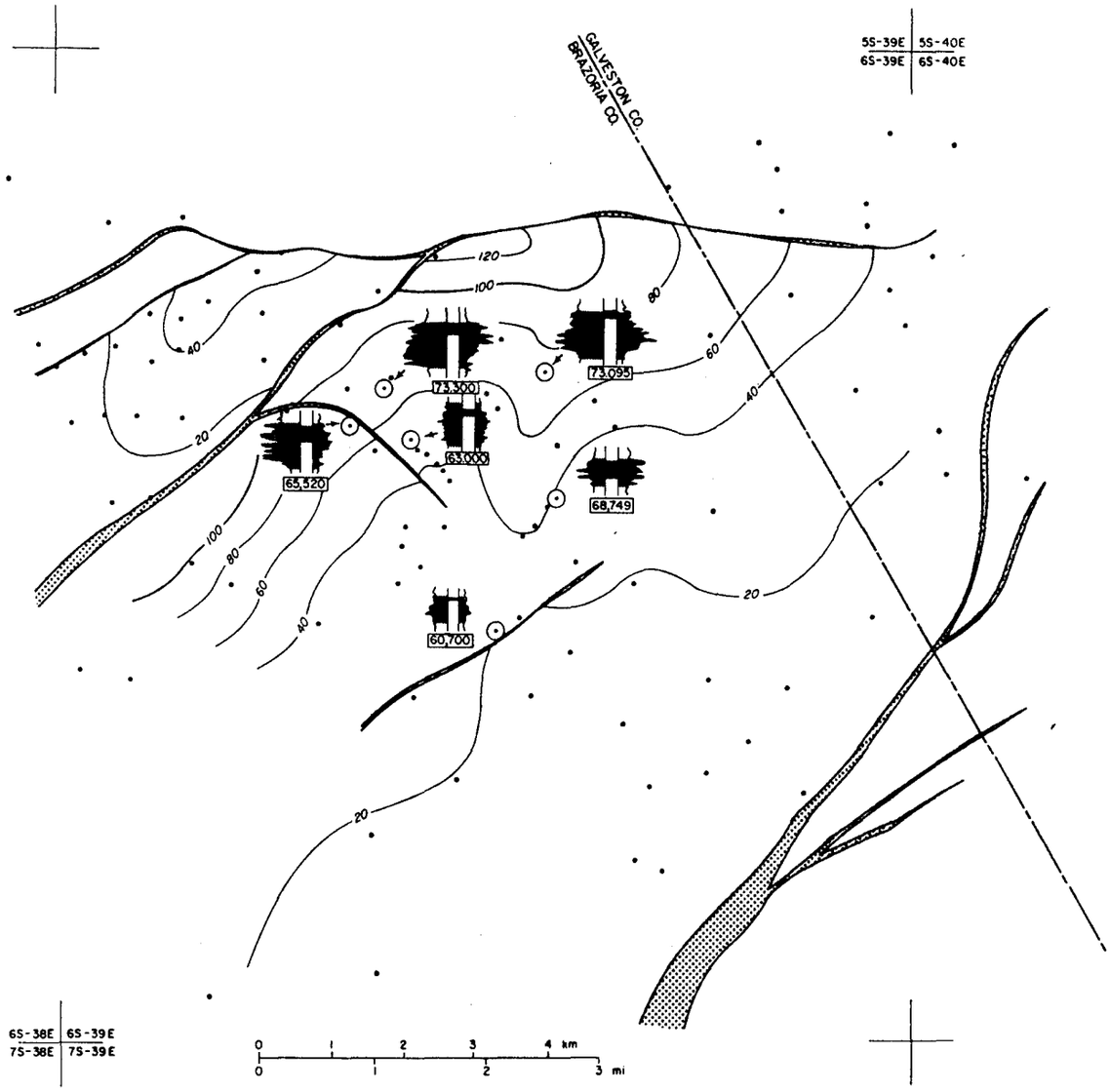

Figure 10. Isopachous map of Upper Weiting sandstone showing log sections and salinities of the unit.

Geochemical Trends

Vertical variations in salinity between reservoirs appear to be more significant than lateral variations within the same reservoir. As reported by Fowler (1970) significant changes in salinity distribution cannot be anticipated in single aquifer sandstone units that were formed during specific stratigraphic time intervals. This relative uniformity in salinity is also true where the aquifer is separated by small growth faults as illustrated in the Frio A sandstone (fig. 7) in East and West Chocolate Bayou fields. The Frio A sandstone was deposited across a tear fault with 400 ft of maximum displacement.

In the Chocolate Bayou field, salinity values seem to decrease slightly with depth in the transition zone near the base of normally pressured sediments (fig. 11). The transition zone, which ranges in depth from approximately 8,000 ft to 10,000 ft subsea, has a pressure gradient of about 0.46 psi/ft and a thermal gradient of about 1.20°F/100 ft in this area. The lowest salinity value, about 12,000 mg/L, is found in the T3 sandstone (fig. 4), which corresponds to the boundary between normally pressured and geopressured sediments (fig. 11). The T3 sandstone is characterized by facies that change from thick, blocky, and massive sandstones in updip areas to thin sandstones with serrate log patterns in downdip areas (fig. 4); the sandstone has good lateral continuity (fig. 5) throughout the Chocolate Bayou field area.

Kharaka and others (1977) reported that salinities in the geopressured zone are higher than those in the normally pressured zone, and this is substantiated by available data that show a gradual increase with depth down to 14,500 ft (fig. 11). This zone is characterized by an abnormally high thermal gradient of 2.33°F/100 ft (Gregory and Backus, 1980) and intermediate pressure gradients between 0.465 and 0.75 psi/ft. Water with the highest salinity (129,000 mg/L) is produced from the Andrau sandstone (Pleasant Bayou No. 2, Appendix A) of the

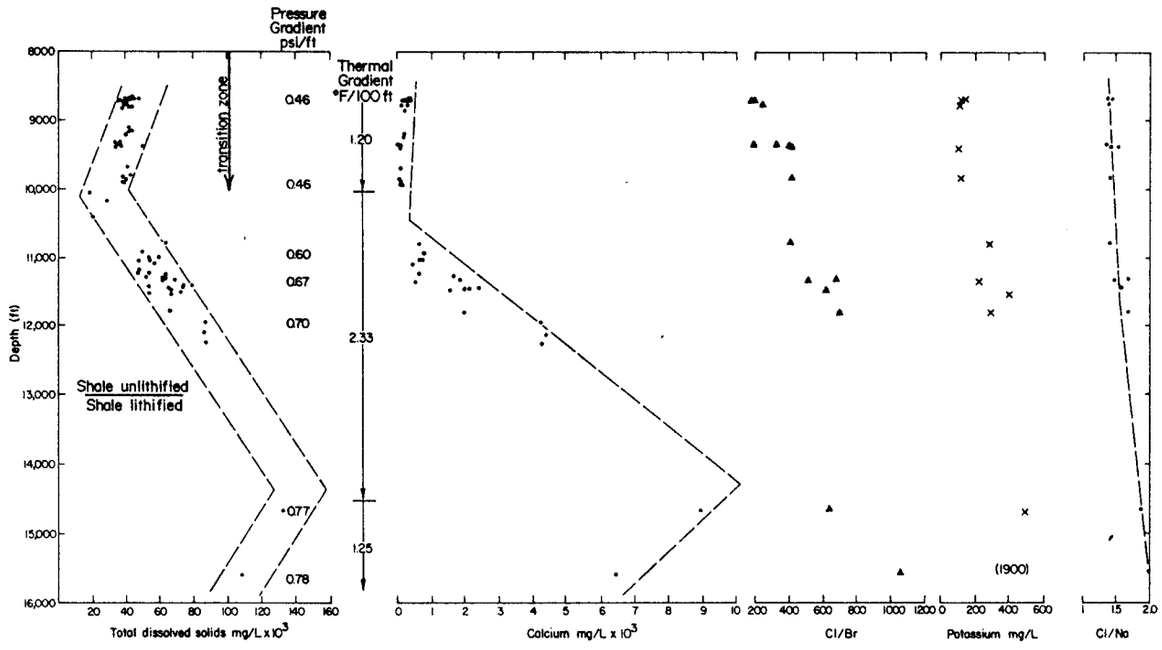

Figure 11. Concentrations of total dissolved solids and major cations and ion ratios in the Frio Formation, Chocolate Bayou field. Chemical data from unpublished files, Phillips Petroleum Co., Kharaka and others (1977, 1980), and Appendix A; thermal gradients from Gregory and Backus (1980).

Pleasant Bayou field area. Milliken and others (1981) designated this zone as a major zone of diagenesis and reported that nearly 90 percent of the smectite-illite transition, albitization, and carbonate precipitation were completed at the base of the zone. Below about 14,500 ft, a decrease in salinity with depth corresponds with a lower thermal gradient of 1.25°F/100 ft and higher pressure gradients varying from 0.77 to 0.93 psi/ft.

The top of the deep decreasing salinity trend correlates with the Andrau interval composed of several thick alternating sandstone and shale sequences, which formed the largest depocenter of the Frio Formation during early Frio time. This interval has a high sandstone percent (maximum 52 percent), which is greater than any other overlying stratigraphic horizon (e.g. T5-30 percent, T3-24 percent, and T2-22 percent).

The direct relationship between salinity variations and individual sandstone thickness seems to be minor if it is important at all. For example, only minor lateral changes of salinity occur in the same reservoir in the Upper Weiting sandstone of the lower Frio Formation (fig. 10). The thicker part of the sandstone in the updip area contains water with slightly higher salinities than does the thinner, basinward part of the sand. The salinity gradually decreases from 73,300 to 60,700 mg/L.

Salinity trends occur at different depths in the Alta Loma and Halls Bayou fields compared with the Chocolate Bayou field. In the Alta Loma and Halls Bayou fields, the Frio sediments are deeply buried on the downthrown side of a major growth fault.

Salinities in the shallower section of the Alta Loma field increase with depth in a trend similar to that of the Chocolate Bayou field; however, salinities abruptly decrease with depth below 12,000 ft. The upper zone of increasing salinities corresponds to intermediate pressure gradients, whereas the lower

zone has distinctively higher pressure gradients of 0.79 and 0.85 psi/ft. The decreasing trend in salinities is continuous down to 15,000 ft, and the freshest formation water measured is 21,125 mg/L at a depth of 14,500 ft in the middle of the Alta Loma field.

Variations in calcium and sodium concentrations with depth closely correspond to those of total dissolved solids (fig. 11); however, calcium increases with depth at a greater rate than does sodium. In contrast, potassium concentrations gradually increase with depth below 8,000 ft (100 to 1,900 mg/L), possibly indicating that reactions involving potassium are not as sensitive to pressure and temperature gradients as are those involving calcium and sodium. The chloride to bromide ratio also gradually increases with depth (390 to 910), whereas the chloride to sodium ratio is fairly uniform (1.5) in the hydropressure zone but shows a slight increase with depth in the geopressure zone (fig. 11).

Corpus Christi Area

The Corpus Christi study area extends from eastern Nueces County across Nueces Bay and into eastern San Patricio County (fig. 1). Oil and gas fields in the area from which salinity data were used include Corpus Christi, Nueces Bay, East White Point, Portland, Gregory, Midway, Geronimo, Harvey Deep, Encinal Channel, and Corpus Channel (fig. 12). The area extends approximately 24 mi in the strike direction and 15 mi in the dip direction. Reservoir sandstones in this area are primarily of the Frio Formation, which increases in thickness from 3,000 ft in the western portion of the area to more than 8,000 ft in the eastern portion (fig. 13); it also thickens in a regional dip direction to more than 9,000 ft in the Encinal Channel and Corpus Channel fields (fig. 14). The top of the Frio Formation varies in depth in the strike direction from approximately 4,700 ft in the Corpus Christi field to 5,200 ft in the Harvey Deep field and in

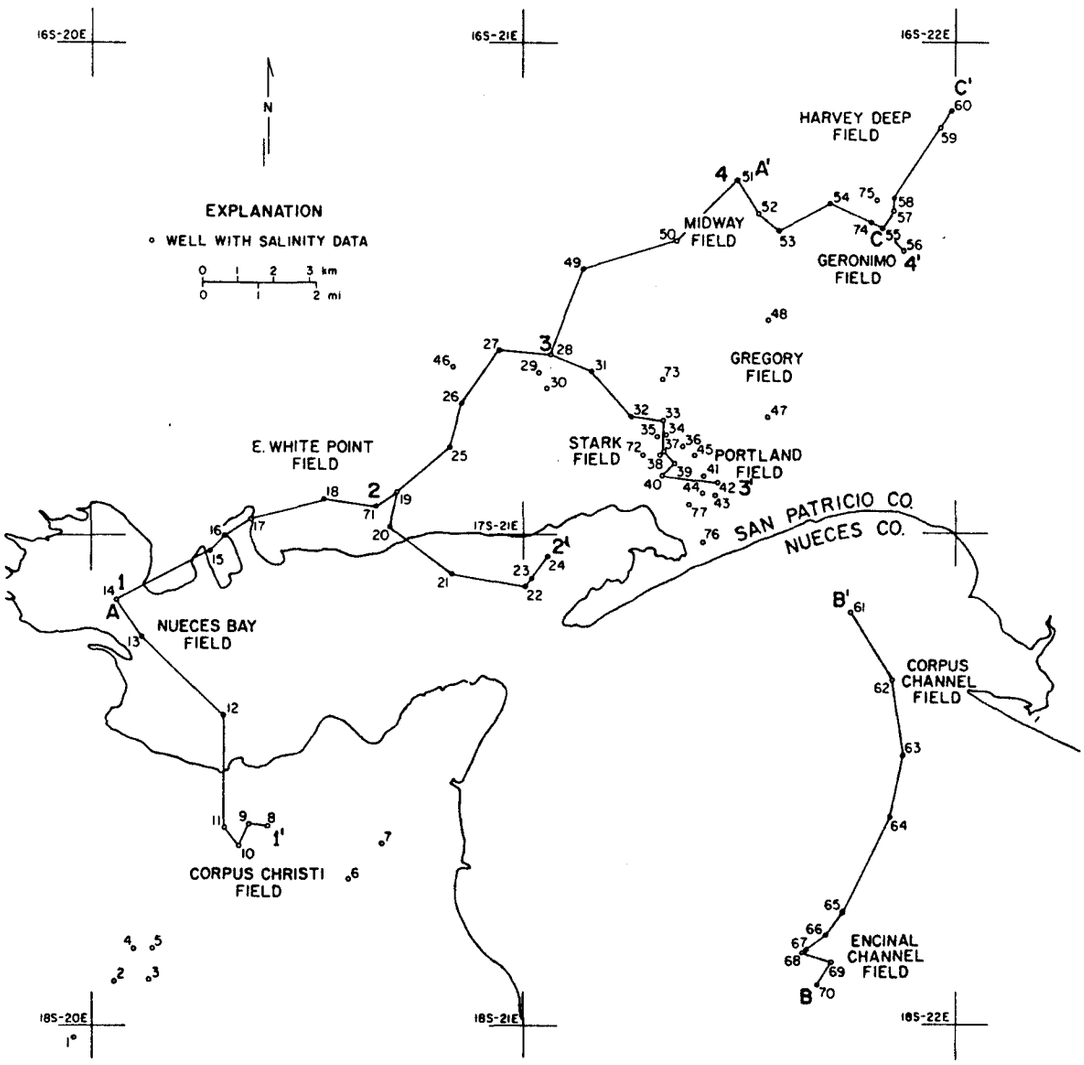

Figure 12. Location of wells with salinity analyses and lines of section, Corpus Christi area.

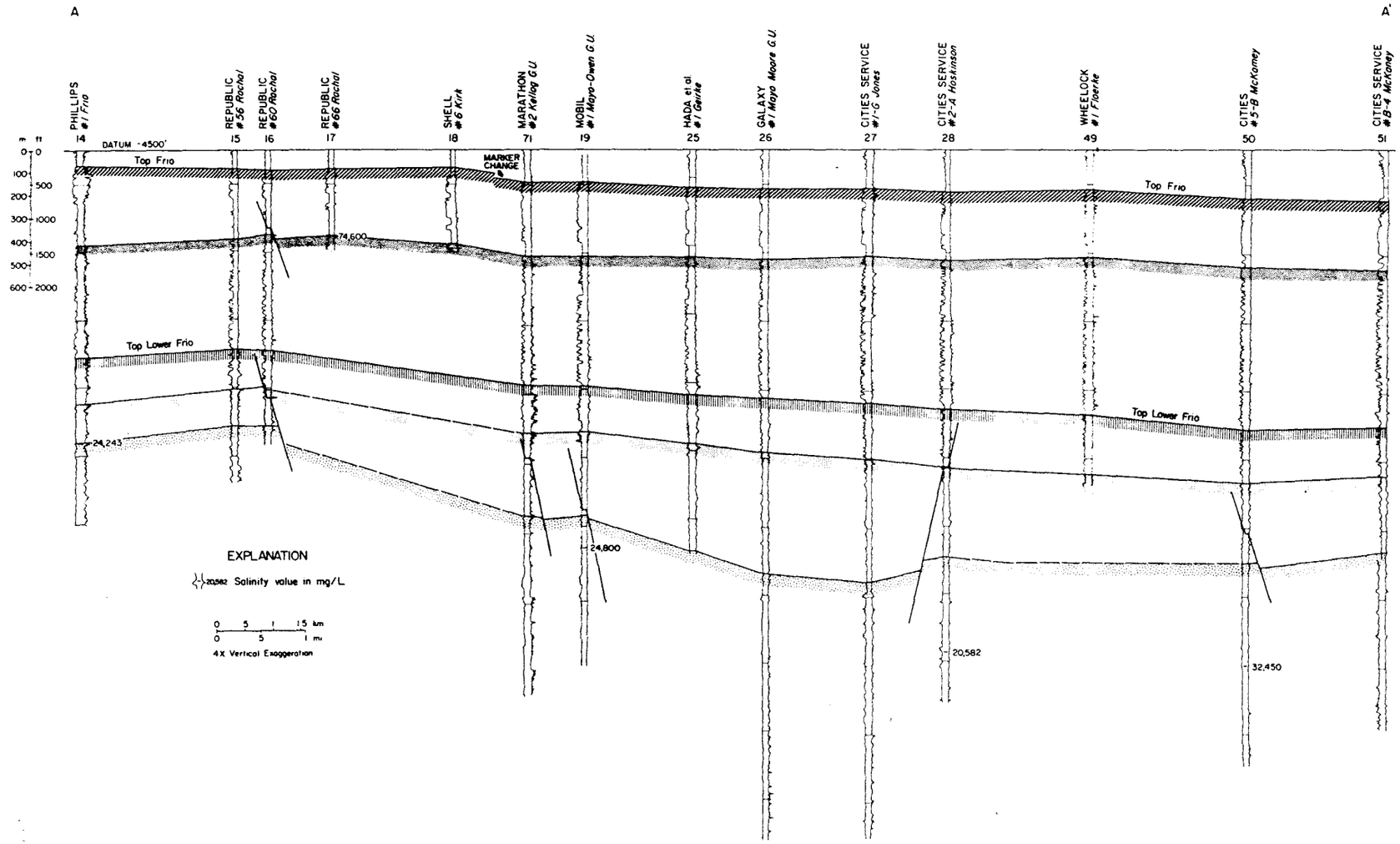

Figure 13. Structural strike section A-A' through Corpus Christi area.

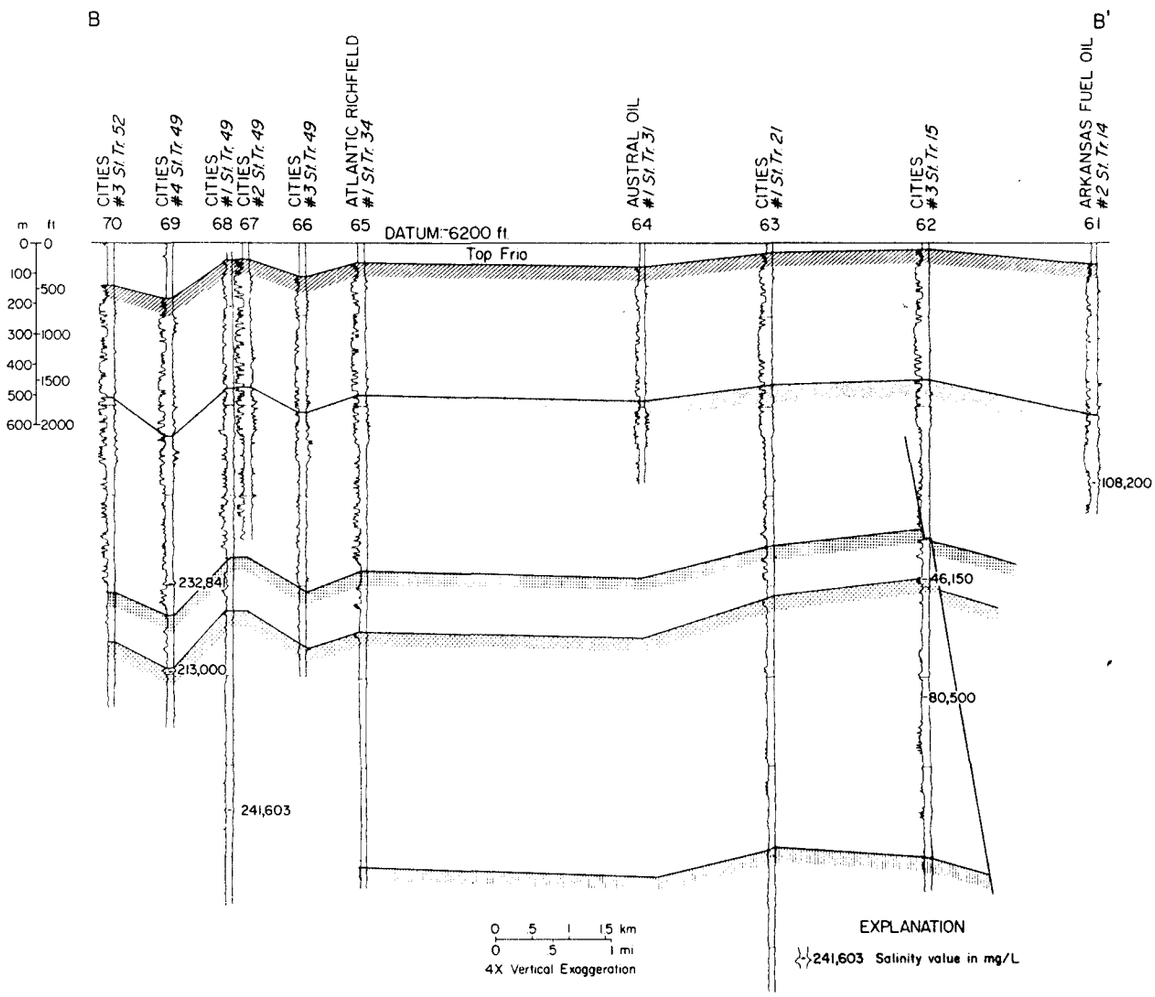

Figure 14. Structural strike section B-B' through Corpus Christi area.

the dip direction to 6,400 ft in the Encinal Channel field. The top of the Frio is picked near the Heterostegina marginulina foraminifera zone underlying the Anahuac Shale.

Structure

Large faults with displacements of 150 ft or more at a depth of 8,000 ft divide the area into major strike-aligned fault blocks (figs. 15 and 16), which extend in the dip direction for less than 5 mi and in the strike direction for tens of miles. Minor, closely spaced faults with displacements of less than 100 ft subdivide major blocks into compartments commonly as small as 0.5 mi^2 in area (fig. 16). Because of the numerous faults, structure in the area is complicated and correlations even within fields are often difficult.

The large growth fault that separates the Encinal Channel and Corpus Channel fields from the rest of the Corpus Christi area (fig. 16) divides the study area respectively into the channel and the onshore areas. Displacement along this fault is as much as 2,000 ft in the lower Frio, and correlation markers used in the onshore cross sections could not accurately be carried across the fault.

For this report three structural strike sections and four structural dip sections were constructed (fig. 12), although only three sections are included. Correlation markers for the onshore area are from Weise and others (1980). Correlation markers for the channel area were taken from type logs of the area.

Stratigraphic Relationships

Earlier studies of the Frio Formation describe the area as a coastal environment but disagree as to whether it was a deltaic (Martin, 1969) or barrier coastline (Boyd and Dyer, 1964) setting. Galloway and others (in press) suggest that deposition occurred within the Greta/Carancahua barrier/strandplain system

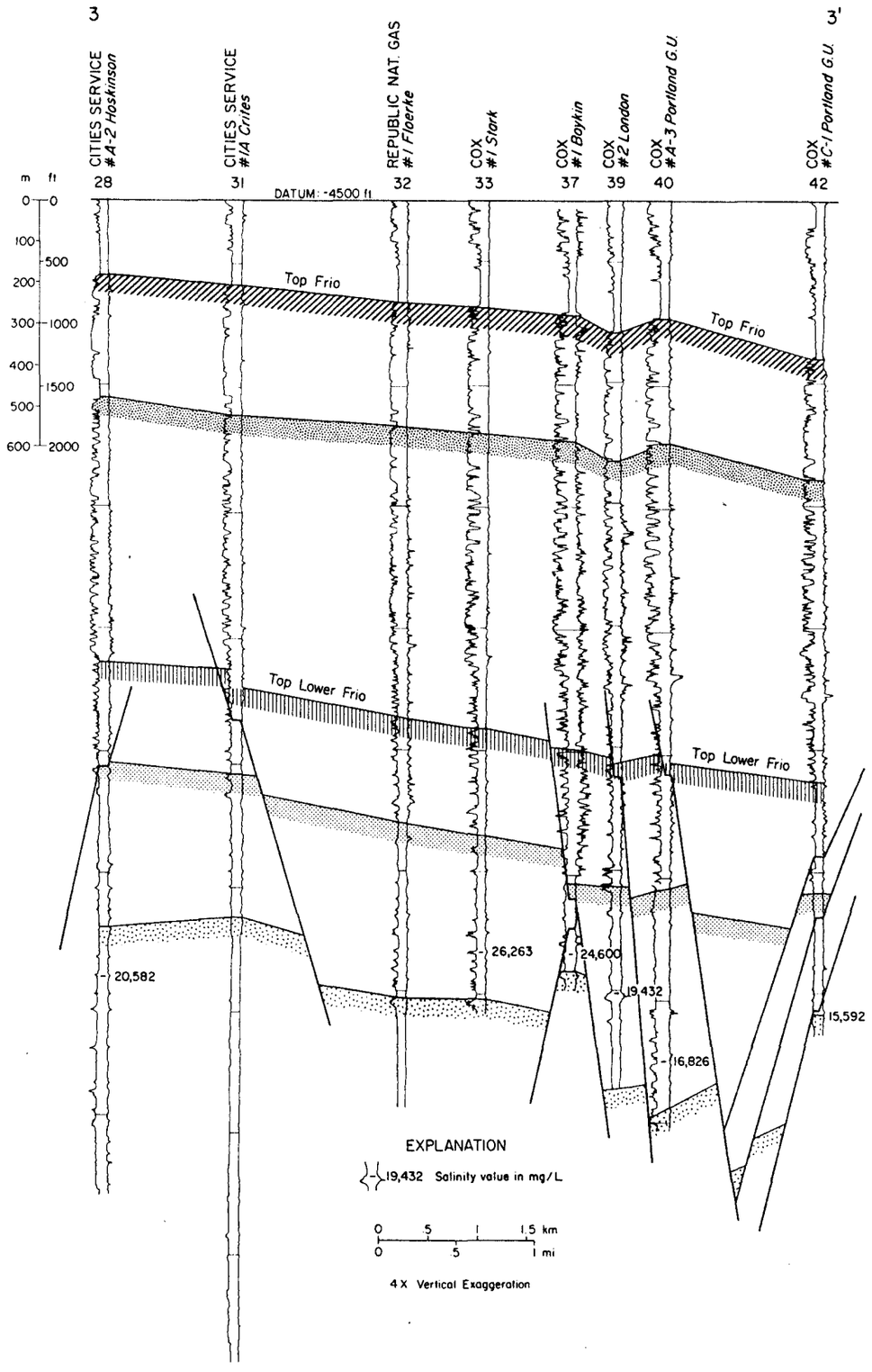

Figure 15. Structural dip section 3-3' through Corpus Christi area.

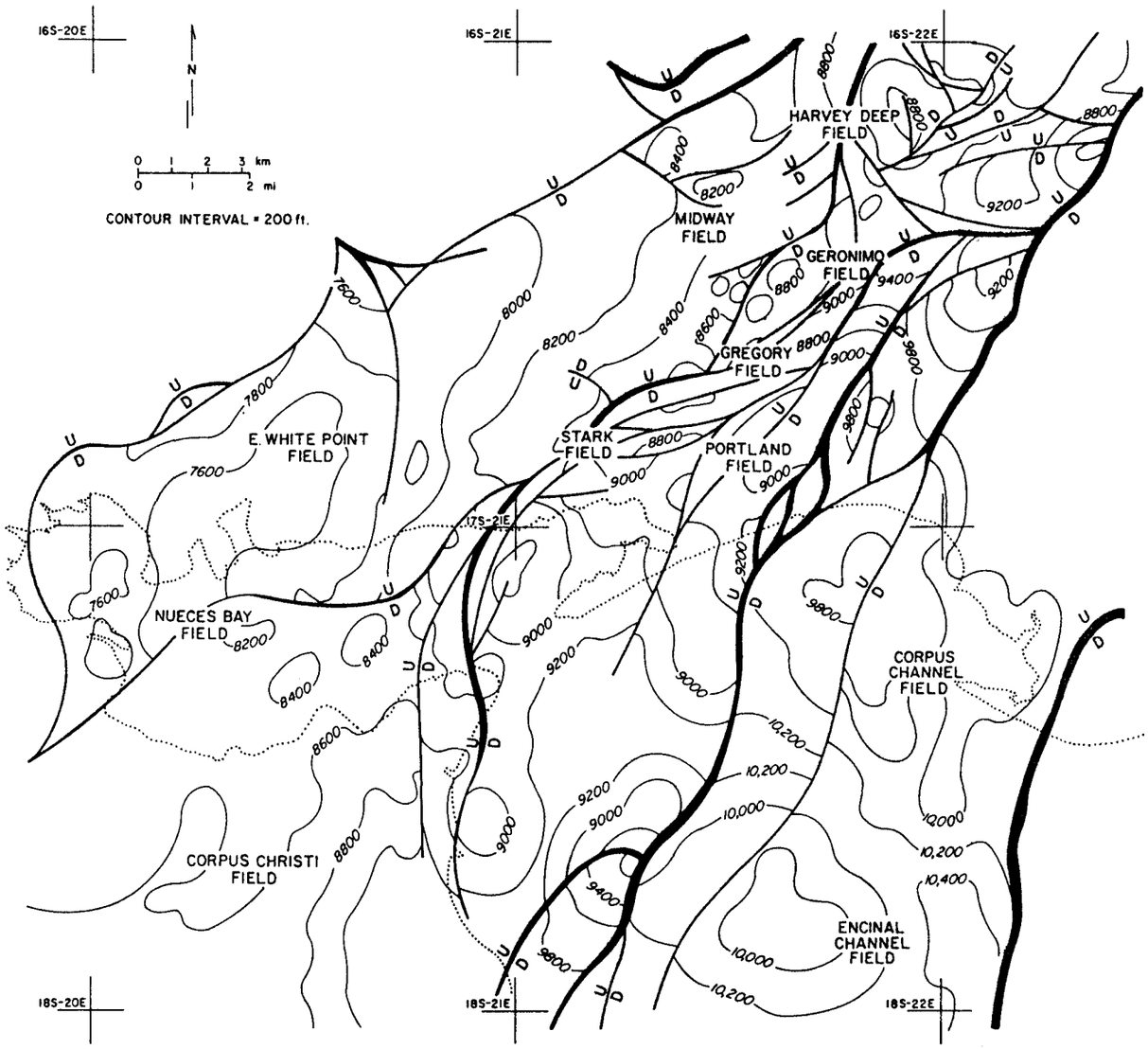

Figure 16. Structure on a horizon in the middle Frio, Corpus Christi area, modified from the Executive's Geologic Atlas (1981), Geomap Company, Dallas, Texas.

adjacent to major deltaic depocenters located along depositional strike from the study area.

Sand packages in the upper Frio Formation resemble a stacked barrier-bar/strandplain sequence. Individual sand bodies 100 to several hundred ft thick interfinger with shales 10 to 20 ft thick. Electric log (SP) patterns for these sandstones are dominantly blocky with a few upward-coarsening or upward-fining patterns; sand percentages are commonly 60 to 70 percent. In the lower Frio Formation, sand packages become thinner and less blocky with depth. Shale breaks become several hundreds of feet thick, and sand percentages range from 10 to 20 percent. Sand bodies are cyclic in nature even at depths of 14,000 ft and can be traced across the entire area. Sand packages and electric log patterns in the channel area are essentially the same as those in the onshore area.

Boyd and Dyer (1964) suggested the strike-aligned delta system centered in the Rio Grande Embayment was the source of the stacked barrier/strandplain sequence in the upper Frio Formation. Most likely sand was also supplied from the Houston delta system located to the northeast. This would be analogous to the modern central Texas coast. The origin of the cyclic sand bodies in the lower Frio Formation, however, is probably different. In both the updip and downdip direction these sands thin considerably, suggesting a strike-aligned rather than dip-aligned source. Yet, to the south, the equivalent lower Frio sands in Kenedy County are massive and vertically stacked. To the north the delta system centered in the Houston Embayment changed position frequently (Galloway and others, in press), but this does not adequately explain the regular cyclic pattern of the lower Frio sands in the Corpus Christi area. In the Nine Mile Point field (fig. 1), Berg and Powell (1976) document aprons of sand and silt deposited in shallow water by storm-generated density currents. In the Red Fish Bay field east of the Corpus Christi area (fig. 1), a core from the lower Frio

exhibits interbedded sandstones and shales that have been interpreted as shelf and slope deposits (Bebout and others, 1978). The cyclic sheet-like sands of the lower Frio are probably shelf deposits equivalent to the massive delta deposits to the north and south.

Geochemical Trends

Salinity data for the area were obtained from three sources: water analyses from Coastal Oil and Gas Corporation, Cities Service Company, and Edwin L. Cox Company; published analyses (Kharaka and others, 1977); and analyses of water samples collected by the Bureau of Economic Geology. Where duplication occurred, chemical analyses showed similar concentrations. Most of the analyses for the Corpus Christi area are from reservoirs within the lower Frio Formation where sands are separated by thick sections of shale.

Salinity values within the Corpus Christi area range from about 15,000 mg/L in the Portland field to over 200,000 mg/L in the Encinal Channel field. Structural mapping shows that in the lower Frio Formation, within a major fault block, salinity values are fairly consistent. For example, within one major fault block, salinity values range from 20,582 to 32,450 mg/L (fig. 13). Other salinities from wells within the same fault block are consistent with these values. In the channel area, which is in another fault block, salinity values are generally much higher than those in the onshore area (fig. 14). Dip section 3 - 3' (fig. 15), which crosses a large fault between wells 37 and 39, illustrates the variations in salinity values within adjacent fault blocks. The salinity values in the updip fault block are in the 25,000 mg/L range, while salinities in the downdip fault block are consistently less than 20,000 mg/L.

In the Portland field, total dissolved solids show a decrease with depth (fig. 17). The three points that fall in the area above the 0.75 psi/ft

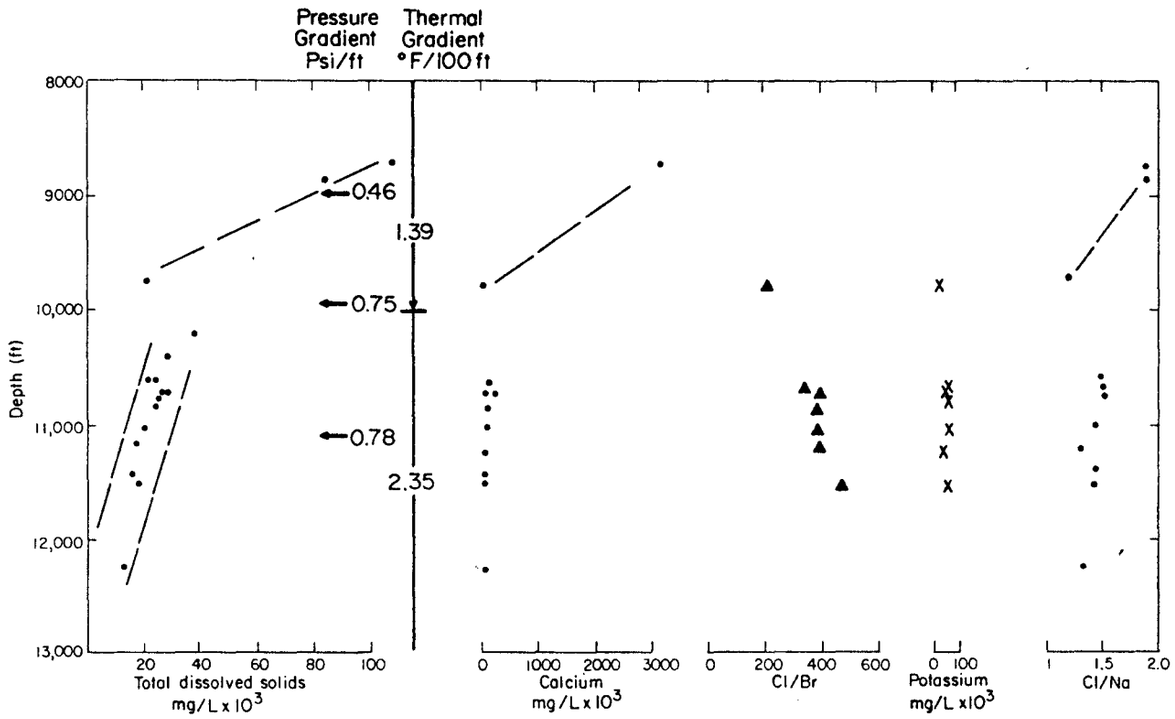

Figure 17. Concentrations of total dissolved solids and major cations and ion ratios in the Frio Formation, Portland field. Chemical data from Appendix A; thermal gradient from Weise and others (1980).

pressure gradient are from wells on the fringes of the field. Below 10,000 ft, where pressure gradients exceed 0.75 psi/ft, the systematic decrease in salinity with depth coincides with the decrease in salinity in the dip direction through the field (fig. 15).

In highly geopressured reservoirs of the Portland field, there is little or no variation in calcium, potassium, and chloride to sodium ratio with depth (fig. 17). A slight increase is seen in the chloride to bromide ratio with depth from 200 to over 400.

The Corpus Christi field shows a similar reduction in salinity at depths below 10,000 ft where pressure gradients are greater than 0.7 psi/ft (fig. 18). As in the Portland field, calcium and the chloride to sodium ratio remain essentially unchanged with depth. Potassium, however, shows an increase with depth, whereas the chloride to bromide ratio is relatively uniform with depth.

Both fields show comparable decreases in total dissolved solids over similar depth intervals and similar pressure and temperature gradients. These salinity gradients substantiate the finding of the other study areas where salinity decreases with depth where sandstones are highly geopressured.

Candelaria Area

The geology of the Candelaria field area (figs. 1 and 19) was previously studied by Bebout and others (1978) and by Weise and others (1980). These former studies provided a basis for the structural and stratigraphic interpretations presented herein. For the present study a total of 62 induction-electric logs (Appendix B) were used to interpret sandstones and shales of the Frio Formation in the Candelaria field area. Two cross sections and a structure map were constructed to illustrate structural and stratigraphic relationships of reservoir sandstones and variations in the salinity of formation waters

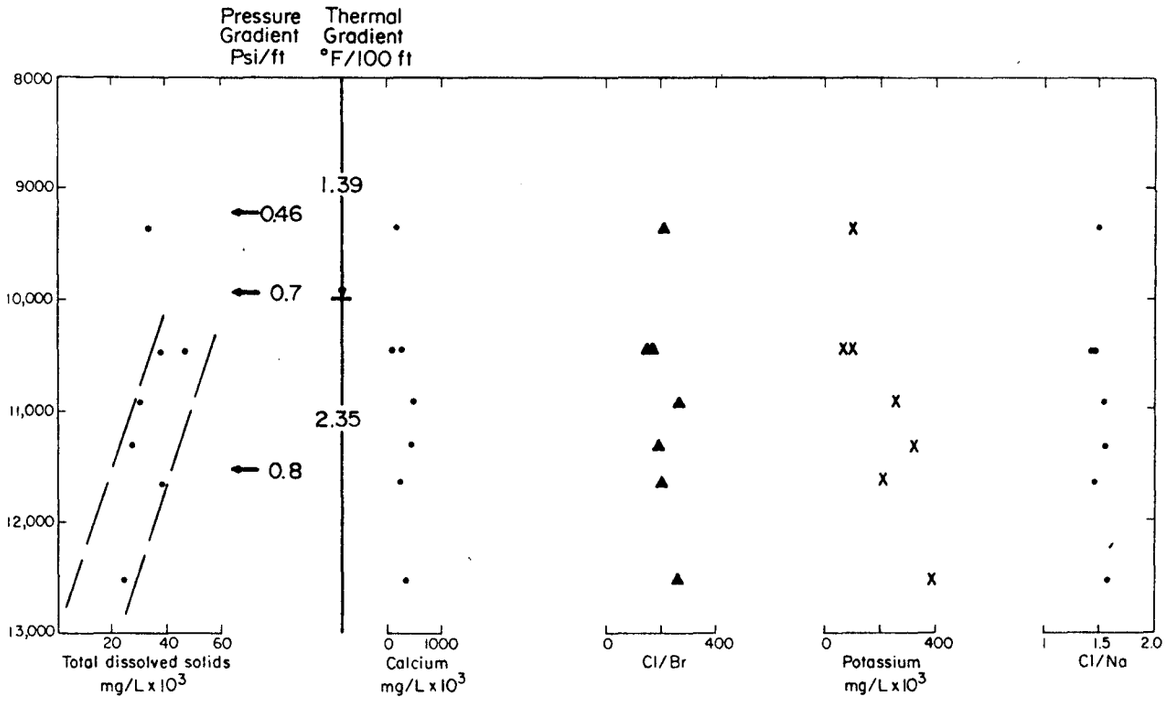

Figure 18. Concentrations of total dissolved solids and major cations and ion ratios in the Frio Formation, Corpus Christi field. Chemical data from Appendix A; thermal gradient from Weise and others (1980).

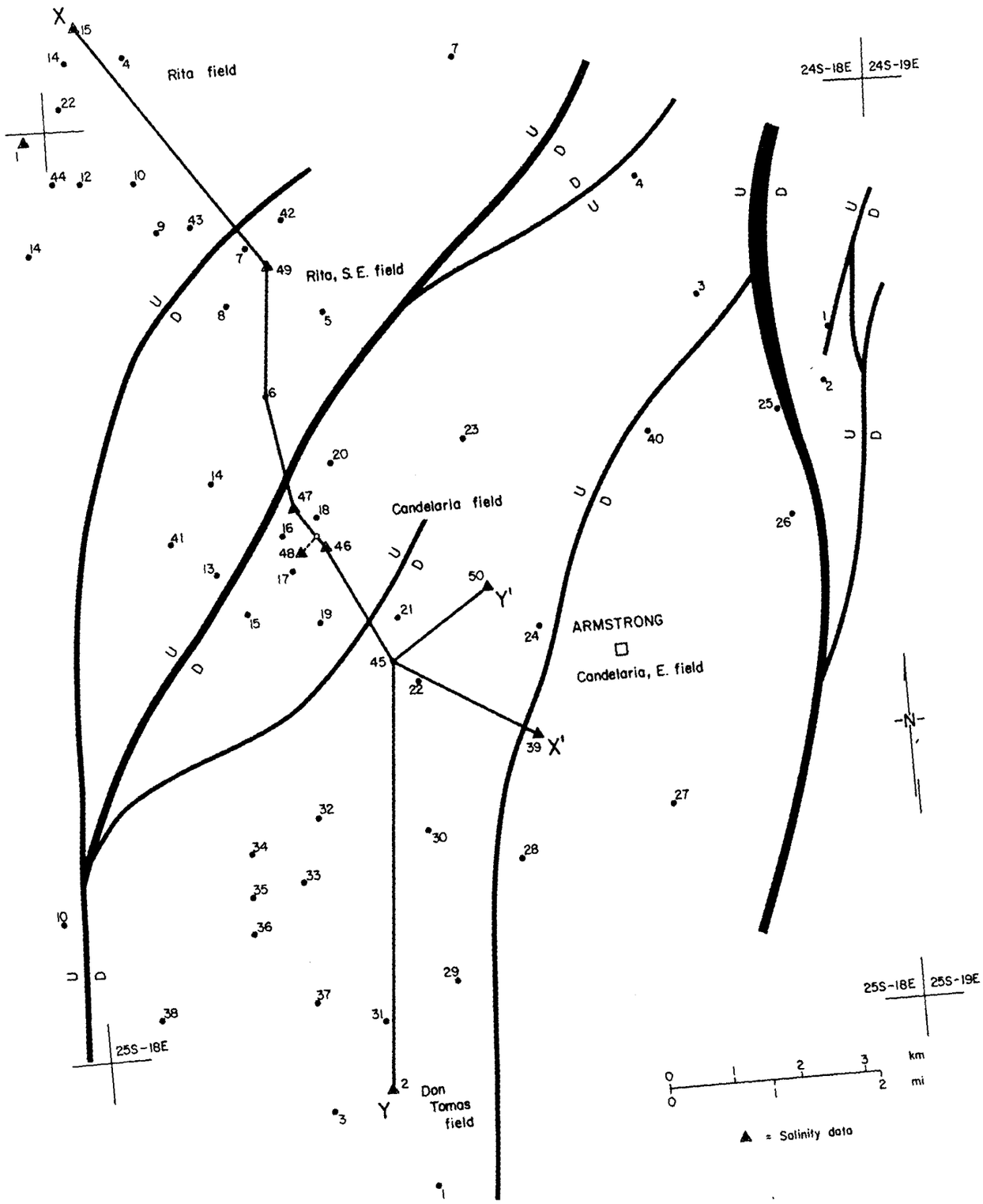

Figure 19. Location map showing well control, wells sampled, lines of section, and faults, Candelaria field area.

(figs. 20, 21, and 22) collected from wells in the Candelaria, Candelaria E., Rita, Rita S.E., and Don Tomas fields (Appendix A). In addition, one water analysis was provided by the Exxon Corporation.

Structure

The structural style of the Frio Formation in South Texas is controlled by complex syndepositional folding and faulting. Deposition of the Norias Delta system (Galloway and others, in press) in the Rio Grande Embayment and near the shelf margin resulted in large vertical displacements along growth faults, massive accumulation of sandstones, and in many areas, reversal of regional dip (rollover) into the downthrown side of the faults. Continued progradation of deltaic sands over undercompacted slope and basinal muds formed multiple zones of down-to-the-basin faults. The Candelaria field lies within this complexly faulted zone of the Frio trend.

The major structural feature of the Candelaria field is a segmented rollover anticline, a low-relief feature commonly associated with syndepositional faulting. Several down-to-the-basin and up-to-the-basin faults compartmentalize the structure. Vertical displacements at mapped horizons range from 50 to 500 ft (fig. 22), but displacements generally increase at greater depths.

Stratigraphic Relationships

The Norias Delta system constitutes the main Frio depocenter along the lower Texas coast. Active progradation during early and middle Frio time advanced the shoreline 60 mi basinward. Progradation continued through late Frio time until it was eventually terminated by the Anahuac transgression (Galloway and others, in press).

In the Candelaria field, typical sand content ranges from 30 to 55 percent of the Frio section, which is more than 11,000 ft thick. Electric-log

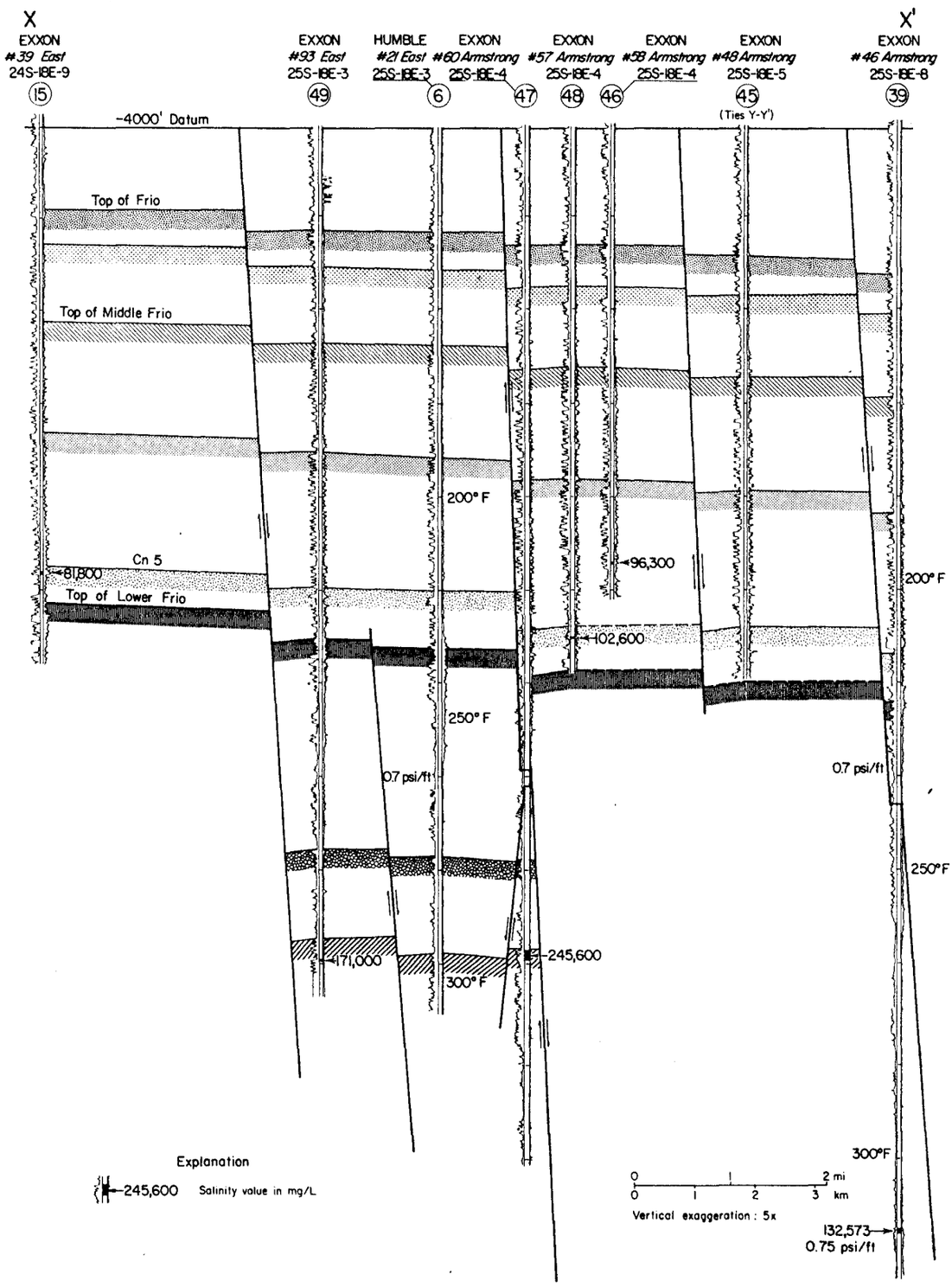

Figure 20. Structural dip section X-X', Candelaria field area.

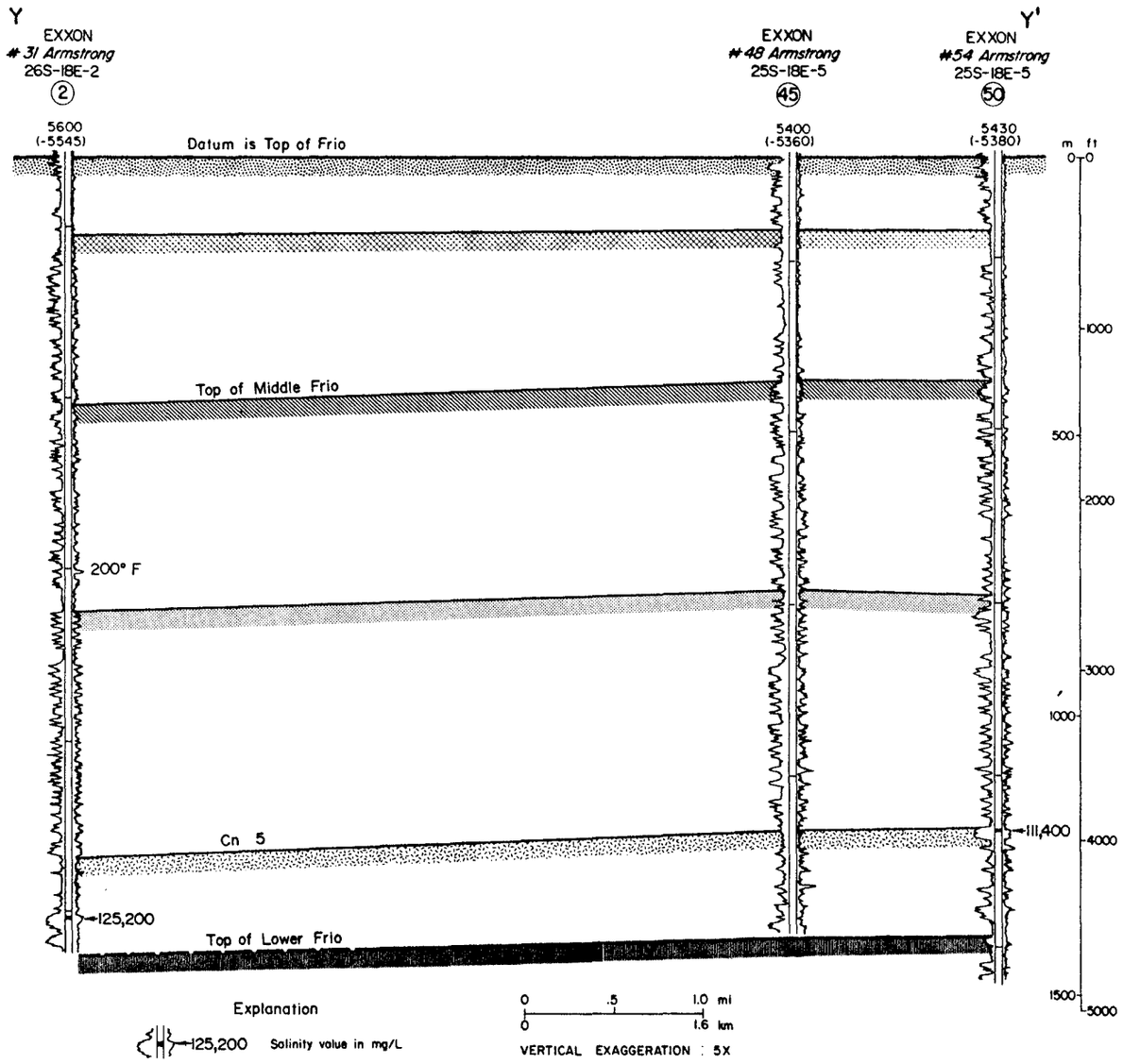

Figure 21. Stratigraphic strike section Y-Y', Candelaria field area.

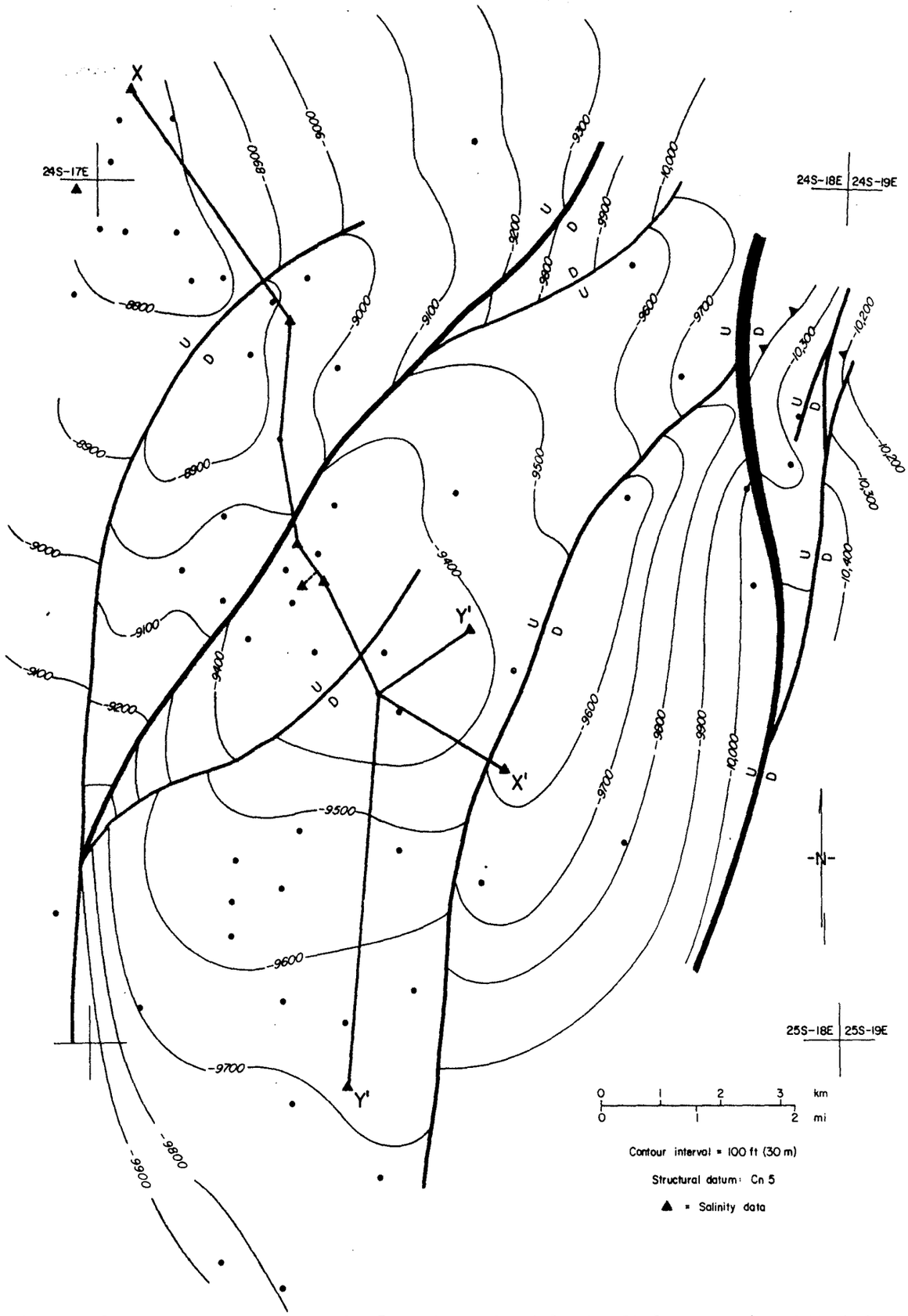

Figure 22. Structure at the Cn 5 marker, Candelaria field area (modified from Weise and others, 1980).

examination of sedimentary characteristics reveals two lithologically distinct sections: a lower section containing the lower Frio operational unit, and an upper section consisting of both the middle and upper Frio operational units (correlation markers after Galloway and others, in press). The lower Frio sandstones are characterized by generally upward-coarsening sandstone and shale sequences several hundred feet thick separated by equally thick shales (well #47, fig. 20). These sequences are interpreted as progradational deltaic facies grading from prodelta muds into delta-front sandstones and associated facies assemblages. The upper section consists of relatively homogeneous middle and upper Frio strata, characterized by predominantly thin (10 to 50 ft), blocky, and laterally discontinuous sandstones separated by thin shales. A few discontinuous and moderately thick (50 to 90 ft) sandstones with upward-coarsening and blocky SP patterns also occur in the section (well #39, fig. 20). This combination of log facies patterns suggests deposition of dominantly aggradational delta-plain facies, an assemblage including distributary-channel fills, crevasse splays, and destructional bar and beach ridge environments (Galloway and others, in press).

Geochemical Trends

Water sample analyses from six wells in the Candelaria and adjacent fields are included in the evaluation of salinity trends with depth. Repeat analyses of samples taken from the same reservoir indicate variations of about 5 percent. Salinity values (TDS) range from 96,300 mg/L to 245,600 mg/L over depths ranging from 8,604 ft to 15,775 ft (Appendix A).

Although numerous physical and chemical factors may be responsible for the wide variations in the salinity of formation water, the principal objective of this study is to delineate interrelationships among local structures,

stratigraphy, fluid temperatures and pressures, and variations in ionic concentrations with depth.

Vertical variations of salinity in the Candelaria field follow trends observed and described elsewhere in this report. Salinity increases at depths, where pressure gradients are between 0.465 psi/ft and 0.7 psi/ft, are a maximum approximately where pressure gradients equal or exceed 0.7 psi/ft, then decrease with depth through the underlying highly geopressured zone (fig. 23). On the basis of available data, the trend of increasing salinity with depth through intermediate pressure gradients is clearly documented (fig. 23). Unfortunately, only a limited number of samples from deep geopressured reservoirs were available, causing the deep decrease in salinity to be questionable. However, data obtained from deep wells in the adjacent Rita and Rita S.E. fields support the observed salinity maximum and subsequent decrease in the underlying zone.

Ionic concentrations of calcium (Ca), potassium (K), and ratios of chlorides to bromides (Cl/Br) and chlorides to sodium (Cl/Na) were examined for vertical variations and trends (fig. 23). Both calcium concentrations and chloride to sodium ratios increase with depth at intermediate pressure gradients and decrease with depth at higher pressure gradients. Chloride to bromide ratios show a slight overall decrease with depth. Potassium concentrations remain relatively constant above 10,000 ft but appear to increase within the geopressured zone. The apparent decrease with depth (fig. 23) at highest pressure gradients is uncertain.

Variations in concentrations of TDS and ions in brines also correlate with changes in geothermal gradients. Lewis and Rose (1970) suggested that geopressured zones also have abnormally high geothermal gradients, and indeed that relationship has been well documented. In the Candelaria field, geothermal gradients are high through the geopressured zone (Weise and others, 1980).

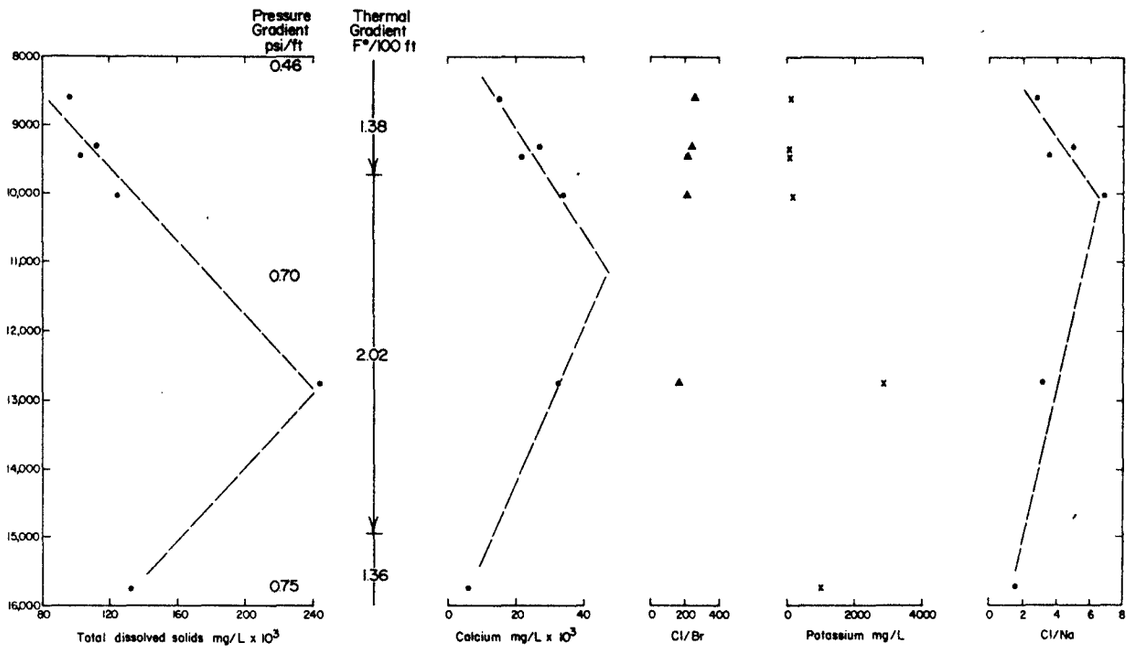

Figure 23. Concentration of total dissolved solids and major cations and ion ratios in the Frio Formation, Candelaria field. Chemical data from Appendix A.

Concentrations of TDS, calcium, and the chloride to sodium ratio increase through the zone where the geothermal gradient is 1.38°F/100 ft (the hydropressured-transition zone). Where the geothermal gradient abruptly changes to 2.02°F/100 ft, corresponding to pressure gradients of 0.7 psi/ft, the chloride to sodium ratio begins to decrease. Concentrations of calcium, potassium, and TDS each reach maximums deeper within the zone of high thermal gradients, then decrease as the thermal gradient declines to 1.36°F/100 ft (fig. 23).

Structural effects on observed chemical variations appear to be minor in the Candelaria field. The anticline is segmented into five fault blocks at the mapped horizon with additional faults compartmentalizing reservoirs at greater depths (figs. 20 and 22). Three downdip fault blocks contain data used in the analysis of salinity trends. None of the sandstone reservoirs sampled are stratigraphic equivalents, making direct comparison of the effects of faulting on salinity variations impossible. Two samples, however, are from reservoirs confined within a single fault block and with similar temperatures and pressures. The observed variation in TDS values is less than 10 percent, agreeing with other field studies that have demonstrated relative uniformity among salinity values from wells within the same fault-bounded reservoir. A somewhat anomalous value (245,600 mg/L) is noted in well #47 (fig. 20). Compartmentalization and restriction of fluid migration through the reservoir sandstone at high temperatures and pressures may be responsible, in part, for the high salinity.

REGIONAL COMPARISON OF WATER COMPOSITION

Ionic Concentrations

As shown by area plots (figs. 11, 17, 18, and 23), the concentrations of specific ions and ratios of selected ion pairs commonly correspond to the

measured values for total dissolved solids, but they can also exhibit spatial patterns that are independent from the salinity trends. The value of such an analysis lies in documenting where changes in ionic concentration occur and attempting to explain those changes in terms of general chemical reactions expected at depth in the Frio sediments. Some of the variability in ionic concentrations (calcium, sodium, potassium) and ionic ratios (Cl/Br, Cl/Na) can be explained by the general geologic setting and the Frio depositional systems, but other chemical components such as silica are low throughout the Frio trend and apparently are not dependent on regional differences in geology.

Perhaps the most influential geographic controls on compositional differences are the major structural features and depositional systems that were active before and during Frio deposition. In a broad sense, Frio deposition is attributed to major delta systems in southeast and far South Texas (Houston and Norias) that respectively occupied the Houston and Rio Grande Embayments (Galloway and others, in press). These same areas roughly coincide with the known occurrence of Louann salt and related salt structures (Murray, 1966). The interdeltaic area was occupied by the Carancahua barrier-strandplain system, which coincided with the San Marcos Arch, an area where salt is absent. For the present discussion these three tectonic/paleogeographic areas are referred to as upper, middle, and lower subregions of the Texas coast.

Salinity

Depth-dependent salinity trends in sedimentary basins and their corresponding relationship to pressure gradient, shale compaction, and clay mineral transformation are well established for hydropressured and shallow geopressured aquifers. The shallowest trend shows a general increase in salinity with depth resulting from the juxtaposition of two different water zones: a shallow zone of

fresh-water circulation from meteoric sources and an underlying zone of connate water that occurs at burial depths greater than a few thousand feet. These connate waters are usually more saline than seawater owing to the chemical reactions and sediment compaction (mainly shale) that accompanies early stage diagenesis.

The trends most widely reported throughout the Gulf Coast and other young basins are (1) a salinity increase that occurs between shallow circulating surface waters and a salinity maximum in the thick well-developed sandstones under hydrostatic pressure and (2) an underlying salinity decrease that occurs near the base of normal pressure or in the transition zone of slightly abnormal pressure. The data of this study not only corroborate the second salinity-depth trend, but they also indicate two deeper turning points and associated trends. The first of these two trends occurs within the intermediate geopressured section and comprises waters with salinities that increase with depth. This trend is present in the Red Fish Reef, Alta Loma, Chocolate Bayou, and Candelaria fields (figs. 2, 11, and 23, Appendix A). The deep salinity maximum apparently coincides with pressure gradients of about 0.75 psi/ft. Where pressure gradients exceed 0.75 psi/ft, the trend again reverses, and salinities decrease with depth to the limit of the data. This deep trend of decreasing salinities is well documented in the Alta Loma, Portland, and Corpus Christi fields (figs. 17 and 18) and appears to be present in the Chocolate Bayou and Candelaria fields (figs. 11 and 23).

As previously reported (Kharaka and others, 1978), most salinity values for the Corpus Christi area are lower than those for surrounding areas, but unlike previous reports some exceptionally high salinities occur in this area (Appendix A). Furthermore, highly saline waters (greater than 80,000 mg/L) are produced from the Frio Formation in South Texas fields (Kenedy County), where Jones

(1975) and Wallace and others (1977) suggested that low salinity waters would be encountered. Total dissolved solids in waters produced from the Candelaria, Sarita, and El Paistle Deep field commonly range between 80,000 and 100,000 mg/L, but salinities as high as 245,600 mg/L have been measured.

Calcium

The range of calcium concentrations varies greatly from area to area and covers several orders of magnitude. Calcium concentrations are high along the upper coast (northeast of central Matagorda County) and along the lower coast (Kleberg and Kenedy Counties), and low along the middle coast. Formation waters from the upper coast subregion contain from 200 to 900 mg/L calcium, the lowest concentrations occurring near the top of geopressure or deep within the highly geopressured zone (Red Fish Reef, Alta Loma, and Chocolate Bayou fields). In the middle coast subregion, calcium generally ranges between 50 and 500 mg/L (Corpus Christi, Midway, Portland, and Harvey Deep fields). Of all the waters analyzed, highest calcium concentrations occur in Kleberg and Kenedy Counties, where values between 2,000 and 34,000 mg/L have been measured (Appendix A). Indeed, calcium ions are more abundant than sodium ions in some high TDS samples from Candelaria, El Paistle Deep, and Rita fields. Within these subregions, calcium may or may not vary appreciably with depth depending on the pressure and thermal gradients and the concentration of total dissolved solids. In the upper and lower coast subregions, calcium generally increases with depth at intermediate pore-pressure gradients and decreases with depth in the zone of high pore-pressure gradients. In contrast, calcium is high in normally pressured sediments and uniformly low with depth in highly geopressured sediments in the Corpus Christi area.

Milliken and others (1981) summarized the sources and sinks of calcium in the Frio sandstones near the Pleasant Bayou well. The general increase in

calcium with depth below the top of geopressure corresponds to a decrease in calcite in the shales (Freed, 1980; Kaiser and others, 1981) and decrease of calcite cements in the sandstones (Loucks and others, 1981). It also corresponds to the zone of albitization (Loucks and others, 1981; Milliken and others, 1981) and smectite-illite transition (Freed, 1980). These general relationships and sources of calcium should be applicable throughout the upper coast subregion of high calcium. Although data are fewer, some of these same relationships may apply in the lower coast subregion. A notable exception is the lack of late stage leaching of carbonate cements. However, the abundance of volcanic and carbonate rock fragments (Loucks and others, 1979) in addition to the smectite-illite transition and albitization could be sources of the calcium. Other possible but undetermined sources of calcium include cation exchange between calcium montmorillonite and sodium montmorillonite, kaolinization of plagioclase, formation of ferroan calcite at the expense of calcite, and the dissolution of calcite in shales. These sources of calcium rely on the in situ interaction of the rocks and interstitial waters. A lesser possibility is the upward migration of calcium-rich waters from underlying Mesozoic carbonate rocks. However, this explanation is highly speculative, and compelling evidence as to the source of the calcium is unavailable.

Potassium

The concentration of potassium in produced brines is substantially less than calcium; nevertheless, their spatial patterns of distribution are similar. Concentrations of potassium ions in excess of 150 mg/L occur in the upper and lower coast subregions, whereas waters in the middle coast subregion usually have less than 150 mg/L. Most samples from the upper coast (Sugar Valley, Alta Loma, Chocolate Bayou, Red Fish Reef) contain between 150 and 600 mg/L. Potassium in samples from Kleberg and Kenedy Counties generally fall within the same

range; however, a few deep wells with high total dissolved solids have between 1,000 and 2,900 mg/L (Candelaria, El Paistle, and Rita fields). The middle coast subregion of low potassium not only includes fields in the Corpus Christi area but also the Maude Traylor, Trull, Tidehaven, and Southwest Pheasant fields (Appendix A).

Potassium concentrations within a field do not appear to be as depth dependent as calcium, and many analyses suggest that potassium is relatively uniform at depth despite major changes in pressure and thermal gradient. Fields where potassium is essentially unchanged at depth include Alta Loma, East White Point, Portland, South May, and Sarita. Fields where potassium increases slightly in the zones of intermediate or high pressure gradients include Chocolate Bayou (fig. 11), Corpus Christi (fig. 18), Rita, and Candelaria (fig. 23).

Potential sources of potassium in these areas are albitization and leaching of feldspars. Only one area exhibiting an increase in potassium in the highly geopressured zone (Chocolate Bayou) has sufficient data for comment on the abundance of K feldspar in shales. Of the two wells analyzed in detail (Freed, 1980), one (State Lease 53034 No. 2) showed that potassium feldspar was very low or absent below 10,000 ft, whereas the other well (Pleasant Bayou No. 2) showed that feldspar was rarely preserved below 12,000 ft (Kaiser and Richmann, 1981).

Sodium

Like calcium and potassium, sodium concentrations are generally highest (>15,000 mg/L) in the upper and lower coast subregions and generally lowest (<15,000 mg/L) in the middle coast subregion. Sodium usually increases at depths of intermediate pore-pressure gradient and decreases at depths of high pore-pressure gradient. Consequently, variations in sodium with depth closely parallel those of total dissolved solids and commonly are similar to those of calcium.

Sodium enrichment of Tertiary formation waters is usually attributed to salt dissolution, but this may not explain the high sodium values in South Texas, where clay mineral diagenesis may be a major contributor of sodium. In some areas, the decrease in sodium within the highly geopressured zone may reflect albitization, a process that depends on availability of silica as well as sodium. Although depth-related changes in sodium and calcium are similar, the rates of change for these major cations are substantially different. Hence, the sodium to calcium ratio also varies with depth and geographic area. For example in Kleberg and Kenedy Counties, ratio values are uniformly low and range from <1 to 6. Highest ratio values are found in the middle coast subregion where sodium is commonly 75 to 125 times more abundant than calcium. From a geochemical perspective, the variations of greatest interest are those related to depth that transcend the geographical boundaries. In most of the fields (Red Fish Reef, Alta Loma, Chocolate Bayou, Maude Traylor, Portland, Corpus Christi) the sodium to calcium ratio reaches a maximum near the top of geopressure and decreases with depth in the geopressure zone. Ratio minimums usually occur in the hydropressure zone or in the highly geopressured interval. Marked decreases in the sodium to calcium ratio in the geopressure zone are caused by the greater increases in calcium than sodium with depth.

Chloride to Sodium Ratio

With a few exceptions in South Texas (South May, Sarita, Rita, Candelaria), Frio Formation waters are dominantly a sodium chloride type; hence, the changes in relative proportions of these ions could provide clues to the origin of the waters. Subtle distinctions in the distribution of Cl/Na values show that most values fall between 1.2 and 1.8, with many values being about 1.5. Highest chloride to sodium ratios, in excess of 2, are found along the lower coast subregion, where high total dissolved solids are products of high calcium as well

as high sodium and chloride concentrations. Sodium is less abundant in this area than elsewhere when similar chlorinity values are compared. Available data (Appendix A) show that chloride to sodium ratios in the upper coast subregion (Red Fish Reef, Chocolate Bayou, Alta Loma) are either unchanged or increase slightly with depth, especially below the top of geopressure. The decrease in sodium and attendant increase in chloride to sodium ratio with depth may result in part from albitization reported for these rocks (Milliken and others, 1981). In the middle coast subregion (East White Point, Portland, Corpus Christi fields), chloride to sodium ratios are either relatively uniform or decrease slightly with depth in the geopressure zone. Unfortunately data are too sparse to determine depth relationships in Kleberg and Kenedy Counties, although it is anticipated that the chloride to sodium ratios would be unchanged or decrease with depth.

Chloride to Bromide Ratio

The effect of evaporite dissolution on the chemical composition of Frio Formation waters is uncertain. Clearly it is not the most important factor determining high salinity for the upper coast and low salinity for the middle coast as previously reported (Kharaka and others, 1978, 1980). On the other hand, it cannot be ignored given the predominance of shallow piercement domes and deep-seated, salt-cored structures in the Houston Embayment. The chloride to bromide ratio may serve as an indicator of the contribution from dissolved salt. In this regard, the Frio trend can be subdivided again into three areas according to the ratio of Cl to Br concentrations in seawater, which is approximately 250. The areas are (1) the upper coast subregion where chloride to bromide ratios exceed 400 and increase with depth (fig. 11), (2) the middle coast subregion where ratio values range from 250 to 400 and either remain unchanged or increase with depth (figs. 17 and 18), and (3) the lower coast subregion

where chloride to bromide ratios are generally less than 250 and remain unchanged or decrease with depth (fig. 23).

The enrichment in these brines of chloride with respect to bromide and the evaporation line for seawater is evidence for salt dissolution in the upper coast subregion according to Rittenhouse (1967) and Kharaka and others (1978, 1980). Indeed a strong case can be made for this interpretation given the high ratio values, the increase in ratio value with depth (Red Fish Reef, Chocolate Bayou fields, fig. 11), and the proximity of salt domes in the area. However, the usefulness of these criteria is less certain when they are applied to the middle coast subregion where the magnitudes and depth trends for chloride to bromide are mixed. Chemical data for this area can be subdivided into two groups (1) fields in which chloride to bromide ratios are less than 250 and remain unchanged or increase with depth (Maude Traylor, East White Point, Corpus Christi, fig. 18) and (2) fields in which chloride to bromide ratios exceed 250 and increase with depth (Portland, fig. 17, Harvey Deep, Brannon, and possibly Midway). The latter fields are problematical because they are not underlain by salt, and yet they display the same characteristics as those in salt dome provinces. The only difference is that the chloride to bromide ratio for these fields may show less departure from the evaporation line for seawater than do some fields near salt domes. Chloride to bromide data from salt and non-salt areas (Kharaka and others, 1978; Appendix A) overlap considerably in the 300 to 500 range, which suggests that the chloride to bromide ratio is not an accurate measure of salt dissolution and is typically definitive only for extreme cases. Judging from the calculated chloride to bromide ratio, produced waters from fields in Kleberg and Kenedy Counties (South May, Sarita, Rita, Candelaria) are unaffected by salt dissolution.

CO_2 Concentration

Determining the composition of gases in formation water at in situ conditions is important because the solution pH and certain chemical reactions depend in part on the concentration of CO_2. According to Kaiser (personal communication, 1981), in situ pHs in Frio Formation waters are probably 2 to 3 units lower (more acidic) than field measurements would suggest because of CO_2 losses at the surface. Although few attempts have been made to accurately measure the level of water saturation with respect to CO_2 in deep geopressured brines, the U.S. Department of Energy's design well and well of opportunity test program has provided data that show the concentration of CO_2 in select wells at relatively high temperatures (figs. 24 and 25).

The Institute of Gas Technology performed analyses of gas composition primarily using flare line samples and gas chromatography. Typical field and laboratory techniques used in the DOE testing program are presented by Eaton Operating Company (1981). Mole percent values of CO_2 (figs. 24-26) represent an average of several samples collected for each well at different times during the testing period. The accuracy of these values is uncertain because the $CO_2/HCO_3^-/CO_3^=$ system in geothermal brines is complex and because measured CO_2 concentration partly depended on separator conditions (temperature, pressure, flowrate). Although absolute concentrations of CO_2 in Gulf Coast brines are unknown, the relative CO_2 concentrations and reservoir conditions (figs. 24-26) as well as differences in composition of associated gases are worth considering when studying the origins of subsurface fluids.

The laboratory experiments of Ellis and Golding (1963) have shown that the salting-out effect on CO_2 falls to a minimum at 300°F and the solubility of CO_2 in brines also reaches a minimum near this temperature. Although the experimental work of Ellis and Golding (1963) indicates that salinity affects

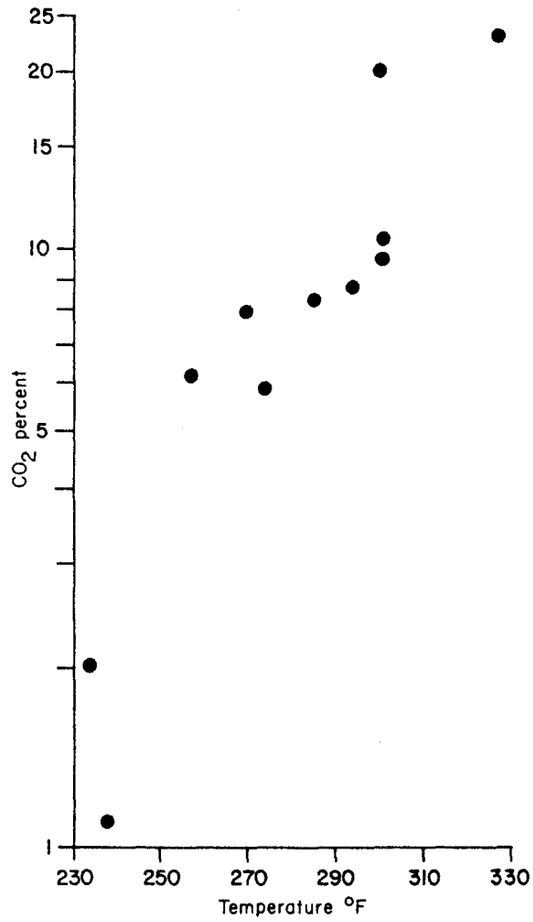

Figure 24. Concentration (mole percent) of CO_2 in formation water as a function of temperature. Data from DOE test well program.

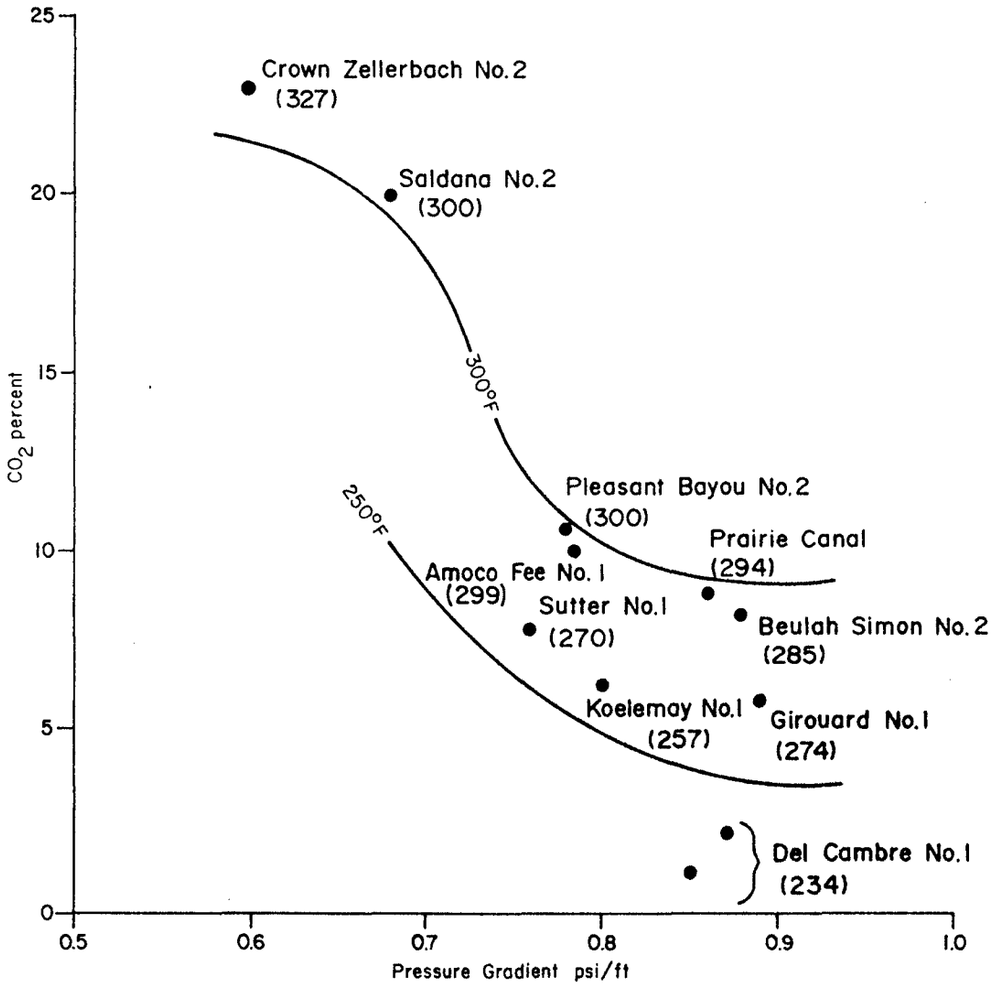

Figure 25. Concentration (mole percent) of CO_2 in formation water as a function of pressure gradient and temperature. Data from DOE test well program.

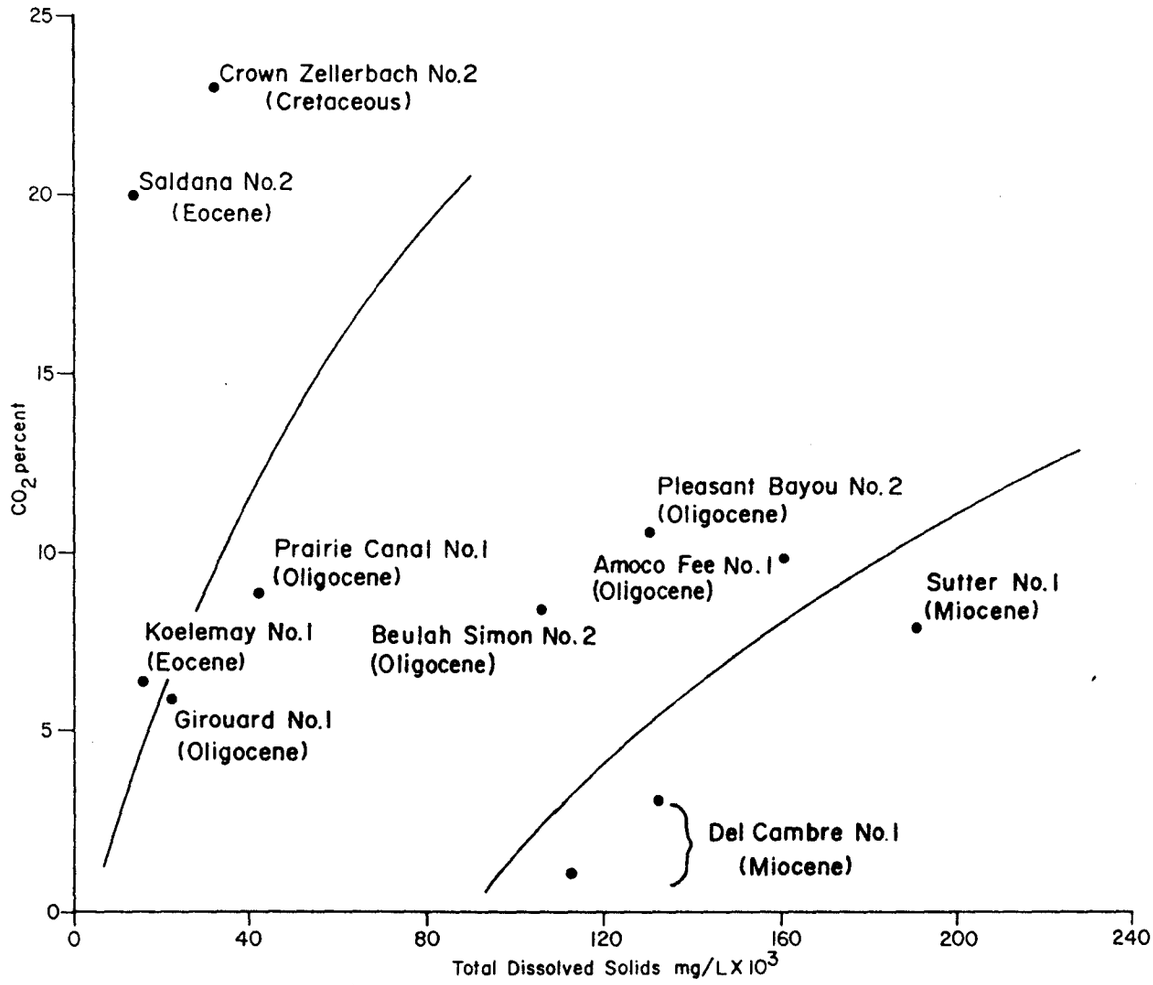

Figure 26. Concentration (mole percent) of CO_2 in formation water as a function of salinity and geologic age. Lines separate samples from rocks of different geologic ages. Data from DOE test well program.

CO_2 solubility at temperatures less than 300°F, the salinity effects are less than the temperature effects over the ranges for which field data are available (fig. 24). A comparison of salinity and CO_2 (fig. 26) shows a weak inverse relationship between the two variables. It also suggests that CO_2 concentrations may be a function of sediment age, older formation waters being enriched in CO_2.

The generation of CO_2 in conjunction with thermal maturation of organic material would partially explain the differences in CO_2 concentrations for waters of different ages. In the temperature and pressure range of available data, CO_2 is inversely related to pressure gradient given the temperature dependency (fig. 25).

CONCLUSIONS

Regional differences in chemical composition of Frio Formation waters are closely related to the major tectonic features (Houston and Rio Grande Embayments and intervening San Marcos Arch) and the associated depositional systems (Houston and Norias deltas and Carancahua barrier-strandplain) that were active during middle Tertiary time. Despite this general relationship, salinity variations within a subregion are generally greater than variations between the upper, middle, and lower Texas Coast. Within a given area, salinity variations are depth dependent and appear to be closely related to gradients of formation temperature and pore pressure. Major growth faults act as barriers to fluid movement as evidenced by substantial differences in salinity that occur at the same depth but across faults with large displacements. In contrast, minor faults do not appear to significantly influence salinity distribution. As a result, stratigraphically equivalent sandstones in the same fault block or

adjacent fault blocks with minor displacement produce waters with remarkably similar salinities and chemical compositions.

Although log calculations suggest that thick, well-developed sandstones with substantial SP deflections contain highly saline brines, chemical analyses of produced water indicate that brine concentrations and reservoir thickness are poorly correlated. Thick sands near the base of hydropressure generally produce high TDS water, but thin sands can produce water with either high or low TDS concentrations. Moreover, highly geopressured sandstones that produce water with low salinities generally are restricted or have low permeabilities, but permeability and salinity are not necessarily related; in fact, low permeability sandstones such as those found in Kleberg and Kenedy County can also produce concentrated brines. Hence it is unlikely that many thick, high-permeability reservoirs containing low salinity water will be encountered by deep subsurface drilling.

Judging from the available data, the concentration of CO_2 in formation waters is directly related to reservoir temperature and sediment age and inversely related to fluid pressure gradient and water salinity. However, these conclusions are tentative owing to the uncertainties of gas composition sampled at the flow line as compared to dissolved gases at in situ conditions. Whereas reported CO_2 values represent the best available data, additional studies will be necessary before CO_2 saturation levels at reservoir conditions can be determined. Similarly, additional work on mineral-solution equilibria will be required before the range of salinity variations can be adequately explained by geochemical processes.

ACKNOWLEDGMENTS

We would like to thank the many individuals and companies who cooperated in furnishing analyses and samples and the companies and individuals who assisted in arranging for sampling of the selected wells. The companies providing assistance are as follows:

Amoco Production Company
Andover Oil Company
Anschutz Corporation
Arco Oil & Gas Company
Chevron U.S.A., Incorporated
Cities Service Company
Coastal Corporation
Conoco, Incorporated
Edwin L. Cox
Exxon Company U.S.A.
Fort Worth Oil & Gas Co.
Galaxy Oil Company
Getty Oil Company
Goldston Oil Corporation
Halbouty, Michel T.
Jake L. Hamon Company
Houston Natural Gas Company
Houston Oil and Minerals
Hunt Oil Company
Lawbar Petroleum Company
Maynard Oil Company
Mitchell Energy Corporation
Mobil Producing, Texas and New Mexico
Patrick Petroleum Company
Phillips Petroleum Company
Prudential Drilling Company
Reading and Bates Petroleum Company
Royal Oil and Gas Corporation
Shell Oil Company
Sun Production Company
Superior Oil Company
Texaco, Incorporated
Texas Oil and Gas Company
Texas International Petroleum Company
Union Texas Petroleum Corporation
Wainoco Oil and Gas Company

Special thanks are extended to Jim O'Connell who conducted the field sampling and prepared the samples for analysis. In addition we would like to thank the manuscript processing, editing, and cartographic sections of the Bureau of Economic Geology for assistance in preparing the manuscript. The text was typed by Margaret T. Chastain and Dorothy C. Johnson under the direction of Lucille C. Harrell, and illustrations were prepared under the direction of Dan F. Scranton. Funding for this research was provided by the U.S. Department of Energy, Division of Geothermal Energy under contract no. DE-AC08-79ET27111.

REFERENCES

Amdurer, M., 1978, Geochemistry, hydrology, and mineralogy of the Laguna Madre Flats, South Texas: The University of Texas at Austin, Master's thesis, 172 p.

Bebout, D. G., Loucks, R. G., and Gregory, A. R., 1978, Frio sandstone reservoirs in the deep subsurface along the Texas Gulf Coast--their potential for the production of geopressured geothermal energy: The University of Texas at Austin, Bureau of Economic Geology Report of Investigations 91, 92 p.

Berg, R. R., and Powell, R. R., 1976, Density flow origin for Frio reservoir sandstones, Nine Mile Point field, Aransas County, Texas: Transactions, Gulf Coast Association of Geological Societies, v. 26, p. 310-319.

Boyd, D. R., and Dyer, B. F., 1964, Frio barrier bar system of South Texas: Transactions, Gulf Coast Association of Geological Societies, v. 14, p. 309-322.

Bredehoeft, J. D., Blyth, C. R., White, W. A., and Maxey, G. B., 1963, Possible mechanism for concentration of brines in subsurface formations: American Association of Petroleum Geologists Bulletin, v. 47, p. 257-269.

Burst, J. R., 1969, Diagenesis of Gulf Coast clayey sediments and its possible relation to petroleum migration: American Association of Petroleum Geologists Bulletin, v. 53, p. 73-93.

Core Laboratories, Inc., 1972, A survey of the subsurface saline water of Texas: Texas Water Development Board, Report 157, v. 1, 12 p.

De Sitter, L. V., 1947, Diagenesis of oil field brines: American Association of Petroleum Geologists Bulletin, v. 31, p. 2030-2040.

Dickey, P. E., 1969, Increasing concentration of subsurface brines with depth: Chemical Geology, v. 4, p. 361-370.

Dickey, P. A., Collins, A. G., and Fajardo, I. M., 1972, Chemical composition of deep formation waters in southwestern Louisiana: American Association of Petroleum Geologists Bulletin, v. 56, p. 1530-1570.

Ellis, A. J., and Golding, R. M., 1963, The solubility of carbon dioxide above 100°C in water and in sodium-chloride solutions: American Journal of Science, v. 261, p. 47-60.

Engelhardt, W. V., and Gaida, K. H., 1963, Concentration changes of pore solutions during compaction of clay sediments: Journal of Sedimentary Petrology, v. 33, p. 919-930.

Fertl, W. H., 1976, Abnormal formation pressures, in Developments in petroleum science: New York, Elsevier, v. 2, 382 p.

Fowler, W. A., 1970, Pressures, hydrocarbon accumulation, and salinities--Chocolate Bayou Field, Brazoria County, Texas: Journal of Petroleum Technology, v. 22, p. 411-422.

Eaton Operating Company, 1981, Final report, Prairie Canal well no. 1, Calcasieu Parish, Louisiana: Eaton Operating Company, Houston, Texas, contract report

No. DE-AC08-80ET27081 prepared for the U.S. Department of Energy, v. 1, section 12, p. 1-146.

Freed, R. L., 1980, Shale mineralogy and burial diagenesis in four geopressured wells, Hidalgo and Brazoria Counties, Texas, in Loucks, R. G., Richmann, D. L., and Milliken, K. L., Factors controlling reservoir quality in Tertiary sandstones and their significance to geopressured geothermal production: The University of Texas at Austin, Bureau of Economic Geology, Report to the Department of Energy, Contract No. DE-AC08-79ET27111, Appendix A, p. 111-172.

Galloway, W. E., Hobday, D. K., and Magara, K., in press, Frio Formation of the Texas Gulf Coast Basin--depositional systems, structural framework, and hydrocarbon origin, migration, distribution, and exploration potential: The University of Texas at Austin, Bureau of Economic Geology Report of Investigations.

Gregory, A. R., and Backus, M. M., 1980, Geopressured formation parameters, geothermal well, Brazoria County, Texas: The University of Texas at Austin, Proceedings, Fourth Geopressured-Geothermal Energy Conference, p. 235-311.

Hedberg, W. H., 1967, Pore-water chlorinities of subsurface shales: University of Wisconsin, Ph.D. dissertation, 121 p.

Jessen, F. W., and Rolshausen, F. W., 1944, Waters from the Frio Formation, Texas Gulf Coast: Transactions, American Institute of Mining and Metallurgical Engineers, v. 155, p. 23-38.

Jones, P. H., 1969, Hydrodynamics of geopressure in the northern Gulf of Mexico: Journal of Petroleum Technology, v. 21, p. 802-810.

Jones, P. H., 1975, Geothermal and hydrocarbon regimes, northern Gulf of Mexico Basin: The University of Texas at Austin, Center for Energy Studies, Proceedings, First Geopressured-Geothermal Energy Conference, p. 15-89.

Kaiser, W. R., Magara, K., Milliken, K. L., and Richmann, D. L., 1981, Using presence of calcite cap rock in shales to predict occurrence of reservoirs composed of leached secondary porosity in the geopressured zone: The University of Texas at Austin, Bureau of Economic Geology, Report to the Department of Energy, Division of Geothermal Energy, Contract No. DE-AC08-79ET27111, 31 p.

Kaiser, W. R., and Richmann, D. L., 1981, Predicting diagenetic history and reservoir quality in the Frio Formation of Brazoria County, Texas, and Pleasant Bayou test wells: Proceedings, Fifth Geopressured-Geothermal Energy Conference, Baton Rouge, Louisiana, p. 67-74.

Kharaka, Y. K., and Berry, F. A., 1974, The influence of geological membranes on the geochemistry of subsurface waters from Miocene sediments at Ketterman North Dome in California: Water Resources Research, v. 10, p. 313-327.

Kharaka, Y. K., Challender, E., and Carothers, W. W., 1977, Geochemistry of geopressured geothermal waters from the Texas Gulf Coast: Proceedings, Third Geopressured-Geothermal Energy Conference, Lafayette, Louisiana, v. 2, p. GI-121 - GI-164.

Kharaka, Y. K., Carothers, W. W., and Brown, P. M., 1978, Origins of water and solutes in the geopressured zones of the Northern Gulf of Mexico Basin: Society of Petroleum Engineers of AIME, Proceedings, 53rd Annual Conference, preprint SPE 7505, 8 p.

Kharaka, Y. K., Lico, M. S., Wright, V. A., and Carothers, W. W., 1980, Geochemistry of formation waters from Pleasant Bayou No. 2 well and adjacent areas in coastal Texas: Proceedings, Fourth Geopressured-Geothermal Energy Conference, v. 1, p. 168-193.

Lewis, C. R., and Rose, S. C., 1970, A theory relating high temperatures and overpressures: Journal of Petroleum Technology, v. 22, p. 11-16.

Loucks, R. G., Dodge, M. M., and Galloway, W. E., 1979, Sandstone consolidation analysis to delineate areas of high-quality reservoirs suitable for production of geopressured geothermal energy along the Texas Gulf Coast: The University of Texas at Austin, Bureau of Economic Geology, Report to the Department of Energy, Division of Geothermal Energy, Contract No. EG-77-5-05-554.

Loucks, R. G., Richmann, D. L., and Milliken, K. L., 1981, Factors controlling reservoir quality in Tertiary sandstones and their significance to geopressured geothermal production: The University of Texas at Austin, Bureau of Economic Geology Report of Investigations 111, 41 p.

Magara, K., 1978, Compaction and fluid migration, practical petroleum geology: New York, Elsevier, 319 p.

Mangelsdorf, P. C., Jr., Manheim, F. T., and Gieskes, J. M. T. M., 1970, Role of gravity, temperature gradients, and ion-exchange media in formation of fossil brines: American Association of Petroleum Geologists Bulletin, v. 54, p. 617-626.

Manheim, F. T., and Bischoff, J. L., 1969, Geochemistry of pore waters from Shell Oil Company drill holes on the continental slope of the northern Gulf of Mexico: Chemical Geology, v. 4, p. 63-82.

Manheim, F. T., and Horn, M. K., 1968, Composition of deeper subsurface waters along the Atlantic continental margin: Southeastern Geology, v. 9, p. 215-236.

Martin, G. B., 1969, Depositional history: key to Frio exploration: Transactions, Gulf Coast Association of Geological Societies, v. 19, p. 489-501.

McKelvey, J. G., and Milne, I. H., 1962, The flow of salt solutions through compacted clay, in Swineford, A. (ed.), Clays and clay minerals: Ninth National Conference, Clays and Clay Minerals, p. 248-259.

Milliken, K. L., Land, L. S., and Loucks, R. G., 1981, History of burial diagenesis determined from isotopic geochemistry, Frio Formation, Brazoria County, Texas: American Association of Petroleum Geologists Bulletin, v. 65, p. 1397-1413.

Mills, R. V. A., and Wells, R. C., 1919, The evaporation and concentration of water associated with petroleum and natural gas: U.S. Geological Survey Bulletin 693, 104 p.

Minor, H. E., 1934, Oil field waters of the Gulf coastal plain, in Wrather, W. E., and Lahee, F. H. (eds.), Problems of petroleum geology: American Association of Petroleum Geologists, Tulsa, Oklahoma, p. 891-906.

Morton, R. A., Ewing, T. E., and Tyler, N., 1981, Continuity and internal properties of Gulf Coast sandstones and their implications for geopressured energy development: The University of Texas at Austin, Bureau of Economic Geology, Report to the Department of Energy, Division of Geothermal Energy, Contract No. DE-AC08-79ET27111.

Murray, G. E., 1966, Salt structures of Gulf of Mexico Basin - a review: American Association of Petroleum Geologists Bulletin, v. 50, p. 439-478.

Myers, R. L., and Van Siclen, D. C., 1964, Dynamic phenomena of sediment compaction in Matagorda County, Texas: Transactions, Gulf Coast Association of Geological Societies, v. 14, p. 241-252.

Overton, H. L., and Timko, D. J., 1969, The salinity principles - a tectonic stress indicator in marine sands: Oil and Gas Journal, v. 67, p. 115-124.

Rittenhouse, G., 1967, Bromine in oil field waters and its use in determining possibilities of origin of these waters: American Association of Petroleum Geologists Bulletin, v. 51, p. 2340-2440.

Russell, W. L., 1933, Subsurface concentration of chloride brines: American Association of Petroleum Geologists Bulletin, v. 17, p. 1213-1228.

Schmidt, G. W., 1973, Interstitial water composition and geochemistry of deep Gulf Coast shales and sandstones: American Association of Petroleum Geologists Bulletin, v. 57, p. 321-337.

Stout, E., 1961, Red Fish Reef, South field, Chambers-Galveston Counties, Texas (abst.): Houston Geological Society Bulletin, v. 3, no. 7, p. 13-14.

Timm, B. C., and Maricelli, J. J., 1953, Formation waters in Southwest Louisiana: American Association of Petroleum Geologists Bulletin, v. 37, p. 397-409.

Wallace, R. H., Taylor, R. E., and Wesselman, J. B., 1977, Use of hydrogeologic mapping techniques in identifying potential geopressured-geothermal reservoirs in the Lower Rio Grande Embayment, Texas: Proceedings, Third Geopressured-Geothermal Energy Conference, v. 2, p. GI1-GI88.

Weise, B. R., Edwards, M. B., Gregory, A. R., Hamlin, H. S., Jirik, L. A., and Morton, R. A., 1980, Geologic studies of geopressured and hydropressured zones in Texas: test-well site selection: The University of Texas at Austin, Bureau of Economic Geology, Report to the Gas Research Institute, Contract No. 5011-321-0125.

White, D. E., 1965, Saline waters of sedimentary rocks, in Young, A., and Galley, J. E. (eds.), Fluids in subsurface environments: American Association of Petroleum Geologists, Memoir 4, p. 342-366.

APPENDIX A

Chemical analyses of water samples collected from the deep Frio Formation in Texas. Analyses by Bureau of Economic Geology Mineral Studies Laboratory, Clara Ho, Chemist-in-Charge.

†Samples provided by the well operator.

*Temperatures estimated by average thermal gradient for the county.

nm not measured.

County	Aransas	Aransas	Aransas	Aransas	Aransas	Brazoria	Brazoria
Field	Bartell Pass	Blackjack	Headquarters	Nine Mile Pt.	Nine Mile Pt.	Alvin, S.	Alvin, S.
Operator Well-Lease	Getty† Texas State Tract 118 #1L	Conoco Inc. St. Charles #34	Conoco Inc. St. Charles #50	Getty† Texas State Tract 142 #1	Getty† Texas State Tract 143 #1	Superior† Lockhart Bank Unit 1 #2	Superior† L. B. McGinnes Oil Unit 1 #3
Depth (ft)	11,204-11,250	9,198-9,244	9,506-9,518	10,904-10,960	11,697-11,712	10,497-10,574	9,711-9,724
Gas-Water Ratio (mcf/bbl)	43.0	oil well	oil well	12.0	5.0	16.0	oil well
Parameter							
TDS mg/L	28,400	16,600	18,200	22,400	22,900	98,500	79,300
Na mg/L	10,500	7,050	6,700	8,400	8,400	37,900	30,600
K mg/L	112	49.0	47.5	122	130	292	216
Mg mg/L	50.0	5.3	2.5	17.0	29.0	180	196
Ca mg/L	460	30.0	130	315	330	1,010	903
Fe mg/L	4.0	2.0	0.4	0.6	2.6	<0.025	<0.03
Al mg/L	<0.5	<0.4	<0.4	<0.4	<0.5	<0.5	<0.5
Mn mg/L	2.2	0.1	0.07	0.4	0.4	0.5	0.29
Sr mg/L	42.0	4.8	9.5	27.0	28.0	157	154
Ti mg/L	<0.13	<0.1	<0.1	<0.1	<0.13	<0.13	<0.13
B mg/L	74.0	38.6	37.0	41.0	41.5	65.4	45.5
P mg/L	<1.3	<1.0	<1.0	<1.0	<1.3	<1.3	<1.3
SiO_2 mg/L	46.0	97.0	93.0	86.0	87.5	60.0	56.0
HCO_3 mg/L	490	2,040	2,950	580	540	600	340
Field alkalinity mg/L	nm	nm	1,428.3	nm	nm	nm	nm
Cl mg/L	17,150	8,700	9,050	13,050	13,400	59,500	49,100
NH_3 mg/L	10.1	4.4	3.4	7.2	7.9	66.4	35.8
SO_4 mg/L	7.4	86.0	82.3	17.0	49.0	12.4	11.4
F mg/L	1.2	3.5	3.2	1.5	1.5	1.0	2.8
Br mg/L	89.0	49.0	45.0	75.0	78.0	94.0	63.0
pH	8.0	8.5	8.3	8.3	8.0	7.8	7.8
Field pH	nm	nm	8.0	nm	nm	nm	nm
Temp °F	273	217	232	235	274	217	208*
cations meq/L	486.7	309.8	299.4	385.6	387.6	1,725	1,400
anions meq/L	493	281.4	305.9	378.9	388.8	1,690	1,391

County	Brazoria	Brazoria	Brazoria	Calcasieu Parish (La.)	Calhoun	Calhoun	Calhoun
Field	Danbury, SW.	Pleasant Bayou	Rowan, N.	Sabine Lake	Maude B.Traylor, N.	Maude B.Traylor, N.	Maude B.Traylor, N.
Operator Well-Lease	Anschutz Corp. H. L. Peterson #1	Gen. Crude† Pleasant Bayou #2	Union Texas E. L. Summers #1	Coastal Oil & Gas† St. Lse. 3459 #1	Superior Oil† M. B.Traylor #8L	Superior Oil† M. B.Traylor #2	Superior Oil† M. M. Brooking #1
Depth (ft)	12,558-12,568	14,640-14,704	10,858-10,864	11,070-11,080	8,362-8,399	7,636-7,639	8,840-8,848
Gas-Water Ratio (mcf/bbl)	38.0	<1.0	<1.0	2.0	72.0	oil well	56.0
Parameter							
TDS mg/L	235,000	129,600	56,600	108,150	43,700	19,200	57,300
Na mg/L	69,700	42,100	22,700	42,400	17,300	7,900	23,000
K mg/L	1,218	570	171	240	90.0	56.4	139
Mg mg/L	1,535	625	59.7	240	39.5	15.7	52.5
Ca mg/L	22,600	8,980	330	1,770	158	34.0	189
Fe mg/L	0.05	62.0	8.0	2.15	.034	<0.013	0.04
Al mg/L	<0.5	<0.5	<0.5	<0.5	<0.5	<0.25	<0.5
Mn mg/L	33.0	22.0	0.5	1.5	0.15	<0.025	<0.03
Sr mg/L	1,080	1,005	49.7	134	36.5	14.0	55.2
Ti mg/L	<0.13	<0.2	<0.13	<0.2	<0.13	<0.063	<0.13
B mg/L	96.5	30.0	56.0	62.0	58.0	40.0	49.5
P mg/L	<1.3	<1.5	<1.3	<1.5	<1.3	<0.6	<1.3
SiO_2 mg/L	60.0	131	95.2	68.0	55.5	61.0	61.3
HCO_3 mg/L	30.0	nm	1,280	562	1,110	1,710	1,130
Field alkalinity mg/L	nm	nm	nm	nm	nm	nm	nm
Cl mg/L	152,000	78,500	34,000	64,700	25,800	10,800	34,100
NH_3 mg/L	182	91.0	32.8	70.0	14.3	5.4	17.9
SO_4 mg/L	15.6	14.0	21.0	760	35.2	44.0	15.3
F mg/L	0.5	0.7	1.4	0.8	0.4	1.1	1.2
Br mg/L	342	92.0	80.5	81.0	89.0	49.4	110
pH	5.2	nm	8.2	7.7	8.4	8.7	8.4
Field pH	nm	nm	nm	nm	nm	nm	nm
Temp °F	258	297	246	248*	194	200	206
cations meq/L	4,328	nm	1,015	1,959	766.8	348.4	1,019
anions meq/L	4,291	nm	981.3	1,850	747.6	334.2	918.9

County	Calhoun	Calhoun	Calhoun	Calhoun	Calhoun	Calhoun	Chambers
Field	Maude B.Traylor, N.	Maude B.Traylor, N.	Panther Reef, NW.	Panther Reef, SW.	Panther Reef, SW.	Panther Reef	Red Fish Reef
Operator Well-Lease	Superior Oil† W. L. Traylor #2	Superior Oil† W. L. Traylor D #6	Getty† Texas State Tract 95 #1	Getty† Texas State Tract 116 #1AL	Getty† Texas State Tract 117 #1	Getty† Texas State Tract 125 #1	Exxon† Galveston Bay State A-120
Depth (ft)	8,910-8,917	9,293-9,323	10,212-10,860	8,780-8,790	8,796-8,802	8,882-8,892	12,145-12,161
Gas-Water Ratio (mcf/bbl)	9.0	3.0	4.0	1.0	3.0	30.0	oil well
Parameter							
TDS mg/L	59,500	70,100	20,000	49,100	31,000	59,800	123,440
Na mg/L	25,000	27,200	7,400	17,100	11,200	22,600	43,600
K mg/L	132	171	63.0	110	85.0	130	450
Mg mg/L	61.7	111	7.0	105	31.3	170	465
Ca mg/L	231	450	44.0	740	185	2,100	4,280
Fe mg/L	0.05	0.04	0.14	0.2	0.04	0.3	0.28
Al mg/L	<0.5	<0.5	<0.4	<1.0	<0.5	<1.0	<0.5
Mn mg/L	0.2	0.025	0.2	0.5	0.2	0.7	3.4
Sr mg/L	46.2	162	7.8	95.0	19.0	160	415
Ti mg/L	<0.13	<0.13	<0.1	<0.25	<0.13	<0.25	<0.2
B mg/L	58.8	50.6	33.5	50.0	46.0	46.0	43.0
P mg/L	<1.3	<1.3	<1.0	<2.5	<1.3	<2.5	<1.5
SiO_2 mg/L	61.5	58.0	81.5	46.5	66.0	10.5	73.0
HCO_3 mg/L	1,100	574	1,800	710	1,300	120	289
Field alkalinity mg/L	nm	nm	nm	nm	nm	nm	nm
Cl mg/L	35,900	41,500	10,550	27,800	17,050	42,050	73,300
NH_3 mg/L	20.3	23.7	4.4	12.8	7.5	14.1	56.0
SO_4 mg/L	6.5	5.2	47.0	23.0	45.0	5.1	<10.0
F mg/L	1.0	1.5	2.8	1.2	1.6	0.8	0.4
Br mg/L	129	131	63.0	125	105	140	82.0
pH	8.1	8.1	8.6	8.0	8.4	7.5	7.5
Field pH	nm	nm	nm	nm	nm	nm	nm
Temp °F	191	225	238	236*	245	228	240
cations meq/L	1,109	1,221	326.3	792.2	501.2	1,060	2,160
anions meq/L	1,032	1,182	328.9	797.7	504.5	1,190	2,072

County	Chambers	Galveston	Galveston	Galveston	Galveston	Galveston	Galveston
Field	Red Fish Reef	Algoa	Algoa	Alta Loma	Alta Loma	Alta Loma	Alta Loma, W.
Operator Well-Lease	Exxon† Galveston Bay State A-124	Superior† Cooper Unit B #1	Superior† Winton Unit #1	Hunt Oil F. Chinavdo #1	Hunt Oil Green #2	Hunt Oil Sayko #2	Hunt Oil Tacquard #1
Depth (ft)	11,594-11,607	11,398-11,408	11,472-11,499	10,800 (mid point)	11,278-11,282	11,250-11,254	12,270-12,280
Gas-Water Ratio (mcf/bbl)	oil well	3.0	24.0	oil well	oil well	oil well	oil well
Parameter							
TDS mg/L	77,025	139,000	133,000	62,500	55,800	58,900	79,900
Na mg/L	27,450	44,000	42,400	24,900	20,900	22,700	29,800
K mg/L	340	624	643	180	185	192	230
Mg mg/L	430	710	670	88.4	153	95.1	151
Ca mg/L	2,485	8,350	8,580	606	1,190	783	1,490
Fe mg/L	0.03	0.10	<0.05	0.1	4.5	0.07	3.9
Al mg/L	<0.5	<1.0	<1.0	<0.5	<0.05	<0.5	<0.5
Mn mg/L	1.5	4.0	6.5	0.7	1.5	0.97	1.4
Sr mg/L	230	350	380	116	143	145	272
Ti mg/L	<0.2	<0.25	<0.25	<0.13	<0.13	<0.13	<0.13
B mg/L	22.0	67.7	64.5	43.7	38.4	39.2	53.6
P mg/L	<1.5	<2.5	<2.5	<1.3	<1.3	<1.3	<1.3
SiO_2 mg/L	63.0	25.0	22.0	102	44.5	114	83.5
HCO_3 mg/L	358	88.0	94.3	848	547	628	536
Field alkalinity mg/L	nm	nm	nm	nm	nm	nm	nm
Cl mg/L	46,700	83,600	80,900	36,700	33,100	35,200	46,300
NH_3 mg/L	40.0	120	125	23.3	24.0	17.8	27.0
SO_4 mg/L	720	2.0	2.9	6.2	1.0	7.5	18.3
F mg/L	0.6	0.5	1.7	0.8	0.6	0.8	0.9
Br mg/L	59.0	81.3	80.0	48.0	43.7	43.3	57.4
pH	7.8	6.1	5.9	8.0	8.0	8.1	7.4
Field pH	nm	nm	nm	nm	nm	nm	nm
Temp °F	250	228	263	218	227*	241	264
cations meq/L	1,362	2,412	2,351	1,101	987.3	1,040	1,390
anions meq/L	1,337	2,360	2,284	1,050	943.0	1,004	1,316

County	Galveston	Jefferson	Jefferson	Kenedy	Kenedy	Kenedy	Kenedy
Field	Hastings, SE.	High Island	Hildebrandt Bayou	Candelaria	Candelaria	Candelaria	Candelaria
Operator Well-Lease	Superior† Eastham Jocku Sonn Unit #1	Superior† High Is. BLK 14L #5	Coastal† Rubye Parr Gas Unit #1	Exxon C. M. Armstrong #60	Exxon C. M. Armstrong #58F	Exxon C. M. Armstrong # 54F	Exxon C. M. Armstrong #57D
Depth (ft)	9,767-9,784	10,421-10,434	9,468-9,512	12,781-12,870	8,604-8,608	9,304-9,316	9,476-9,484
Gas-Water Ratio (mcf/bbl)	66.0	22.0	13.0	13.0	oil well	101	37.0
Parameter							
TDS mg/L	136,000	57,200	42,700	245,600	96,300	111,400	102,600
Na mg/L	49,300	22,600	17,250	39,900	19,750	14,200	17,870
K mg/L	371	146	99.0	2,900	143	135	140
Mg mg/L	660	100	55.4	220	26.2	46	117
Ca mg/L	4,260	480	204	32,240	15,400	27,500	22,260
Fe mg/L	0.1	0.04	0.04	35.0	2.8	8.5	24.6
Al mg/L	<0.5	<0.5	<0.5	<0.5	<0.4	<0.4	<0.4
Mn mg/L	4.5	0.15	0.05	56.2	1.3	2.1	4.1
Sr mg/L	381	69.8	44.7	1,670	800	1,280	1,220
Ti mg/L	<0.13	<0.13	<0.2	<0.2	<0.1	0.14	<0.1
B mg/L	62.1	65.5	52.0	100	64.0	36.9	46.9
P mg/L	<1.3	<1.3	<1.5	<1.5	<0.6	<1.0	<1.0
SiO_2 mg/L	8.5	58.0	66.0	56.0	54.0	72.8	144
HCO_3 mg/L	219	1,130	1,678	47.5	58.6	42.9	48.4
Field alkalinity mg/L	nm	nm	nm	nm	62.9	40.8	61.2
Cl mg/L	83,600	33,800	24,400	129,400	56,300	70,000	65,400
NH_3 mg/L	76.5	36.3	20.0	147	7.8	10.0	32.0
SO_4 mg/L	51.0	14.3	460	12.0	5.0	<1.0	2.0
F mg/L	0.7	0.9	1.3	1.4	2.8	2.1	1.9
Br mg/L	95.4	66.7	72.0	800	225	287	299
pH	7.4	8.0	7.9	nm	6.7	6.4	6.4
Field pH	nm	nm	nm	nm	6.75	6.7	6.3
Temp °F	214	219*	254	287	223	235.0	236
cations meq/L	2,425	1,021.0	767.6	3,436	1,633	1,997	1,901
anions meq/L	2,363	972.9	725.2	3,650	1,591	1,978	1,849

County	Kenedy	Kenedy	Kenedy	Kenedy	Kenedy	Kenedy
Field	Don Tomas	Rita	Rita, SE.	Sarita	Sarita	Sarita, E.
Operator Well-Lease	Exxon C. M. Armstrong #31	Exxon S. K. East #58D	Exxon S. K. East #93	Exxon Sarita Oil & Gas Unit #32F	Exxon Sarita Oil & Gas Unit #123F	Exxon S. K. East #B-24
Depth (ft)	10,028-10,040	7,492-7,496	12,939-12,946	7,439-7,443	7,321-7,328	13,837-14,667
Gas-Water Ratio (mcf/bbl)	3.0	oil well	3.0	oil well	oil well	10.0
Parameter						
TDS mg/L	125,200	94,600	171,000	95,900	97,700	95,440
Na mg/L	11,300	23,400	33,300	25,950	29,000	27,190
K mg/L	200	148	1,870	137	142	1,160
Mg mg/L	12.5	74.2	98.5	112	287	178
Ca mg/L	34,000	14,100	28,700	7,670	6,675	6,510
Fe mg/L	0.53	6.6	21.6	0.6	6.7	65.0
Al mg/L	<0.5	<0.5	<0.5	<0.5	<0.5	<0.5
Mn mg/L	1.6	1.8	22.5	2.6	1.3	5.2
Sr mg/L	1,180	860	2,120	643	290	500
Ti mg/L	0.14	<0.13	<0.13	<0.1	<0.1	<0.2
B mg/L	36.4	66.0	122	76.0	41.0	84.0
P mg/L	<1.3	5.7	<1.3	<1.0	<1.3	<1.5
SiO_2 mg/L	82.0	55.0	103	56.0	33.0	76.0
HCO_3 mg/L	70.0	120.0	127.0	143	51.4	175
Field alkalinity mg/L	35.4	57.8	102.0	nm	59.8	nm
Cl mg/L	76,650	59,300	105,300	55,900	57,800	56,300
NH_3 mg/L	12.0	5.7	160	10.5	9.0	74.0
SO_4 mg/L	2.0	9.7	2.4	3.0	5.0	21.5
F mg/L	1.9	2.1	2.0	1.5	0.8	1.1
Br mg/L	353	237	567	239	220	157
pH	6.6	7.0	6.2	6.8	7.0	nm
Field pH	6.4	6.5	5.7	nm	6.9	nm
Temp °F	234	197	295	198	196	309
cations meq/L	2,194	1,732	2,946	1,524.9	1,622	1,552
anions meq/L	2,167	1,678	2,980	1,578.9	1,633	1,591

County	Kleberg	Kleberg	Kleberg	Matagorda	Matagorda	Matagorda
Field	Alazan, N.	May, S.	May, S.	Pheasant, SW.	Sugar Valley	Sugar Valley
Operator Well-Lease	Exxon Unit #354	Cities Service Hubert #23	Cities Service Mittag #6	Mobil† Mat'l. Trull "H" Sand Unit #2	Superior† S.Thomasson #1UT	Superior† S.Thomasson #1LT
Depth (ft)	7,262-7,340	8,854-8,862	8,496-8,504	11,655-11,716	8,708-8,712	8,948-8,965
Gas-Water Ratio (mcf/bbl)	<1.0	1.0	<1.0	29.0	<1.0	oil well
Parameter						
TDS mg/L	91,200	55,600	62,100	15,380	93,700	104,000
Na mg/L	25,600	18,990	20,860	5,840	35,900	38,900
K mg/L	150	131	95.0	60.8	260	379
Mg mg/L	95.0	77.0	61.0	9.4	225	296
Ca mg/L	8,100	1,780	3,490	100	1,070	1,770
Fe mg/L	1.4	23.0	85.0	0.05	0.03	0.05
Al mg/L	<1.0	<0.5	<0.5	<0.5	<0.5	<1.0
Mn mg/L	1.9	0.8	1.4	0.14	0.18	1.01
Sr mg/L	500	288	335	8.2	182	217
Ti mg/L	<0.25	<0.1	<0.1	<0.1	<0.13	<0.25
B mg/L	69.0	66.0	60.0	80.0	50.1	49.1
P mg/L	<2.5	<1.0	<1.0	<1.0	<1.3	<1.3
SiO_2 mg/L	44.0	70.0	23.0	112	52.5	51.5
HCO_3 mg/L	84.0	415	132	806	257	207
Field alkalinity mg/L	59.8	nm	nm	nm	nm	nm
Cl mg/L	53,850	33,150	37,000	8,470	56,900	62,700
NH_3 mg/L	12.0	14.0	7.5	4.8	37.3	87.5
SO_4 mg/L	25.0	7.0	7.0	60.0	6.8	6.2
F mg/L	1.8	1.7	1.0	1.8	0.9	0.8
Br mg/L	245	137	186	56	66.0	82.4
pH	6.9	7.5	6.5	nm	7.7	7.6
Field pH	6.9	nm	nm	nm	nm	nm
Temp °F	192	195*	192*	258*	195*	200*
cations meq/L	1,530	925.4	1,089.4	261.4	1,642	1,820
anions meq/L	1,524	941.9	1,045.8	253.1	1,610	1,773

County	Matagorda	Matagorda	Matagorda	Matagorda	Matagorda	Matagorda	Nueces
Field	Sugar Valley	Sugar Valley	Sugar Valley	Tidehaven, Deep	Tidehaven	Trull	Corpus Channel NW.
Operator Well-Lease	Superior† S.Thomasson #2	Superior† W.J. Culbertson A #3	Superior† W.J. Culbertson A #4	Coastal† Elma Ayers #1	Coastal† N. Heffelfinger #1	Coastal† L.P. Neuszer #1	Cities Serv. Co.† Texas State Tract 15 #3LT
Depth (ft)	8,727-8,734	8,940-8,945	8,996-9,000	10,768-10,815	9,396-9,406	9,370-9,390	11,182-11,260
Gas-Water Ratio (mcf/bbl)	oil well	<1.0	<1.0	103	oil well	oil well	3.0
Parameter							
TDS mg/L	92,000	100,000	98,800	51,380	32,780	14,230	80,500
Na mg/L	36,200	37,400	36,000	12,590	12,097	4,822	21,600
K mg/L	270	310	359	144	80.0	30.0	270
Mg mg/L	239	286	277	130	20.0	2.4	200
Ca mg/L	1,188	1,620	1,660	4,784	92.0	16.0	7,660
Fe mg/L	0.025	0.1	0.07	40.8	1.34	0.13	85.0
Al mg/L	<0.5	<0.5	<0.5	<0.5	<0.5	<0.5	<0.4
Mn mg/L	0.37	0.42	1.36	8.5	0.37	0.17	10.5
Sr mg/L	188	213	213	607	26.0	2.1	508
Ti mg/L	<0.13	<0.13	<0.13	<0.2	<0.2	<0.2	<0.1
B mg/L	48.8	47.6	51.0	8.2	31.0	29.0	53.0
P mg/L	<2.5	<1.3	<1.3	<1.5	<1.5	<1.5	<1.0
SiO_2 mg/L	46.5	47.0	49.0	21.0	63.0	67.0	32.5
HCO_3 mg/L	267	230	242	20.0	1,310	2,475	170
Field alkalinity mg/L	nm	nm	nm	nm	nm	nm	nm
Cl mg/L	57,000	61,000	59,100	29,300	18,500	6,100	47,750
NH_3 mg/L	37.4	40.9	40.3	10.8	5.9	0.5	36.0
SO_4 mg/L	5.9	14.7	6.2	22.0	7.0	22.0	1.0
F mg/L	1.1	0.8	0.9	0.6	1.6	3.6	1.0
Br mg/L	75.5	80.0	79.0	33.0	45.0	45.0	250
pH	7.7	7.7	7.8	4.7	8.3	8.8	6.9
Field pH	nm	nm	nm	nm	nm	nm	nm
Temp °F	198	203	189	240	208	211	229
cations meq/L	1,663	1,742	1,683	800.8	534.4	211.6	1,345
anions meq/L	1,613	1,725	1,672	826.7	543.3	213.1	1,352

County	Nueces	Nueces	Nueces	Nueces	Nueces	Nueces	Nueces
Field	Corpus Channel, NW.	Corpus Channel, NW.	Corpus Christi, W.	Corpus Christi, W.	Corpus Christi, W.	Corpus Christi, W.	Corpus Christi, W.
Operator Well-Lease	Cities Serv. Co.† Texas State Tract 15 #3UT	Cities Serv. Co.† Texas State Tract 14 #2	Andover Oil Co. Talbert #2	Andover Oil Co. Peterson-Nuss et al. Unit #1	Andover Oil Co. Eleanor Kelly #3	Andover Oil Co. P.W. Kelly #1	Maynard Oil Co. N.A. Caldwell #1
Depth (ft)	9,903-9,929	8,838-8,906	11,314-11,334	10,879-10,898	12,538-12,586	11,658-11,670	9,340-9,346
Gas-Water Ratio (mcf/bbl)	<1.0	20.0	110.0	30.0	60.0	10.0	66.0
Parameter							
TDS mg/L	46,150	108,200	22,150	29,900	24,500	38,900	34,200
Na mg/L	11,400	30,200	8,850	10,600	8,860	15,200	13,300
K mg/L	124	300	328	264	375	211	105
Mg mg/L	93.0	240	47.9	44.8	25.8	38.2	30.0
Ca mg/L	6,450	9,100	459	491	375	271	181
Fe mg/L	200	7.0	37.5	2.6	21.2	0.06	4.3
Al mg/L	<0.4	<0.5	<0.4	<0.4	<0.4	<0.4	<0.4
Mn mg/L	10.0	12.0	0.73	0.64	0.91	0.49	0.2
Sr mg/L	350	680	40.0	46.3	31.0	58.0	51.0
Ti mg/L	<0.1	<0.1	<0.1	<0.1	<0.1	<0.1	<0.5
B mg/L	18.0	38.0	59.0	47.0	67.1	43.0	35.6
P mg/L	<1.0	<1.0	<1.0	<1.0	<1.0	<1.0	<1.0
SiO_2 mg/L	18.0	61.0	142	108	192	86.8	90.0
HCO_3 mg/L	114	215	450	570	400	1,070	990
Field alkalinity mg/L	nm	nm	nm	nm	nm	nm	357.1
Cl mg/L	28,550	61,970	13,800	16,700	14,000	22,000	20,000
NH_3 mg/L	26.0	42.0	14.6	12.3	9.9	10.0	11.3
SO_4 mg/L	1.0	4.7	1.0	46.0	4.6	2.8	18.0
F mg/L	0.06	1.1	0.8	0.9	0.3	1.1	1.4
Br mg/L	145	280	59.5	63.4	56.1	104	92.5
pH	5.8	6.9	7.7	8.1	8.1	8.2	8.2
Field pH	nm	nm	nm	nm	nm	nm	5.2
Temp °F	229	205	247	265	272	230	226
cations meq/L	828.6	1,795	421.1	496.8	416.4	683.9	593.4
anions meq/L	808.8	1,755	397.3	482.1	402.2	639.4	581.8

County	Nueces	Nueces	Nueces	Nueces	San Patricio	San Patricio	San Patricio
Field	Corpus Christi, Uptown	Corpus Christi, Uptown	Encinal Channel	Mobil-David	Brannon	Geronimo	Geronimo
Operator Well-Lease	Ft. Worth Oil & Gas H. Mange Gas Unit D #1	Ft. Worth Oil & Gas Wilson Trust Gas Unit B #1	Cities Serv. Co.† Texas State Tract 49 #4LT	Mobil Prod.† W.F.L. Lehman #1LT	Wainoco Oil & Gas J.R.C. Brannon Gas Unit #1	Goldston Oil J.E. Garrett #1	Getty† Q.M. Priday #1
Depth (ft)	10,460-10,482	10,440-10,452	10,954-10,960	11,102-11,140	10,521-10,535	10,475-10,490	10,960-11,000
Gas-Water Ratio (mcf/bbl)	12.0	5.0	2.0	16.0	154	74.0	35.0
Parameter							
TDS mg/L	37,900	46,700	213,000	43,250	18,600	21,000	25,200
Na mg/L	14,400	17,700	53,600	17,140	7,170	7,900	9,400
K mg/L	76.5	91.0	485	177	32.3	35.8	71.0
Mg mg/L	28.2	48.1	715	70.0	8.5	8.9	26.0
Ca mg/L	166	298	21,000	590	45	27.4	158
Fe mg/L	4.8	0.34	38.0	0.04	35.9	1.9	0.1
Al mg/L	<0.4	<0.4	<0.5	<0.25	<0.25	0.26	<0.5
Mn mg/L	0.15	0.22	41.0	0.14	0.86	0.12	0.3
Sr mg/L	19.6	31.2	1,300	54.0	4.2	5.0	11.3
Ti mg/L	<0.1	<0.1	<0.1	<0.1	<0.06	<0.06	<0.13
B mg/L	43.8	49.2	34.0	52.0	51.4	41.5	83.3
P mg/L	<1.0	<1.0	<1.0	<1.0	<0.6	<0.6	<1.3
SiO_2 mg/L	114	80.0	33.5	86.0	81.6	88.0	76.0
HCO_3 mg/L	1,550	1,310	114	510	1,720	1,750	870
Field alkalinity mg/L	nm	nm	nm	nm	nm	986.2	nm
Cl mg/L	20,600	25,600	125,600	26,800	9,400	10,300	14,100
NH_3 mg/L	18.4	14.7	56.0	8.4	8.3	8.1	7.4
SO_4 mg/L	28.0	33.0	8.0	9.5	64.0	58.0	120
F mg/L	1.5	1.2	1.1	0.9	2.0	1.8	1.5
Br mg/L	127	155	580	150	34.5	36.5	45.5
pH	8.4	8.1	6.0	nm	8.6	8.6	8.4
Field pH	nm	nm	nm	nm	nm	7.1	nm
Temp °F	235*	263	258	242	260	250	257
cations meq/L	640	792	3,451	785.4	316.2	347.1	420.7
anions meq/L	608.6	746.1	3,551	764.4	295.2	320.9	415

County	San Patricio	San Patricio	San Patricio	San Patricio	San Patricio	San Patricio	San Patricio
Field	Harvey Deep	Harvey Deep	Harvey Deep	Midway, S.	Midway, S.	Midway, S.	Midway, E.
Operator Well-Lease	Galaxy Oil K. Moore #1	Jake L. Hamon Co. Harvey #4	Jake L. Hamon Co. McKamey #2	Cities Serv. Co. Hoskinson A #2	Reading & Bates Eda Crites #1L	Reading & Bates G. Hoskinson #1	Cities Serv. Co. McKamey B #5
Depth (ft)	10,606-10,874	10,510-10,566	10,906-10,914	10,693-12,582	9,656-9,695	9,660-9,702	11,074-13,162
Gas-Water Ratio (mcf/bbl)	20.0	<1.0	12.0	11.0	7.0	oil well	7.0
Parameter							
TDS mg/L	31,100	18,200	27,900	20,700	77,800	19,900	32,500
Na mg/L	11,900	7,230	10,500	7,550	31,300	8,100	12,690
K mg/L	81.2	45.4	80.1	73.0	173	41.4	92.0
Mg mg/L	33.8	9.7	31.1	22.5	29.5	12.3	46.2
Ca mg/L	207	55.9	190	282	484	24.0	398
Fe mg/L	12.5	0.44	8.0	1.6	317	0.78	3.4
Al mg/L	<0.4	<0.4	<0.4	<0.5	<0.5	<0.25	<0.5
Mn mg/L	0.21	0.09	0.18	0.2	4.7	0.23	0.3
Sr mg/L	17.9	6.1	15.5	22.7	16.0	10.2	34.3
Ti mg/L	<0.1	<0.1	<0.1	<0.1	<0.13	<0.06	<0.1
B mg/L	72.3	67.2	96.5	40.0	33.5	37.0	48.0
P mg/L	<1.0	<1.0	<1.0	<1.0	<1.3	<0.6	<1.0
SiO_2 mg/L	119	112	90.0	134	33.5	53.5	124
HCO_3 mg/L	950	1,520	880	687	237	1,220	820
Field alkalinity mg/L	1,142.6	nm	nm	nm	nm	nm	nm
Cl mg/L	17,800	9,700	15,500	12,150	46,100	10,900	19,000
NH_3 mg/L	9.3	7.6	17.3	9.0	29.9	7.5	12.6
SO_4 mg/L	38.0	3.5	75.0	15.0	270	9.5	9.0
F mg/L	1.3	1.9	1.2	1.6	4.8	1.9	1.2
Br mg/L	49.1	33.6	42.5	40.0	44.7	45.0	54.2
pH	8.1	8.6	8.0	8.4	5.0	8.5	8.4
Field pH	6.8	nm	nm	nm	nm	nm	nm
Temp °F	272	250	259	265	220	199	270
cations meq/L	533.9	319.7	471.9	346.8	1,394	356.1	578.7
anions meq/L	519	299.1	453.7	354.3	1,310	328.1	549.5

County	San Patricio	San Patricio	San Patricio
Field	Midway, E.	Portland, N.	Portland, W.
Operator Well-Lease	Jake L. Hamon Co. Hunt #1	Galaxy Oil Simons Gas Unit A #3	Ft. Worth Oil & Gas Portland Gas Unit D #1L
Depth (ft)	10,647-10,663	10,665-10,745	9,715-9,724
Gas-Water Ratio (mcf/bbl)	oil well	<1.0	<1.0
Parameter			
TDS mg/L	37,700	27,400	16,900
Na mg/L	13,300	10,500	7,330
K mg/L	156	78.1	40.2
Mg mg/L	83.6	22.9	8.0
Ca mg/L	748	156	48.0
Fe mg/L	182	0.20	0.36
Al mg/L	<0.4	<0.4	<0.4
Mn mg/L	5.0	0.16	0.17
Sr mg/L	33.6	17.7	5.5
Ti mg/L	<0.1	<0.1	<0.1
B mg/L	33.2	74.2	56.6
P mg/L	<1.0	<1.0	<1.0
SiO_2 mg/L	128	83.0	111
HCO_3 mg/L	420	1,120	2,760
Field alkalinity mg/L	nm	nm	nm
Cl mg/L	21,000	15,200	8,900
NH_3 mg/L	30.4	9.2	6.2
SO_4 mg/L	47.0	52.0	37.0
F mg/L	5.5	1.3	2.0
Br mg/L	46.8	43.0	40.2
pH	5.9	8.4	8.7
Field pH	nm	nm	nm
Temp °F	248	253	230*
cations meq/L	628.5	469	322.9
anions meq/L	600.9	448.7	297.6

APPENDIX B: LIST OF WELLS USED IN AREA STUDIES

Chocolate Bayou Area

Tobin Grid	Well Number	Well Name
6S-38E-1	1	Kelly Brock, #1 Brown Walling
6S-38E-1	2	Phillips, #1 Peterman
6S-38E-1	3	Phillips, #1 Kitchen
6S-38E-1	4	Phillips, #1 Basordi
6S-39E-3	5	Phillips, #1 Kresling
6S-39E-3	6	Phillips, #1 Pardue
6S-39E-3	8	Phillips, #1 Newlin
6S-39E-3	8A	Phillips, #2-A Houston
6S-39E-3	9	Phillips, #1 Bernand
6S-39E-3	10	Phillips, #1 Smiley Benson
6S-39E-3	11	Phillips, #4 Bernand
6S-39E-3	12	Phillips, #6 Bernand
6S-39E-3	13	Phillips, #1 Andrau
6S-39E-3	14	Phillips, #1 Bernadino
6S-39E-3	15	Phillips, #1 Triangle
6S-39E-3	16	Phillips, #1 Plummer
6S-39E-3	17	Quintana, #1 Herring
6S-39E-3	18	Burna, #1 Potter
6S-39E-3	19	Phillips, #1 Westheimer
6S-39E-3	21	Phillips, #4 Angle
6S-39E-2	23	Phillips, #1 Kempner
6S-39E-2	24	Texaco, #1 Weiting
6S-39E-2	25	Phillips, #1 Kentzleman
6S-39E-2	26	Phillips, #1 Grubbs
6S-39E-2	27	Ambassador, #1 Perkins
6S-39E-2	28	Phillips, #1 Schenk
6S-39E-2	29	Phillips, #1 Rebnett
6S-39E-2	30	Pan American, #1 Knutson
6S-39E-1	31	Gulf Board, #1 Millburn
6S-39E-1	32	Texaco, #1 Eggers
6S-40E-3	33	Texas Eastern Trans, #1 Newton

Chocolate Bayou Area (cont.)

Tobin Grid	Well Number	Well Name
6S-39E-1	34	Texaco, #1-B Harris
6S-39E-1	35	Coastal St., #1 Parker
6S-39E-1	36	Texaco, #1 Tocker
6S-39E-1	37	Placid, #1 Briscoe-Dyche
6S-39E-1	38	Texaco, #6 Orchard
6S-39E-1	39A	Texaco, #1-O/A Orchard
6S-39E-1	40	Texaco, #1 Kainer
6S-39E-1	42	M.P.S., #1 Chapman
6S-40E-3	43	R.E.B., #1 Gunderson
6S-40E-3	44	Del Mar, #1 Harris
6S-40E-3	45	Del Mar, #1 Zinn
6S-40E-3	46	General Crude, #1 Miller
6S-40E-3	47	Phillips, #B-1 Pabst
6S-40E-3	48	Phillips, #1 Adriance
6S-40E-3	49	Phillips, #B-3 Pabst
6S-40E-3	50	Hunt, #2 Sayko
6S-40E-3	50A	Hunt, #1 Sayko
6S-40E-3	53	Phillips, #B-2 Pabst
6S-40E-4	77	Buttes, #2 Marshall
6S-40E-4	78	Sinclair, #1 Marshall
6S-40E-4	79	Nor. Am., #1 Konzack
6S-40E-4	80	Am. Petrofina, #1 Marshall
6S-40E-4	85	General Crude, #1 Reitmeyer Briscoe
6S-40E-4	86	General Crude, #1 Hulen
6S-39E-6	87	Texas Eastern Trans., #1 Nana
6S-39E-6	88	Pan. American, #1 Breeding
6S-39E-6	89	Superior, #1 McIlvaine
6S-39E-6	90	Phillips, #1-A McIlvaine
6S-39E-6	91	Phillips, #1-U Houston
6S-39E-6	92	Phillips, #1-T Houston
6S-39E-6	93	Texaco, #1 Harris
6S-39E-5	94	Phillips, #1-W Houston
6S-39E-5	95	Phillips, #1-H Houston

Chocolate Bayou Area (cont.)

Tobin Grid	Well Number	Well Name
6S-39E-5	97	Phillips, #1-S Houston
6S-39E-5	98	Phillips, #1-K Houston
6S-39E-5	99	Phillips, #2 Gunderson
6S-39E-5	100	Phillips, #1-G Houston
6S-39E-5	101	Phillips, #3-F Houston
6S-39E-5	102	Phillips, #2-F Houston
6S-39E-5	103	Phillips, #1-J Houston
6S-39E-5	104	Phillips, #2 Old
6S-39E-5	105	Texaco, #2-A Wilson
6S-39E-5	106	Phillips, #2 Gewill
6S-39E-5	106A	Phillips, #2 Rekdahl
6S-39E-5	107	Texaco, #1 Wilson
6S-39E-5	108	Phillips, #1 Millington
6S-39E-5	109	Phillips, #2 Millington
6S-39E-5	110	Phillips, #2 Cozby
6S-39E-5	111	Phillips, #1 Cozby
6S-39E-5	112	Phillips, #1 Alibel
6S-39E-5	113	Phillips, #5 Schenk
6S-39E-5	114	Phillips, #2-A Schenk
6S-39E-5	115	Phillips, #1-A Schenk
6S-39E-5	116	Phillips, #3 Schenk
6S-39E-5	117	Phillips, #1 Deicken
6S-39E-5	118	Phillips, #1 Taggert
6S-39E-5	119	Crosby, #1 Wilson
6S-39E-5	120	Texaco, #5 Weiting
6S-39E-5	121	Texaco, #15 Weiting
6S-39E-5	122	Phillips, #3 Angle
6S-39E-4	123	Phillips, #3 Banfield
6S-39E-5	124	Phillips, #1 Banfield
6S-39E-4	125	Phillips, #1 Bullard
6S-39E-4	126	Phillips, #1 Houston
6S-39E-4	126A	Phillips, #1-A Houston
6S-39E-4	127	Phillips, #3-C Houston

Chocolate Bayou Area (cont.)

Tobin Grid	Well Number	Well Name
6S-39E-4	128	Phillips, #2-C Houston
6S-39E-4	129	Phillips, #2-M Houston
6S-39E-4	130	Phillips, #B-1 Houston
6S-39E-4	131	Barnes, #1 Houston
6S-39E-4	132	Lacal, #1 Houston
6S-39E-4	133	General Crude, #1 Houston
6S-39E-4	134	Ft. Bend, #1 Anderson
6S-39E-4	135	Foster, #1-B Anderson
6S-39E-4	136	Phillips, #1-P Houston
6S-39E-9	137	General Crude, #2 Pleasant Bayou
6S-39E-8	138	Monsanto, #2 Houston
6S-39E-8	140	Texaco, #2 Houston
6S-39E-8	141	Phillips, #1-X Houston
6S-39E-7	142	Phillips, #1-Y Houston
6S-39E-7	143	Phillips, #1-Z Houston
6S-39E-7	144	Phillips, #A-A Houston
6S-39E-7	145	Superior, #1 Houston
6S-39E-7	146	Phillips, #R-1 Houston
6S-39E-7	147	Phillips, #1 Gardiner
6S-39E-7	148	Phillips, #1-V Houston
6S-39E-7	149	Phillips, #1 Houston "CC"
6S-39E-7	150	Phillips, #1 Houston "FF"
6S-39E-7	151	Phillips, #1 Houston "JJ"
6S-39E-7	152	Phillips, #1 Houston "KK"
6S-39E-7	153	Phillips, #1 Houston "EE"
6S-39E-7	154	Phillips, #1 Houston "NN"
6S-39E-7	155	Phillips, #1 Houston "DD"
6S-40E-9	156	Phillips, #1 Houston "GG"
6S-40E-9	157	Humble, #1-B Houston
6S-40E-9	158	Callender, #1 Griffith
6S-40E-9	159	Payne, #1 Griffith
6S-40E-9	160	Buttes, #3 Marshall
6S-40E-9	161	Buttes, #1 Marshall
7S-39E-1	152A	Phillips, #1 Houston "LL"

Corpus Christi Area

Tobin Grid	Well Number	Well Name
19S-20E-1	1	Maynard et al., #1 Caldwell
18S-21E-9	2	Canus Petroleum, #1 P. W. Kelly
18S-21E-9	3	Canus Petroleum, #3 E. Kelly
18S-21E-9	4	Canus Petroleum, #2 Talbert
18S-21E-9	5	Canus Petroleum, #1 Peterson-Nuss
18S-21E-8	6	Kelly Bell, #1-D H. Manges
18S-21E-5/6	7	Kelly Bell, #B-1 Wilson Trust
18S-21E-5	8	Bell & Dansfield, #1 Baldwin Farms
18S-21E-5	9	Dansfiell et al., #1 KSIX
18S-21E-5	10	Dansfiell, #1 G. W. Hatch
18S-21E-4	11	Coastal States & Dansfiell, #1 KRYS
18S-21E-4	12	Texas Oil & Gas, #1 St. Tr. 750A
18S-21E-3	13	Phillips, #8 Sand
18S-21E-3	14	Phillips, #1 St. Tr. 686
18S-21E-3	15	Republic Natural Gas, #56 E. M. Rachal
18S-21E-3	16	Republic Natural Gas, #60 E. M. Rachal
17S-21E-8	17	Republic Natural Gas, #66 E. M. Rachal
17S-21E-8	18	Shell, #6 W. E. Kirk
17S-21E-7	19	Mobil, #1 Mayo-Owens G.U.
17S-21E-7	20	Mobil, #1 F. B. Jones
17S-21E-1	21	Sunray et al., #1 St. Tr. "G"
18S-22E-3	22	Republic Natural Gas, #2 St. Tr. 786
18S-22E-3	23	Republic Natural Gas, #8 St. Tr. 786
18S-22E-3	24	Arkansas Fuel Oil, #1 St. Nueces Bay 751
17S-21E-7	25	J. L. Hada et al., #1 B. Gierke
17S-21E-7	26	Galaxy, #1 Mayo Moore G.U.
17S-21E-6	27	Cities, #G-1 Jones
17S-22E-4	28	Cities, #2-A G. Hoskinson
17S-22E-4	29	Midwest Oil, #1-A Hoskinson
17S-22E-9	30	Lance Resources, #1 E. Crites
17S-22E-4	31	Cities, #1-A E. Crites
17S-22E-9	32	Republic Natural Gas, #1 Floerke
17S-22E-9	33	E. L. Cox, #1 Stark

Corpus Christi Area (cont.)

Tobin Grid	Well Number	Well Name
17S-22E-8/9	34	E. L. Cox, #1 Barns
17S-22E-9	35	E. L. Cox, #2 Stark
17S-22E-8	36	E. L. Cox, #1 London
17S-22E-8/9	37	E. L. Cox, #1 Boykin
17S-22E-9	38	E. L. Cox, #2 Boykin
17S-22E-8	39	E. L. Cox, #2 London
17S-22E-9	40	E. L. Cox, #A-3 Portland G.U.
17S-22E-8	41	E. L. Cox, #C-2 Portland G.U.
17S-22E-8	42	E. L. Cox, #C-1 Portland G.U.
17S-22E-8	43	E. L. Cox, #C-4-A Portland G.U.
17S-22E-8	44	E. L. Cox, #B-1 Portland G.U.
17S-22E-8	45	E. L. Cox, #B-3 Portland G.U.
17S-21E-6	46	Cities, #1-H Jones
17S-22E-8	47	Goldston Oil, #1 J. E. Garrett
17S-22E-5	48	Hamon & Cox, #1 J. W. Hunt, Jr.
17S-22E-4	49	R. L. Wheelock, Jr., #1 G. Floerke
17S-22E-5	50	Cities, #B-5 McKamey
17S-22E-2	51	Cities, #B-4 T. A. McKamey
17S-22E-5	52	Cities, #E-2 Taylor
17S-22E-5	53	Wainco, #1 Taylor
17S-22E-1/6	54	Midwest Oil, #1 T. R. Miller
17S-22E-6	55	J. L. Hamon, #1 K. G. McKamey
17S-22E-6	56	Tidewater Oil, #1 Q. M. Priday
17S-22E-6	57	J. L. Hamon, #2 K. G. McKamey
17S-22E-1	58	J. L. Hamon, #3 K. G. McKamey
17S-22E-1	59	J. L. Hamon, #4 J. H. Harvey
17S-22E-1	60	J. L. Hamon, #3 J. H. Harvey
18S-22E-1	61	Arkansas Fuel Oil, #2 St. Tr. 14
18S-22E-1	62	Cities, #3 St. Tr. 15
18S-22E-6	63	Cities, #1 St. Tr. 21
18S-22E-6	64	Austral Oil, #1 St. Tr. 31
18S-22E-7	65	Atlantic Richfield, #1 St. Tr. 34
18S-22E-7	66	Cities, #3 St. Tr. 49

Corpus Christi Area (cont.)

Tobin Grid	Well Number	Well Name
18S-22E-8	67	Cities, #2 St. Tr. 49
18S-22E-7	68	Cities & Sunray, #1 St. Tr. 49
18S-22E-8	69	Cities, #4 St. Tr. 49
18S-22E-7/8	70	Cities, #3 St. Tr. 52
17S-21E-8	71	Marathon Oil, #2 Kellogg G.U.
17S-22E-9	72	Galaxy Oil, #A-3 Simons G.U.
17S-22E-4/9	73	Royal & Cox, #1 Marriott
17S-22E-6	74	Trice Producing, #1 K. Y. Moore
17S-22E-1	75	Galaxy Oil, #1 K. Moore
18S-22E-2	76	Kelly Bell, #D-1 Portland Unit
17S-22E-8	77	Kelly Bell, #B-1 Portland Unit

Candelaria Area

Tobin Grid	Well Number	Well Name
24S-18E-9	7	Humble #54 East
24S-18E-9	14	Humble #32 East
24S-18E-9	15	Humble #39 East
24S-18E-9	22	Humble #34 East
25S-17E-1	1	Exxon #58 East
25S-17E-7	10	Exxon #35 Armstrong
25S-17E-1	14	Exxon #87 East
25S-18E-1	1	Humble #1-E East
25S-18E-1	2	Humble #4 Armstrong
25S-18E-1	3	Exxon #41 East
25S-18E-1	4	Humble #56 East
25S-18E-3	5	Humble #22 East
25S-18E-3	6	Humble #21 East
25S-18E-3	7	Exxon #83 East
25S-18E-3	8	Humble #17 East
25S-18E-3	9	Exxon #71 East
25S-18E-3	10	Humble #36 East
25S-18E-3	11	Humble #2 East
25S-18E-3	12	Exxon #61 East
25S-18E-4	13	Humble #15 Armstrong
25S-18E-4	14	Humble #16 Armstrong
25S-18E-4	15	Exxon #29 Armstrong
25S-18E-4	16	Humble #23 Armstrong
25S-18E-4	17	Humble #10 Armstrong
25S-18E-4	18	Humble #12 Armstrong
25S-18E-4	19	Humble #11 Armstrong
25S-18E-4	20	Humble #14 Armstrong
25S-18E-5	21	Humble #25 Armstrong
25S-18E-5	22	Exxon #32 Armstrong
25S-18E-5	23	Exxon #44 Armstrong
25S-18E-5	24	Humble #21 Armstrong
25S-18E-6	25	Humble #9 Armstrong
25S-18E-6	26	Humble #17 Armstrong

Candelaria Area (cont.)

Tobin Grid	Well Number	Well Name
25S-18E-7	27	Humble #20 Armstrong
25S-18E-8	28	Exxon #34 Armstrong
25S-18E-8	29	Exxon #29 Armstrong
25S-18E-8	30	Humble #8 Armstrong
25S-18E-8	31	Exxon #38 Armstrong
25S-18E-9	32	Humble #18 Armstrong
25S-18E-9	33	Exxon #37 Armstrong
25S-18E-9	34	Exxon #40 Armstrong
25S-18E-9	35	Humble #5 Armstrong
25S-18E-9	36	Exxon #33 Armstrong
25S-18E-9	37	Humble #6 Armstrong
25S-18E-9	38	Humble #7 Armstrong
25S-18E-8	39	Exxon #46 Armstrong
25S-18E-6	40	Exxon #30 Armstrong
25S-18E-4	41	Humble #2 Armstrong
25S-18E-3	42	Exxon #92 East
25S-18E-3	43	Exxon #75 East
25S-18E-3	44	Humble #1 East
25S-18E-5	45	Exxon #48 Armstrong
25S-18E-4	46	Exxon #58 Armstrong
25S-18E-4	47	Exxon #60 Armstrong
25S-18E-4	48	Exxon #57 Armstrong
25S-18E-3	49	Exxon #93 East
25S-18E-5	50	Exxon #54 Armstrong
26S-18E-2	1	Humble #22 Armstrong
26S-18E-2	2	Exxon #31 Armstrong
26S-18E-3	3	Exxon #36 Armstrong
26S-18E-3	4	Humble #27 Armstrong
26S-18E-3	5	Humble #3 Armstrong